THE ANALYTICAL AND EXPERIMENTAL STUDIES OF THE HEAT TRANSFER AROUND A VERTICAL ICE WALL IN FRESH WATER NEAR ITS MAXIMUM DENSITY TEMPERATURE

CATHERINE ROBIN DUTTON

ISBN 0-315-31017-0

THE ANALYTICAL AND EXPERIMENTAL STUDIES OF THE HEAT TRANSFER AROUND A VERTICAL ICE WALL IN FRESH WATER NEAR ITS MAXIMUM DENSITY TEMPERATURE

by

©Catherine Robin Dutton

A thesis submitted to the School of Graduate Studies
in partial fulfillment of the
requirements for the degree of
Master of Engineering

Faculty of Engineering and Applied Science
Memorial University of Newfoundland
September 1985

St. John's Newfoundland Canada

DEDICATION

For my husband and children

John
Johnathan
Taryn
Adam

ABSTRACT

The analytical as well as experimental investigations of the temperature and velocity distribution in fresh water along a vertical ice wall are carried out. The analytical investigation involves the simultaneous solution of the continuity equation, the Navier-Stokes equations for fluid motion in two-dimensions and the thermal energy balance equation, by a finite-difference technique. The general form of these equations can then be solved by the successive-substitution method on a digital computer. The experimental investigation involves taking temperature and velocity measurements through the boundary layer along the ice surface at various bulk fluid temperatures.

The analytical and experimental results are compared, for both the temperature and velocity, the local and average heat transfer coefficients and the Nusselt numbers.

The analytical model is then extended to other bulk fluid temperatures with predictions for the temperature and velocity profiles, the average heat transfer coefficients and the Nusselt numbers.

ACKNOWLEDGEMENTS

I would like to thank my supervisor, Dr. A. M. Sharan for his guidance and support in completing this work. I would also like to thank Dr. B. D. Bowen who helped me at the start of this project and assisted in formulating the problem.

I also express my thanks to the National Research Council of Canada who provided funding for this work, and to the Engineering Department at the Memorial University for the use of their many facilities.

I also thank Levinia Vatcher for her patience in typing this thesis.

TABLE OF CONTENTS

LIST OF FIGURES

LIST OF TABLES

NOMENCLATURE

a_ϕ	a coefficient in the modified general equation
A_E, A_W, A_S, A_N	coefficients in the convection terms
A'_j	a coefficient in the modified general substitution formula
b_ϕ	a coefficient in the modified general equation
B_E, B_W, B_S, B_N	coefficients in the diffusion terms
B'_j	a coefficient in the modified general substitution formula
c_ϕ	a coefficients in the modified general equation
C_E, C_W, C_S, C_N	coefficients in the general substitution formula
e_ϕ	the source term the modified general equation
D	source term in the general substitution formula
C_p	specific heat
k	thermal conductivity
h_x	local heat transfer coefficient
$\bar{h}$	average heat transfer coefficient
Nu_x	local Nusselt number
$\bar{Nu}$	average Nusselt number
P	pressure
u	velocity in the x-direction
v	velocity in the y-direction
x, y	cartesian coordinates
X	body forces in the x-direction

Y	body forces in the y-direction
T	temperature
T_B	bulk fluid temperature
S_1	physical distances between nodes in x-direction
S_2	physical distances between nodes in y-direction
X_N, X_S, X_E, X_W	limits of integration in x-direction
Y_N, Y_S, Y_E, Y_W	limits of integration in y-direction
X1	grid line coordinate
X2	grid line coordinate
ρ	density
μ	viscosity
ψ	stream function
ω	vorticity
ϕ	general dependant variable
L	plate length

CHAPTER 1

INTRODUCTION AND LITERATURE SURVEY

1.1 Introduction

The study of heat transfer around ice surfaces is quite useful in understanding the melting and freezing of lakes, rivers, ponds, etc. The process of melting or thawing is quite complex as far as the mathematical analysis is concerned. The complexity is due to the phase change; the type of the boundary layer at the ice surface, i.e. depending upon the conditions one can have either a turbulent or laminar boundary layer; the mass transfer coupled with the heat transfer in the zone of interest; and the variation of properties which introduce nonlinearities in the corresponding equations. Even after several assumptions for simplification, the mathematical model would still be quite involved. Therefore, it would require numerical techniques for the solution and verification of these solutions through experimentation.

The problem of the heat transfer around a semi-infinite vertical ice wall has been studies by Lee [1]. He carried out the theoretical analysis of free convection melting of a semi-infinite vertical ice wall. In this analysis he obtained the velocity profiles, melt velocities,

streamlines and the Nusselt number as a function of temperature. He also considered salinity as one of the variables. In his work, due to the semi-infinite nature of the ice wall, he did not have the air-water interface in his model which is actually the case in reality. He did not verify his results experimentally. There have been several other studies of the heat transfer process around ice surfaces or heated surfaces.

In the heat transfer around vertical ice surfaces in water, there is an interesting phenomenon that takes place around 4°C; at this temperature the density of water is maximum. For a bulk fluid temperature less than 4°C there is an upflow and for a bulk fluid temperature greater than 6°C there is a downflow. In the range of 4°C to 6°C there is a dual flow. It is in this temperature range that there is an inversion of the direction of flow of the water within the boundary layer from predominantly up to predominantly down. In the temperature range where the flow inverts, there is a value at which there is a minimum Nusselt number which corresponds to a lower heat transfer rate. This phenomenon has also been studied by several researchers.

1.2 Inversion Temperature Studies

The earliest work by Dumoré et al [2] gave a minimum Nusselt number at 4.8°C for the case of ice spheres

melting in water. Their experiments involved studying the gradual decrease in diameter and change in weight of the sphere with time. They compared their results with the theoretical findings of Merk [3]. Merk [3] had applied boundary layer theory to calculate the effects of both the melting process, i.e. a moving boundary and the anomalous thermal expansion of water at about 4.°C on the heat transfer process. His results indicate a minimum Nusselt number at 5.3°C. However, due to some limitations in his theoretical model these results differed from the experimental results given in [2]. Ede [4], also compared his experimental results for a heated plate in water with the theoretical findings of Merk [3], and had good correlation except in the range of low Nusselt number. Schenk and Schenkels [5] carried out experiments on ice spheres and compared their results with Merk [3]. Their results corresponded quite well with the theoretical results yielding a minimum Nusselt number at 5.3°C. Other work on ice spheres was carried out by Vanier and Tien [6] and it gave an inversion temperature range between 5.°C and 6.°C. They used these results for comparison with flat-plate theory to pin-point the effect of the diameter on the Nusselt number and when appropriately scaled, the data corresponded within ±7%.

Work by Saitoh [7] involved a theoretical and experimental analysis of melting ice cylinders at various

water temperatures. His theoretical and experimental values corresponded quite well, verifying the findings of earlier works. Work by Oborin [8] involved studying the effect of the temperature head on the inversion temperature range. His results indicate a minimum heat transfer at 5.3°C for an ice surface.

Additional work in this area involved a vertical surface in water at various temperatures. Schechter and Isbin [9] studied the Nusselt number in unidirectional and inverted convection flow experimentally for a heated plate in water at a variety of temperatures. In doing so, they examined the temperature distribution in the boundary layer. Bendall and Gebhart [10] carried out experiments on melting slabs of ice, by recording the change in weight measurements with time. From their data, a Nusselt number was evaluated and compared with the theoretical results of Gebhart and Mollendorf [11]. They found a minimum Nusselt number at 5.6°C. Several other similar studies have also been carried out in [12-21].

In all these studies the theoretical analysis failed to give satisfactory results for the temperature and velocity distributions in the range of the flow inversion. They did however indicate the temperature of the minimum Nusselt number within the range of bidirectional flow. A representative plot of their findings is shown in Fig. 1.1.

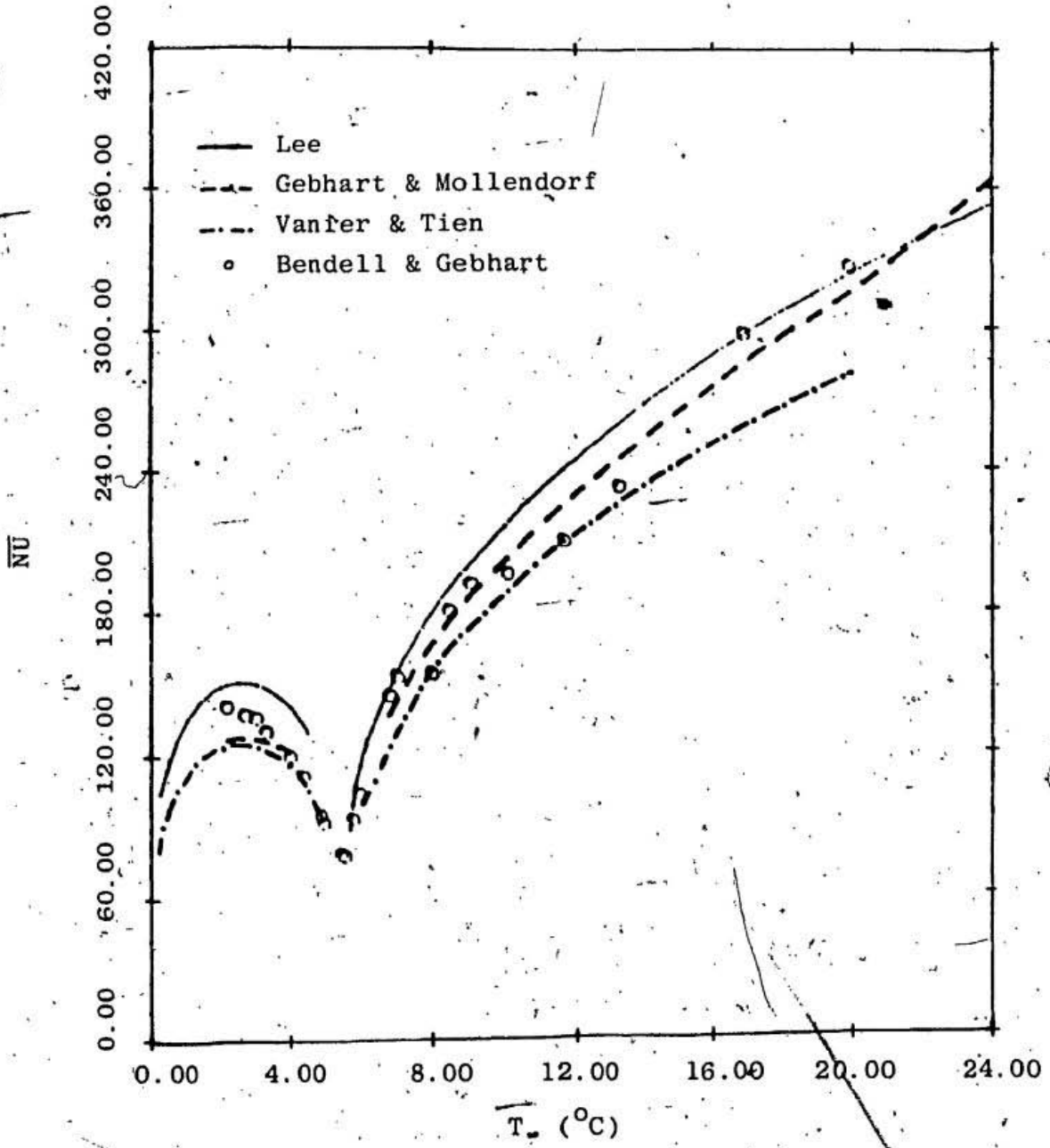

Fig. 1.1 Previous Findings for Nusselt Number as a Function of Temperature, L = 0.7632 m [1]

1.3 Boundary Layer Measurement Techniques

As outlined above, the major experimental approach in these studies has been measurements of observable changes in the ice (size and weight) and little has been done on the makeup of the boundary layer itself. In the experimental studies that have been carried out by other researchers, either the temperature or the velocity distribution within the boundary layer has been measured with respect to an ice surface.

Work by Wilson and Vyas [22] experimentally examined the velocity profiles of an ice surface melting in fresh water. They used an adaptation of a method developed by Baker [23] to create a dye line along the boundary layer. Their results indicated a upward velocity for 0°C to 4°C; an upflow of decreased maximum velocity for 4°C to 4.7°C; an area of dual flow from 4.7°C to 5.6°C with a gradually increasing downflow leading to a downward flow between 5.6°C to 7.0°C.

Another technique for measuring the velocity within the boundary layer is through the use of a hot wire anemometer. Work by Jaluria & Gebhart [24] made use of this technique for velocity measurements within the boundary layer of a heated plate in water. They used a Disa hot wire probe to obtain measurements of the longitudinal and normal components of velocity in the transition flow regime of the boundary layer adjacent to the plate.

Temperature measurements have been obtained through the use of thermocouple and thermistor probes. Work by Warner [25] involved a chromel-constantan thermocouple probe to measure temperature variations in air along a vertical flat plate. Schechter and Isbin [9] used a thermistor probe (a 3.8×10^{-5}m (.0015 in.) diameter glass bead) for the purpose of obtaining the temperature at various points in the field of interest, which was a vertical heated flat plate in water.

There have also been some work done involving simultaneous velocity and temperature measurements. Hishida and Nagano [26] used a two probe configuration - one a hot-wire and the other a temperature wire mounted in close proximity to each other. Their application was the measurement of instantaneous velocity and temperature in non-isothermal flows. Vliet and Liu [27] also used a dual purpose probe, consisting of a hot-wire sensor and a thermocouple in their study of turbulent natural convection boundary layers of a vertical heated plate in water.

1.4 The Objectives of the Present Investigation

The objectives of this work are, therefore, to study the effect of the variations of the bulk temperature on the following:

1. The temperatures of the fluid in the zone of interest (around a vertical ice wall in fresh water).
2. The directions of the fluid flow in this zone.
3. The local and average heat transfer coefficient at the ice surface.
4. The variation of the Nusselt number, both the local and the average .

To accomplish the above mentioned objectives, the mathematical model of the actual process is first developed. Since the exact solution of the resulting set of partial differential equations with variable properties and appropriate boundary conditions is not possible to obtain, these are solved using the finite-difference method. Then, the solutions of these equations under certain special conditions are verified experimentally to check the validity of the theoretical model.

In Chapter 2, the mathematical model of the process is developed, which is a set of partial differential equations along with the appropriate boundary conditions. Then these equations are transformed into a finite-difference form. The algorithm to solve these equations on the digital computer has also been discussed in this chapter.

The details of the experimental techniques as well as the various pieces of equipment used are described in Chapter 3.

Chapter 4 consists of discussion of the analytical, as well as the experimental results and a discussion on the validity of the theoretical model.

The conclusions and recommendations for future work are discussed in Chapter 5.

1.5 Conclusions

In this chapter, the relevant literature survey of the experimental, as well as the theoretical studies on the heat transfer process around various geometrical surfaces has been outlined. Based on these surveys, the objectives of the present work were arrived at and the methods of meeting these objectives were stated.

CHAPTER 2

THE THEORETICAL FORMULATION

2.1 Introduction

The modelling of the heat transfer process around a vertical ice wall in fresh water in the laboratory can be extended to a similar process that takes place in ponds or lakes near the melting point of ice. The flow of the fluid medium is generally laminar. This process can also be mathematically modelled by a set of simultaneous partial differential equations. These equations along with the appropriate boundary conditions can be solved using various numerical techniques. One of these techniques is the finite-difference technique.

In this Chapter the physical process discussed above is mathematically formulated and then solved using the finite-difference technique by using successive-substitution on a digital computer. In the mathematical formulation the unknowns in the partial differential equations are the velocities in the x and y directions and the temperature. The solution involves the transformation of these equations to a new set of equations where the vorticity, the stream function and the temperature are the unkhowns. These

unknowns are solved using the finite-difference technique and the velocities are obtained by back substitution.

2.2 The General Formulation of the Equations

For the system shown in Fig. 2.1, the continuity equation, the complete Navier-Stokes equations for motion in two-dimensions and the thermal energy balance equation can be written as: [1]

$$\frac{\partial u}{\partial x} + \frac{\partial v}{\partial y} = 0 \tag{2.1}$$

$$\rho u \frac{\partial u}{\partial x} + \rho v \frac{\partial u}{\partial y} = - \frac{\partial P}{\partial x} + \frac{\partial}{\partial x} \{\mu[2 \frac{\partial u}{\partial x} - \frac{2}{3}(\frac{\partial u}{\partial x} + \frac{\partial v}{\partial y})]\} + \frac{\partial}{\partial y} \{\mu[\frac{\partial u}{\partial y} + \frac{\partial v}{\partial x}]\} + X \tag{2.2}$$

$$\rho u \frac{\partial v}{\partial x} + \rho v \frac{\partial v}{\partial y} = - \frac{\partial P}{\partial y} + \frac{\partial}{\partial y} \{\mu[2 \frac{\partial v}{\partial y} - \frac{2}{3}(\frac{\partial u}{\partial x} + \frac{\partial v}{\partial y})]\} + \frac{\partial}{\partial x} \{\mu[\frac{\partial u}{\partial y} + \frac{\partial v}{\partial x}]\} + Y \tag{2.3}$$

$$\rho(u \frac{\partial T}{\partial x} + v \frac{\partial T}{\partial y}) = \frac{k}{C_p} (\frac{\partial^2 T}{\partial x^2} + \frac{\partial^2 T}{\partial y^2}) \tag{2.4}$$

Using the continuity equation, and considering viscosity a constant, the momentum equations can be reduced to the following forms:

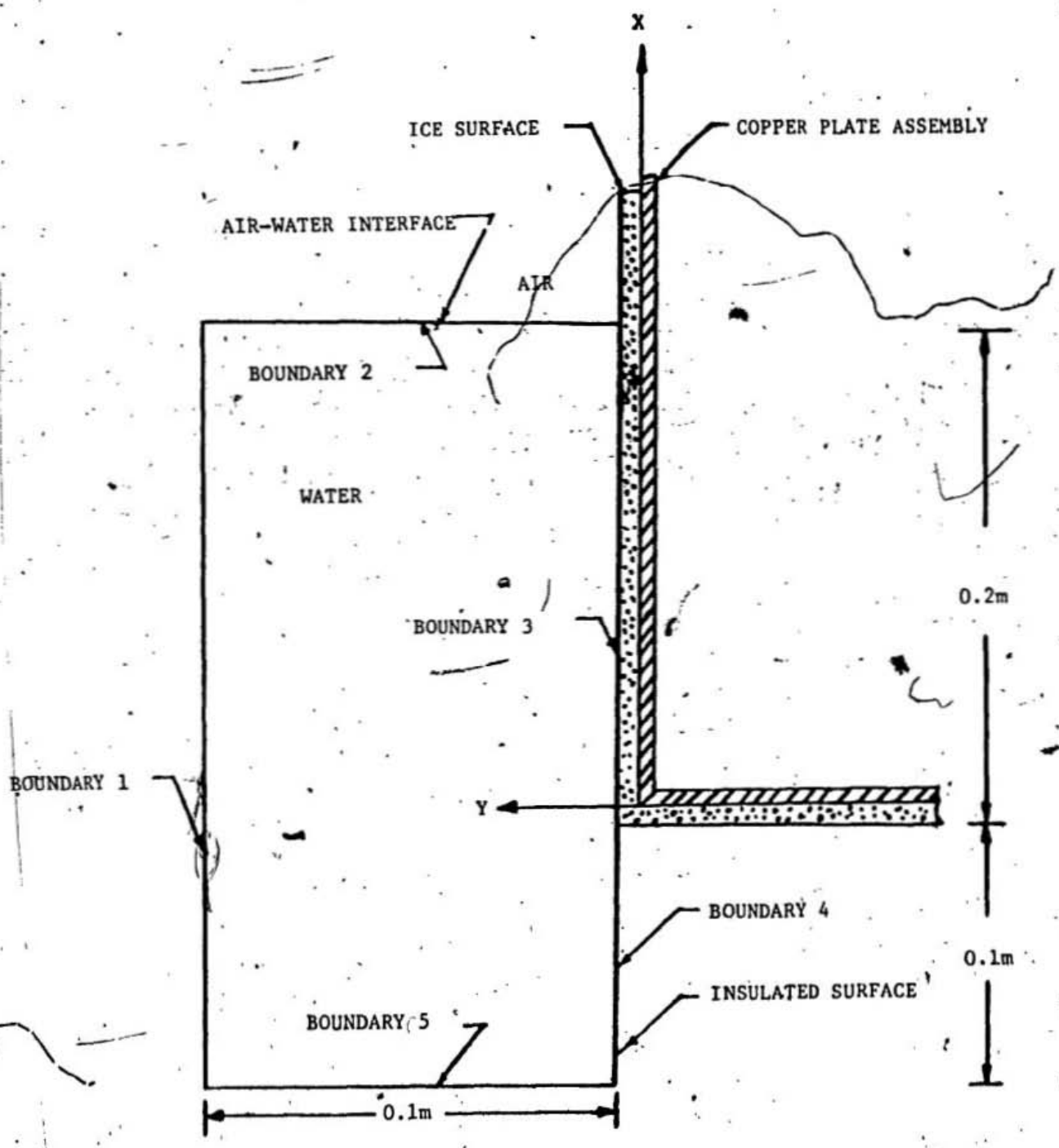

Fig. 2.1 The Schematic of the Area Analyzed

$$\rho\left(u\frac{\partial u}{\partial x} + v\frac{\partial u}{\partial y}\right) = -\frac{\partial P}{\partial x} + \mu\left(\frac{\partial^2 u}{\partial x^2} + \frac{\partial^2 u}{\partial y^2}\right) + X \qquad (2.5)$$

$$\rho\left(u\frac{\partial v}{\partial x} + v\frac{\partial v}{\partial y}\right) = -\frac{\partial P}{\partial y} + \mu\left(\frac{\partial^2 v}{\partial x^2} + \frac{\partial^2 v}{\partial y^2}\right) + Y \qquad (2.6)$$

Elimination of the pressure terms in these equations is accomplished by differentiation of Eqn. (2.5) with respect to y and Eqn. (2.6) with respect to x. Then, using the continuity equation and a few mathematical steps [28] one obtains

$$\underbrace{\frac{\partial}{\partial y}\left[\rho u\frac{\partial u}{\partial x} + \rho v\frac{\partial u}{\partial y}\right] - \frac{\partial}{\partial x}\left[\rho u\frac{\partial v}{\partial x} + \rho v\frac{\partial v}{\partial y}\right]}_{\text{I}}$$

$$\underbrace{-\mu\left[\frac{\partial}{\partial y}\left(\frac{\partial^2 u}{\partial x^2} + \frac{\partial^2 u}{\partial y^2}\right) - \frac{\partial}{\partial x}\left(\frac{\partial^2 v}{\partial x^2} + \frac{\partial^2 v}{\partial y^2}\right)\right]}_{\text{II}} + \frac{\partial X}{\partial y} + \frac{\partial Y}{\partial x} = 0 \qquad (2.7)$$

This equation can be further simplified by suitable manipulations of parts I and II separately. In order to do this it is now necessary to introduce the expressions for stream function and vorticity, which are as follows:

$$\rho u = \frac{\partial \psi}{\partial y} \qquad (2.8)$$

Stream Function

$$\rho v = -\frac{\partial \psi}{\partial x} \qquad (2.9)$$

$$\omega = \frac{\partial v}{\partial x} - \frac{\partial u}{\partial y} \quad \text{Vorticity} \qquad (2.10)$$

2.2.1 Simplification of Part I in Eqn. (2.7)

Starting with part I in Eqn. (2.7) and using Eqns. (2.8) to (2.10) one obtains

$$\frac{\partial}{\partial y}\left[\frac{\partial \psi}{\partial y}\frac{\partial u}{\partial x} - \frac{\partial \psi}{\partial x}\left(\frac{\partial v}{\partial x} - \omega\right)\right] - \frac{\partial}{\partial x}\left[\frac{\partial \psi}{\partial y}\left(\frac{\partial u}{\partial y} + \omega\right) - \frac{\partial \psi}{\partial x}\frac{\partial v}{\partial y}\right]$$

$$= \frac{\partial}{\partial y}\left(\omega \frac{\partial \psi}{\partial x}\right) - \frac{\partial}{\partial x}\left(\omega \frac{\partial \psi}{\partial y}\right) + \frac{\partial}{\partial y}\left(\frac{\partial \psi}{\partial y}\frac{\partial u}{\partial x} - \frac{\partial \psi}{\partial x}\frac{\partial v}{\partial x}\right)$$

$$- \frac{\partial}{\partial x}\left(\frac{\partial \psi}{\partial y}\frac{\partial u}{\partial y} - \frac{\partial \psi}{\partial x}\frac{\partial v}{\partial y}\right)$$

$$= \frac{\partial}{\partial y}\left(\omega \frac{\partial \psi}{\partial x}\right) - \frac{\partial}{\partial x}\left(\omega \frac{\partial \psi}{\partial y}\right) + \frac{\partial}{\partial y}\left(\rho u \frac{\partial u}{\partial x} + \rho v \frac{\partial v}{\partial x}\right)$$

$$- \frac{\partial}{\partial x}\left(\rho u \frac{\partial u}{\partial y} + \rho v \frac{\partial v}{\partial y}\right)$$

$$= -\frac{\partial}{\partial x}\left(\omega \frac{\partial \psi}{\partial y}\right) + \frac{\partial}{\partial y}\left(\omega \frac{\partial \psi}{\partial x}\right) - \frac{\partial}{\partial x}\left(\rho u \frac{\partial u}{\partial y}\right)$$

$$+ \frac{\partial}{\partial y}\left(\rho u \frac{\partial u}{\partial x}\right) - \frac{\partial}{\partial x}\left(\rho v \frac{\partial v}{\partial y}\right) + \frac{\partial}{\partial y}\left(\rho v \frac{\partial v}{\partial x}\right)$$

$$= -\frac{\partial}{\partial x}\left(\omega \frac{\partial \psi}{\partial y}\right) + \frac{\partial}{\partial y}\left(\omega \frac{\partial \psi}{\partial x}\right) - \rho u \frac{\partial^2 u}{\partial x \partial y} - \frac{\partial u}{\partial y}\frac{\partial(\rho u)}{\partial x}$$

$$+ \rho u \frac{\partial^2 u}{\partial x \partial y} + \frac{\partial u}{\partial x}\frac{\partial(\rho u)}{\partial y} - \rho v \frac{\partial^2 v}{\partial x \partial y} - \frac{\partial v}{\partial y}\frac{\partial(\rho v)}{\partial x}$$

$$+ \rho v \frac{\partial^2 v}{\partial x \partial y} + \frac{\partial v}{\partial x}\frac{\partial(\rho v)}{\partial y}$$

Cancelling $\rho u \frac{\partial^2 u}{\partial x \partial y}$ and $\rho v \frac{\partial^2 v}{\partial x \partial y}$, one can write

$$\text{Part I} = -\frac{\partial}{\partial x}\left(\omega \frac{\partial \psi}{\partial y}\right) + \frac{\partial}{\partial y}\left(\omega \frac{\partial \psi}{\partial x}\right) + \left(u \frac{\partial u}{\partial x} + v \frac{\partial v}{\partial x}\right) \frac{\partial \rho}{\partial y}$$

$$- \left(u \frac{\partial u}{\partial y} + v \frac{\partial v}{\partial y}\right) \frac{\partial \rho}{\partial x}$$

$$= -\frac{\partial}{\partial x}\left(\omega \frac{\partial \psi}{\partial y}\right) + \frac{\partial}{\partial y}\left(\omega \frac{\partial \psi}{\partial x}\right) + \frac{\partial}{\partial x}\left(\frac{u^2+v^2}{2}\right) \frac{\partial \rho}{\partial y}$$

$$- \frac{\partial}{\partial y}\left(\frac{u^2+v^2}{2}\right) \frac{\partial \rho}{\partial x} \qquad (2.11)$$

2.2.2 Simplifications of Part II in Eqn. (2.7)

Combining part II of Eqn. (2.7) and Eqns. (2.8) to (2.10) one obtains

$$= -\mu\left[\frac{\partial}{\partial y}\left(\frac{\partial^2 u}{\partial x^2} + \frac{\partial^2 v}{\partial x \partial y} - \frac{\partial \omega}{\partial y}\right) - \frac{\partial}{\partial x}\left(\frac{\partial^2 u}{\partial x \partial y} + \frac{\partial \omega}{\partial x} + \frac{\partial^2 v}{\partial y^2}\right)\right]$$

$$= \mu\left[\frac{\partial^2 \omega}{\partial y^2} + \frac{\partial^2 \omega}{\partial x^2}\right] - \mu\left[\frac{\partial}{\partial y}\left(\frac{\partial^2 u}{\partial x^2} + \frac{\partial^2 v}{\partial x \partial y}\right)\right.$$

$$\left. - \frac{\partial}{\partial x}\left(\frac{\partial^2 u}{\partial x \partial y} + \frac{\partial^2 v}{\partial y^2}\right)\right]$$

Neglecting all the terms containing the third derivatives, one can write

$$\text{Part II} = \mu\left[\frac{\partial^2 \omega}{\partial y^2} + \frac{\partial^2 \omega}{\partial x^2}\right] \qquad (2.12)$$

2.2.3 The Derivation of the Momentum and Energy Equations in the General Form

Using $X = -\rho g$ and $Y = 0$ Eqn. (2.7) becomes

$$-\frac{\partial}{\partial x}\left(\omega \frac{\partial \phi}{\partial y}\right) - \frac{\partial}{\partial y}\left(\omega \frac{\partial \phi}{\partial x}\right) - \mu\left(\frac{\partial^2 \omega}{\partial x^2} + \frac{\partial^2 \omega}{\partial y^2}\right)$$

$$-\frac{\partial}{\partial x}\left(\frac{u^2+v^2}{2}\right)\frac{\partial \rho}{\partial y} + \frac{\partial}{\partial y}\left(\frac{u^2+v^2}{2}\right)\frac{\partial \rho}{\partial x} - g\frac{\partial \rho}{\partial y} = 0 \qquad (2.13)$$

This is the vorticity expression in general form.

Now, the stream function expression is obtained using Eqns. (2.8) to (2.10). Substituting the values of the u and v from Eqns. (2.8) and (2.9) respectively into Eqn. (2.10) yields

$$\omega = -\frac{\partial}{\partial x}\left[\frac{1}{\rho}\frac{\partial \phi}{\partial x}\right] - \frac{\partial}{\partial y}\left[\frac{1}{\rho}\frac{\partial \phi}{\partial y}\right]$$

This can be rewritten as

$$\frac{\partial}{\partial x}\left[\frac{1}{\rho}\frac{\partial \phi}{\partial x}\right] + \frac{\partial}{\partial y}\left[\frac{1}{\rho}\frac{\partial \phi}{\partial y}\right] - \omega = 0 \qquad (2.14)$$

The temperature equation can also be put in the same general form by the following formulation:

$$\rho\left(u\frac{\partial T}{\partial x} + v\frac{\partial T}{\partial y}\right) = \frac{k}{C_p}\left(\frac{\partial^2 T}{\partial x^2} + \frac{\partial^2 T}{\partial y^2}\right)$$

Transposing the right-hand side term to the left, one obtains

$$\rho u \frac{\partial T}{\partial x} + \rho v \frac{\partial T}{\partial y} - \frac{k}{C_p} \left(\frac{\partial^2 T}{\partial x^2} + \frac{\partial^2 T}{\partial y^2}\right) = 0$$

Using Eqns. (2.8) and (2.9), this becomes

$$\frac{\partial \psi}{\partial y} \frac{\partial T}{\partial x} - \frac{\partial \psi}{\partial x} \frac{\partial T}{\partial y} - \frac{k}{C_p} \left[\frac{\partial^2 T}{\partial x^2} + \frac{\partial^2 T}{\partial y^2}\right] = 0$$

Rewriting this equation, one obtains

$$\frac{\partial}{\partial x} \left[T \frac{\partial \psi}{\partial y}\right] - \frac{\partial}{\partial y} \left[T \frac{\partial \psi}{\partial x}\right] - \frac{k}{C_p} \left[\frac{\partial^2 T}{\partial x^2} + \frac{\partial^2 T}{\partial y^2}\right] = 0 \qquad (2.15)$$

The velocity values are determined by back substitution of the stream function and the vorticity values in Eqns. (2.8) to (2.10).

The above partial differential equations, Eqns. (2.13), (2.14) and (2.15) are for obtaining vorticity, stream function and temperature respectively. These equations can be represented by the following general form:

$$a_\phi \left\{\frac{\partial}{\partial x}\left(\phi \frac{\partial \psi}{\partial y}\right) - \frac{\partial}{\partial y}\left(\phi \frac{\partial \psi}{\partial x}\right)\right\} - \frac{\partial}{\partial x}\left\{b_\phi \frac{\partial}{\partial x}(c_\phi \phi)\right\}$$

$$- \frac{\partial}{\partial y}\left\{b_\phi \frac{\partial}{\partial y}(c_\phi \phi)\right\} + e_\phi = 0 \qquad (2.16)$$

where ϕ is the general dependent variable and a_ϕ, b_ϕ, c_ϕ and e_ϕ are outlined in the Table 2.1

Table 2.1: Expression of a_ϕ, b_ϕ, c_ϕ and e_ϕ

ϕ	a_ϕ	b_ϕ	c_ϕ	e_ϕ
ω	1	1	μ	$-[\frac{\partial}{\partial x}(\frac{u^2+v^2}{2})\frac{\partial \rho}{\partial y} - \frac{\partial}{\partial y}(\frac{u^2+v^2}{2})\frac{\partial \rho}{\partial x}] \pm g\frac{\partial \rho}{\partial y}$
ϕ	0	$\frac{1}{\rho}$	1	$-\omega$
T	1	$\frac{k}{C_p}$	1	0

2.3 The Finite-Difference Form of the Equations

Following the procedure outlined by Gosman, Pun and Runchal [28], it is possible to reduce these partial differential equations to a set of simultaneous algebraic finite-difference equations in a form which can be solved by an iterative successive-substitution technique.

The technique outlined in [28] involves integration of the equation over the field of interest as shown in Fig. 2.2. In this figure one can see a typical node P, in an orthogonal grid network, and four surrounding nodes, N, S, E and W. The actual integration is carried out over the smaller rectangle outlined by n, s, e and w around node P, as follows:

$$\underbrace{\int_{Y_s}^{Y_n}\int_{X_w}^{X_e} a_\phi \left\{\frac{\partial}{\partial x}\left(\phi\,\frac{\partial \psi}{\partial y}\right) - \frac{\partial}{\partial y}\left(\phi\,\frac{\partial \psi}{\partial x}\right)\right\} dx\,dy}_{\text{Convection Term, } I_c} -$$

$$\underbrace{\int_{Y_s}^{Y_n}\int_{X_w}^{X_e} \left\{\frac{\partial}{\partial x}\left(b_\phi \frac{\partial}{\partial x}\left(c_\phi\,\phi\right)\right) + \frac{\partial}{\partial y}\left\{b_\phi \frac{\partial}{\partial y}\left(c_\phi\,\phi\right)\right\}dx dy\right.}_{\text{Diffusion Terms, } I_d}$$

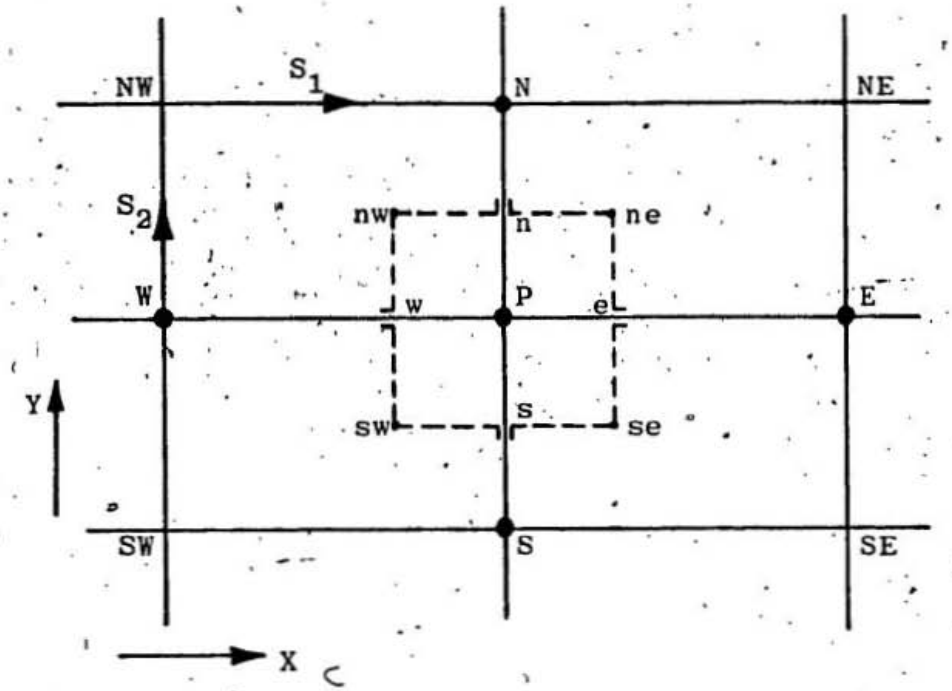

Fig. 2.2 The Domain of Integration

$$+ \int_{Y_s}^{Y_n} \int_{X_w}^{X_e} e_\phi \, dxdy = 0 \qquad (2.17)$$

|——Source Term, I_s——|

It should be noted that all terms but the last can be integrated once since a_ϕ is a constant. (refer to Table 2.1). Therefore, we can carry out the first integration to get

$$a_{\phi P} \Big[\underbrace{\int_{Y_s}^{Y_n} \{\phi_e (\tfrac{\partial \psi}{\partial y})_e - \phi_w (\tfrac{\partial \psi}{\partial y})_w\} dy - \int_{X_w}^{X_e} \{\phi_n (\tfrac{\partial \psi}{\partial x})_n - \phi_s (\tfrac{\partial \psi}{\partial x})_s\} dx}_{I_c} \Big]$$

$$- \underbrace{\int_{Y_s}^{Y_n} \{b_{\phi e} \tfrac{\partial}{\partial x} (c_\phi \phi)_e - b_{\phi w} \tfrac{\partial}{\partial x} (c_\phi \phi)_w\} dy - \int_{X_w}^{X_e} \{b_{\phi n} \tfrac{\partial}{\partial y} (C_\phi \phi)_n\}}_{I_d}$$

$$- b_{\phi s} \tfrac{\partial}{\partial y} (c_\phi \phi)_s \} d x +$$

$$\int_{Y_s}^{Y_n} \int_{X_\omega}^{X_e} e_\phi \, dxdy = 0 \qquad (2.18)$$

|—— I_s ——|

The terms have been grouped together as 'convection', 'diffusion' and 'source' for further manipulations, with different assumptions being introduced for each of these terms.

2.3.1 The Convection Term

In this term there are four integrals all of similar form, therefore it is necessary to look at only one of them to demonstrate the solution procedure. The convection term (I_c) can be expressed as

$$I_c = a_{\phi P} \int_{Y_s}^{Y_n} \phi_e \left(\frac{\partial \psi}{\partial y}\right)_e \, dy$$

For ϕ and ψ well behaved, there exists an average value of ϕ_e which can be written as

$$\bar{\phi}_e \equiv \frac{\int_{Y_s}^{Y_n} \phi_e \left(\frac{\partial \psi}{\partial y}\right)_e \, dy}{\int_{Y_s}^{Y_n} \left(\frac{\partial \psi}{\partial y}\right)_e \, dy} = \frac{I_c}{a_{\phi P}(\psi_{ne} - \psi_{se})}$$

with ne and se are as indicated in Fig. 2.2. Therefore,

$$I_c = a_{\phi P} \, \bar{\phi}_e \, (\psi_{ne} - \psi_{se}) .$$

It is now necessary to make the following assumptions:

1. ϕ is uniform within each rectangle and has the value at P.
2. $\bar{\phi}_e$ takes on the ϕ value possessed by the fluid upstream of the e-face of the rectangle. i.e. if flow is from P to E then $\bar{\phi}_e$ must be equal to ϕ_P.

With these assumptions I_c becomes:

$$I_c = a_{\phi P}\left[\phi_e\left\{\frac{(\phi_{ne} - \phi_{se}) - |\phi_{ne} - \phi_{se}|}{2}\right\} + \phi_P\left\{\frac{(\phi_{ne} - \phi_{se}) + |\phi_{ne} - \phi_{se}|}{2}\right\}\right]$$

If we also assume that the value of the stream function, ϕ, at the interior node is the average of the values of the four neighbouring nodes then

$$\phi_{se} = \frac{\phi_{SE} + \phi_E + \phi_P + \phi_S}{4}$$

and along with similar expressions for ϕ_{ne}, ϕ_{nw} and ϕ_{sw}, the total integral for the convection term can be expressed as

$$I_C = A_E(\phi_P - \phi_E) + A_W(\phi_P - \phi_W) + A_N(\phi_P - \phi_N) + A_S(\phi_P - \phi_S),$$

where $A_E = a_{\phi P}[(\phi_{se} - \phi_{ne}) + |\phi_{se} - \phi_{ne}|]/2$,

$$A_W = a_{\phi P}[(\phi_{nw} - \phi_{sw}) + |\phi_{nw} - \phi_{sw}|]/2,$$

$$A_N = a_{\phi P}[(\psi_{ne} - \psi_{nw}) + |\psi_{ne} - \psi_{nw}|]/2 ,$$

$$A_S = a_{\phi P}[(\psi_{sw} - \psi_{se}) + |\psi_{sw} - \psi_{se}|]/2 ,$$

2.3.2 The Diffusion Term

Again, because of similiarity of terms only one integral needs to be examined, which is

$$I_d = \int_{Y_s}^{Y_n} b_{\phi e} \frac{\partial}{\partial x} (c_\phi \phi)_e \, dy$$

Here we make a substitution of S_1 and S_2, which are the physical distances between the coordinates such that

$$dS_1 = dx \quad ; \quad dS_2 = dy$$

then

$$I_d = \int_{S_{2s}}^{S_{2n}} (b_{\phi e}) \frac{\partial}{\partial S_1} (c_\phi \phi)_e \, dS_2$$

If we assume $b_{\phi e} \approx (b_{\phi E} + b_{\phi P})/2$

and $\frac{\partial}{\partial S_1} (c_\phi \phi)_e \approx \frac{c_{\phi E}\phi_E - c_{\phi P}\phi_P}{S_{1E} - S_{1P}}$

then $I_d = \frac{b_{\phi E} + b_{\phi P}}{2} \cdot \frac{c_{\phi E}\phi_E - c_{\phi P}\phi_P}{S_{1E} - S_{1P}} \cdot \frac{S_{2N} - S_{2S}}{2}$

With similar expressions for the other terms, one obtains

$$I_d = B_E(c_{\phi E}\phi_E - c_{\phi P}\phi_P) + B_W(c_{\phi W}\phi_W - c_{\phi P}\phi_P)$$
$$+ B_N(c_{\phi N}\phi_N - c_{\phi P}\phi_P) + B_S(c_{\phi S}\phi_S - c_{\phi P}\phi_P)$$

where

$$B_E = \frac{b_{\phi E} + b_{\phi P}}{4} \cdot \frac{S_{2N} - S_{2S}}{S_{1E} - S_{1P}} ,$$

$$B_W = \frac{b_{\phi W} + b_{\phi P}}{4} \cdot \frac{S_{2N} - S_{2S}}{S_{1P} - S_{1W}} ,$$

$$B_N = \frac{b_{\phi N} + b_{\phi P}}{4} \cdot \frac{S_{1E} - S_{1W}}{S_{2N} - S_{2P}}$$

$$B_S = \frac{b_{\phi S} + b_{\phi P}}{4} \cdot \frac{S_{1E} - S_{1W}}{S_{2P} - S_{2S}} .$$

2.3.3 The Source Term

The final integral to evaluate is

$$I_s = \int_{Y_s}^{Y_n} \int_{X_w}^{X_e} e_\phi \, dx \, dy .$$

We again substitute S_1 and S_2 as before to obtain

$$I_s = \int_{S_{2s}}^{S_{2n}} \int_{S_{1w}}^{S_{1e}} e_\phi \, dS_1 \, dS_2$$

If we assume that e_ϕ is uniform over the area of integration and takes on the value at P then the integral can be

approximated by:

$$I_s \approx e_{\phi P} V_P$$

where

$$V_P = \left(\frac{S_{1E} - S_{1W}}{2}\right)\left(\frac{S_{2N} - S_{2S}}{2}\right)$$

An expression for $\left(\frac{\partial \phi}{\partial y}\right)_P$ for a non-uniform grid can be written as [28]

$$\left(\frac{\partial \phi}{\partial y}\right)_P = \frac{(\phi_N - \phi_P)\left(\frac{Y_P - Y_S}{Y_N - Y_P}\right) + (\phi_P - \phi_S)\left(\frac{Y_N - Y_P}{Y_P - Y_S}\right)}{Y_N - Y_S}$$

The Eqn. (2.16) in the finite-diference form can now be written as

$$A_E(\phi_P - \phi_E) + A_W(\phi_P - \phi_W) + A_N(\phi_P - \phi_N) + A_S(\phi_P - \phi_S) -$$

$$B_E(c_{\phi E}\,\phi_E - c_{\phi P}\,\phi_P) - B_W(c_{\phi W}\,\phi_W - c_{\phi P}\phi_P) -$$

$$B_N(c_{\phi N}\phi_N - c_{\phi P}\phi_P) - B_S(c_{\phi S}\phi_S - c_{\phi P}\,\phi_P) + e_{\phi P}\,V_P = 0 \qquad (2.19)$$

In this equation, the convection term has A as its coefficients; the diffusion term has B as its coefficients and the source term is represented by a single term $e_{\phi P}\,V_P$.

We can now recast this equation into the successive-substition form as shown below:

$$\phi_P = C_E\phi_E + C_W\phi_W + C_N\,\phi_N + C_S\phi_S + D \qquad (2.20)$$

where

$$C_E = (A_E + B_E\, c_{\phi E}) \;/\; \Sigma AB \;,$$

$$C_W = (A_W + B_W\, c_{\phi W}) \;/\; \Sigma AB \;,$$

$$C_N = (A_N + B_N\, c_{\phi N}) \;/\; \Sigma B \;,$$

$$C_S = (A_S + B_S c_{\phi S}) \;/\; \Sigma AB \;,$$

$$D = (-e_{\phi P}\, V_P) \;/\; \Sigma AB \;, \qquad (2.21)$$

$\Sigma AB = A_E + A_W\ A_N + A_S + c_{\phi P}(B_E + B_W + B_N + B_S)$, and $V_P = \frac{1}{4}(S_{1E} - S_{1W})(S_{2N} - S_{2S})$. The coefficients in the convection term are:

$$A_E = \frac{a_{\phi P}}{8}\{(\phi_{SE} + \phi_S - \phi_{NE} - \phi_N) + |\phi_{SE} + \phi_S - \phi_{NE} - \phi_N|\},$$

$$A_W = \frac{a_{\phi P}}{8}\{(\phi_{NW} + \phi_N - \phi_{SW} - \phi_S) + |\phi_{NW} + \phi_N - \phi_{SW} - \phi_S|\},$$

$$A_N = \frac{a_{\phi P}}{8}\{(\phi_{NE} + \phi_E - \phi_{NW} - \phi_W) + |\phi_{NE} + \phi_E - \phi_{NW} - \phi_W|\}, \qquad (2.23)$$

$$A_S = \frac{a_{\phi P}}{8}\{(\phi_{SW} + \phi_W - \phi_{SE} - \phi_E) + |\phi_{SW} + \phi_W - \phi_{SE} - \phi_E|\}.$$

The coefficients in the diffusion term are:

$$B_E = \frac{b_{\phi E} + b_{\phi P}}{4} \cdot \frac{S_{2N} - S_{2S}}{S_{1E} - S_{1P}} \;,$$

$$B_W = \frac{b_{\phi W} + b_{\phi P}}{4} \cdot \frac{S_{2W} - S_{2S}}{S_{1P} - S_{1W}},$$

$$B_N = \frac{b_{\phi N} + b_{\phi P}}{4} \cdot \frac{S_{1E} - S_{1W}}{S_{2W} - S_{2P}}, \qquad (2.23)$$

$$B_S = \frac{b_{\phi S} + B_{\phi P}}{4} \cdot \frac{S_{1E} - S_{1W}}{S_{2P} - S_{2S}}.$$

2.4 The Equations for the Boundary Nodes and the Boundary Conditions

We have now developed a general successive-substitution formula from the original partial differential equations. It is therefore necessary to specify the boundary conditions for the area under examination and develope the associated substitution formula at these boundaries. Fig. 2.1 shows details of the area analyzed. The dimensions specified correspond to the actual dimensions in the experiments carried out.

Boundary 1 corresponds to the free-stream conditions where the temperature corresponds to the bulk fluid temperature and the velocity is zero. Mathematically this can be written as

$$T = T_B = T_{air},$$

$$u = v = 0,$$

$$\omega = 0, \text{ and}$$

$$\psi = 0. \qquad (2.24)$$

Boundary 2, is the air-water interface. The boundary conditions at this surface are

$$T = T_B = T_{air},$$

$$u = v = 0, \text{ and}$$

$$\omega = \psi = 0 \qquad (2.25)$$

There is no heat transfer through this surface, water and air are at the same temperature, and there is no movement of the fluid through or at the surface, hence the velocities are zero.

Boundary 3 is the actual ice surface with the following boundary conditions:

$$T = T_{ice} = 0\,^{\circ}C \text{ and}$$

$$u = v = 0 \qquad (2.26)$$

The calculation of ω for the boundaries 3 and 4 involves use of a separate equation due to the wall. These calculations are explained in Step 4, page 38. The stream function, ψ, at the wall is constant.

Boundary 4 is considered as an insulated surface. Physically it is a plexiglass wall. The associated boundary conditions here are:

$$-k \frac{\partial T}{\partial y} = 0 \text{ and}$$

$$u = v = 0 , \qquad (2.27)$$

Boundary 5 is similar to boundary 1, i.e.

$$T = T_B ,$$

$$u = v = 0 \text{ and}$$

$$\phi = \omega = 0 \qquad (2.28)$$

2.5 The Computer Programme

With the governing equations in their successive-substitution form and the associated boundary conditions outlined, it is now possible to proceed to the computer programme to solve these equations for the problem of interest.

As this is an iterative technique, it is necessary to lay out the grid network for the domain of interest. It was decided to go with an uneven grid spacing which would allow for more nodes near the ice surface and less nodes out in the vicinity of the other boundaries. Fig. 2.3 shows the grid arrangement chosen. Tables 2.2a and 2.2b lists the grid line coordinates for the 21 x 21 node grid. In Fig. 2.3 CD represents the ice surface; DE the insulated surface below

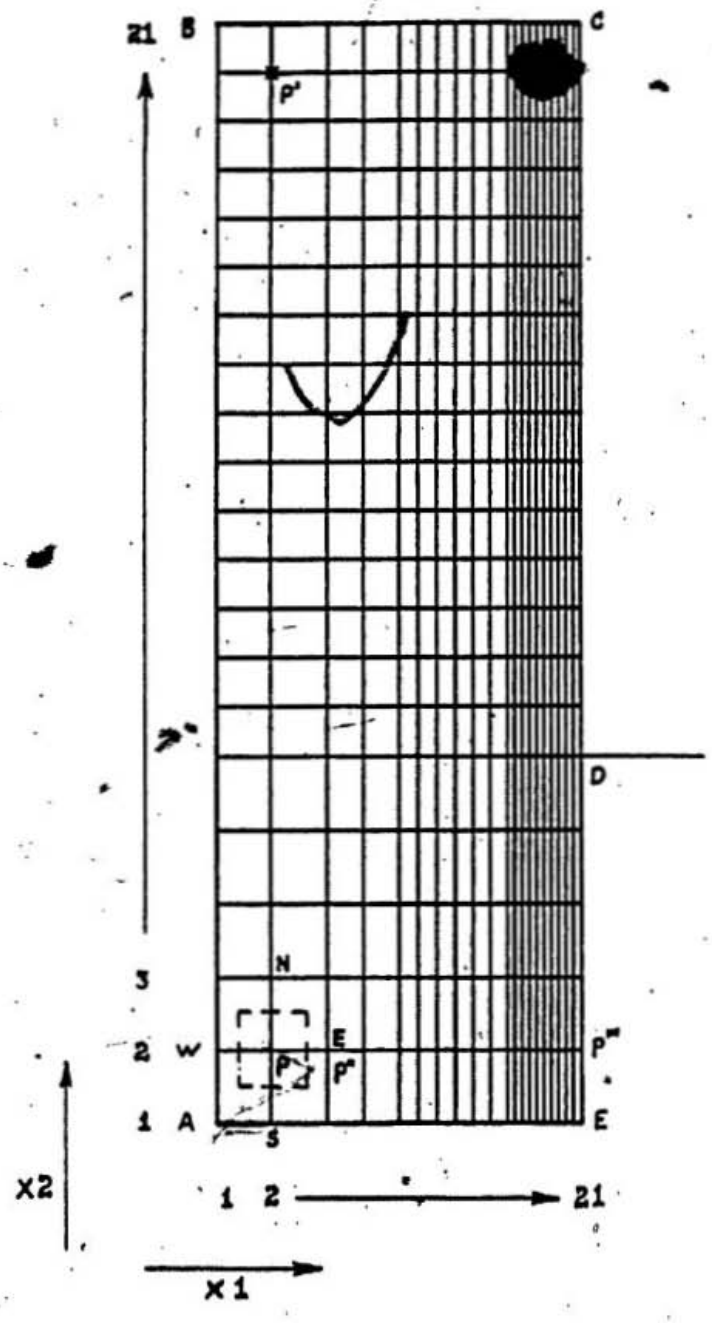

Fig. 2.3 The Grid Network

Table 2.2a: Grid Line Coordinates

Grid Line Number	X1 (m)
1	0.000
2	0.015
3	0.030
4	0.040
5	0.050
6	0.055
7	0.060
8	0.065
9	0.070
10	0.075
11	0.080
12	0.082
13	0.084
14	0.086
15	0.088
16	0.090
17	0.092
18	0.094
19	0.096
20	0.098
21	0.100

Table 2.2b: Grid Line Coordinates

Grid Line Number	X2 (m)
1	0.0000
2	0.0200
3	0.0400
4	0.0600
5	0.0800
6	0.1000
7	0.1138
8	0.1271
9	0.1404
10	0.1537
11	0.1670
12	0.1803
13	0.1936
14	0.2069
15	0.2202
16	0.2336
17	0.2468
18	0.2601
19	0.2734
20	0.2867
21	0.3000

the ice; AE and AB represent the free stream conditions and BC is the air-water interface.

The programme was set up such that when supplied with the differential equations to be solved, the associated boundary conditions, the thermodynamic relationships, and the grid network, it solves the associated set of algebraic equations. This consists of K times M substitutions where K is the number of differential equations (3 in this case) and M is the total number of grid nodes.

It is first, however, necessary to recast the previous successive-substitution equation, Eqn. (2.20) into a form more suitable for programming. Eqn. (2.20) can be rearranged as

$$\phi_P = \frac{\sum_{j=N,S,E,W} \{(A_j + c_{\phi j} B_j)\ \phi_j\} - e_{\phi P}\ V_P}{\sum_{j=N,S,E,W} A_j + c_{\phi P} B_j} \qquad (2.29)$$

where $\sum_{j=N,S,W,W}$ denotes summation over the nodes N, S, E and W and the other terms are as outlined previously.

We now divide both numerator and denominator by V_p to get

$$\phi_P = \frac{\sum_{j=N,S,E,W} \{(A'_j + c_{\phi j}(b_{\phi j} + b_{\phi P})B_j')\}\phi_j - e_{\phi P}}{\sum_{j=N,S,E,W} A'_j + c_{\phi P}\ (b_{\phi j} + b_{\phi P})B_j'} \qquad (2.30)$$

where

$$A_j' = \frac{A_j}{V_p}$$

$$B_j' = \frac{B_j}{V_p(b_{\phi j} + b_{\phi P})}$$

As an example if j refers to the node E then

$$A_E' = a_{\phi P} \frac{|\phi_N - \phi_S + \phi_{NE} - \phi_{SE}| - (\phi_N - \phi_S + \phi_{NE} - \phi_{SE})}{2(S_{1E} - S_{1W})(S_{2N} - S_{2S})}$$

and $$B_E' = \frac{2}{(S_{1E} - S_{1P})(S_{1E} - S_{1W})}$$

The flow diagram for the programme is shown in Fig. 2.4a and 2.4b. A technique of under-relaxation was used to speed up the convergence.

The calculations involved can be summed up in the following steps:

1. Assume initial values for ω, ϕ, T, u and v for all the nodes. In the present work, the density has been assumed to vary with the temperature. Therefore, for any given node, P, the density was calculated at the temperature corresponding to that node. (refer to Fig. 2.2). All other properties were assumed constant over the field of interest, whereas the density was assumed constant only within the area enclosed by the dotted lines. The

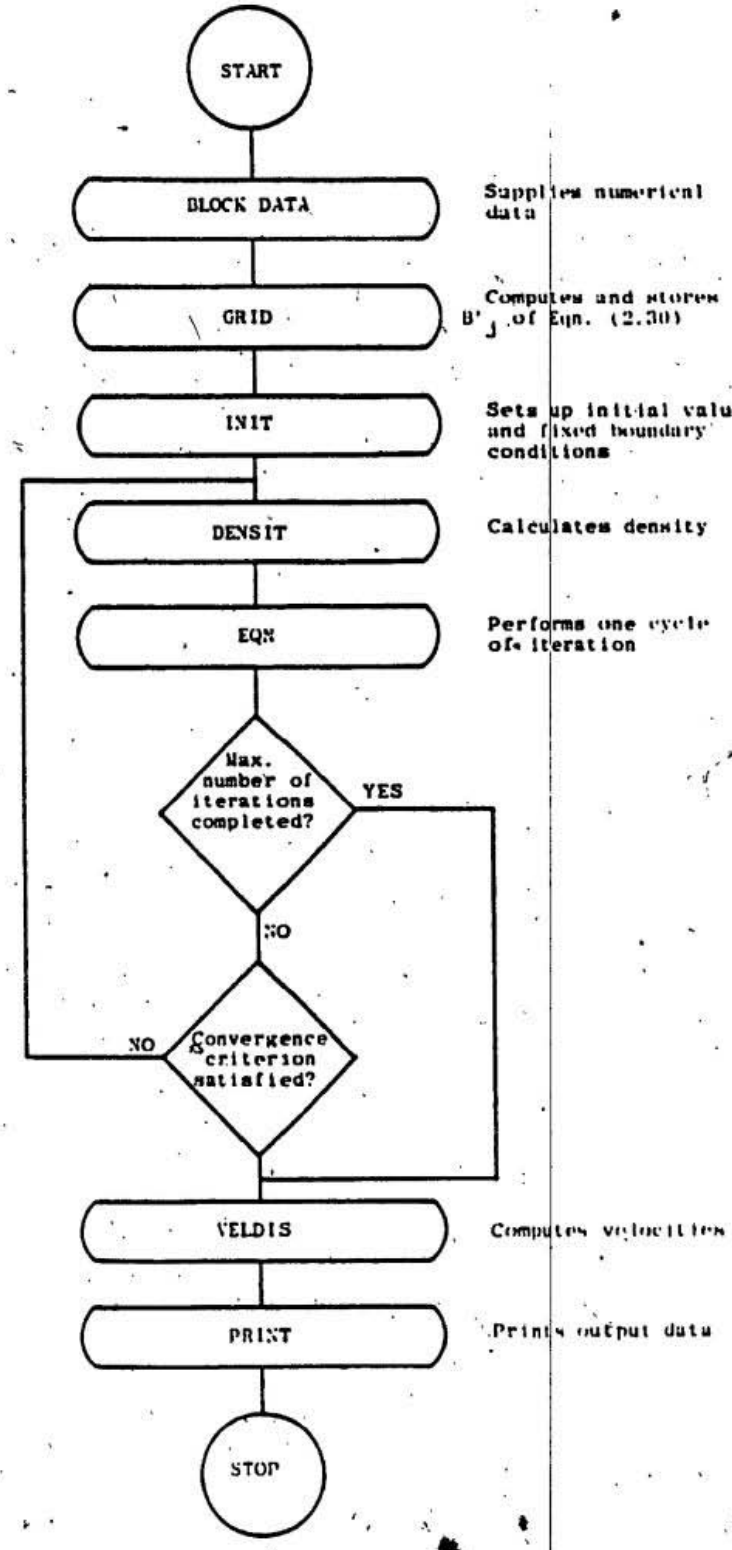

Fig. 2.4a The Main Flow Diagram

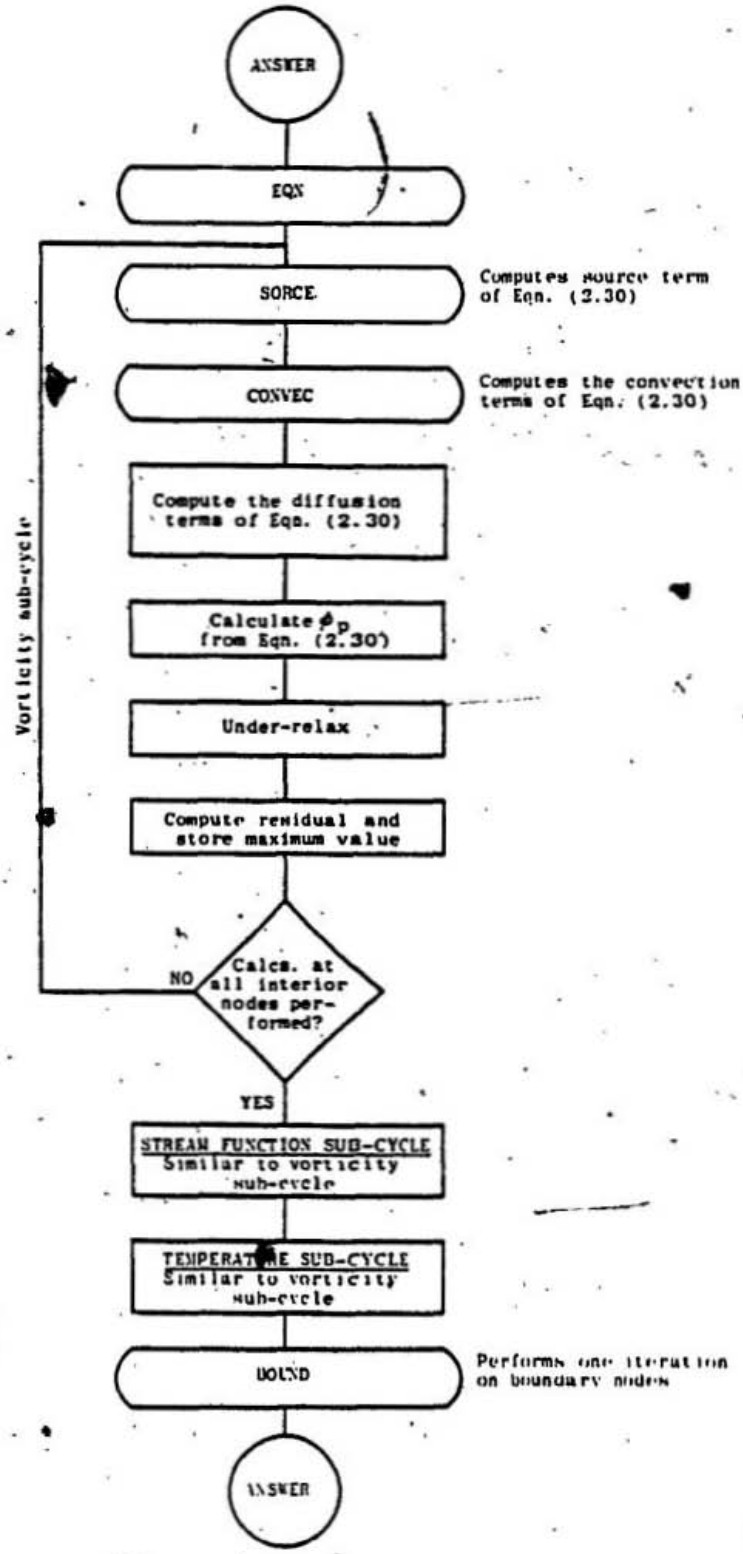

Fig. 2.4b The EQN Subcycle

calculations can now be started at node P in Fig. 2.3.

2. Using Table 2.1, obtain a_ϕ, b_ϕ, c_ϕ and e_ϕ for the vorticity term. To calculate e_ϕ, the finite difference form was used.
3. Calculate ϕ_P for ω using Eqn. (2.30) where all the parameters on the right-hand side are known at this stage.
4. Repeat steps 2 and 3 for all the nodes from P to P' and then to P'' and so on (refer to Fig. 2.3). It should be noted here that the nodes at the wall such as P''' require a different equation which is

$$\omega_P = -\left[\frac{3(\phi_{NP} - \phi_P)}{\rho\, n_{NP}^2} + \frac{\omega_{NP}}{2}\right]$$

where n_{NP} is the distance between nodes NP and P. Node P is the boundary node and node NP is the adjacent interior node (refer to Fig. 2.3).

5. The stream function, ϕ, and the temperature, T, are then calculated using steps similiar to those used for ω. The applicable boundary conditions are applied and the density values are updated for the new temperatures.
6. Repeat steps 2 to 5 using the under-relaxation technique until convergence is achieved.

A flow chart outlining these steps is shown in Figs. 2.4a and 2.4b.

2.6 Conclusions

In this chapter, the partial differential equations which describe the temperature and the velocity variations around the vertical ice wall were obtained. These equations were then transformed into the finite-difference form. Finally, an algorithm to obtain the solution of these equations was described.

CHAPTER 3

THE EXPERIMENTAL INVESTIGATIONS

3.1 Introduction

In the previous chapter, the analytical formulation of the heat transfer process around a vertical ice wall was carried out. For the given boundary conditions, the variation of the temperature and velocity fields could be obtained using the digital computer.

In this chapter, the experimental verification of the theoretical model under certain conditions will be discussed. To carry out the experiments one has to consider various measurement techniques, selection criteria of the instruments used, and the details of hardware needed to accurately obtain the results. In the various sections of this chapter these points have been discussed.

3.2 The Selection Criteria of the Instruments

Before starting the experimental work various techniques for fine measurement of temperature and velocity were examined. The major criteria for any measuring devices were: (a) high sensitivity; (b) the size i.e. the instruments used must not disturb the flow and (c) the linearity over a specified range. Considering these

criteria, it was decided to use a thermistor probe for the temperature measurements. Similarly, the velocity measurements were obtained using a thymol blue indicator solution with a platinum wire probe using a photographic technique.

3.3 The Experimental Equipment

3.3.1 The Tank

The experiments were carried out in a specially designed .0127 m (1/2 in.) thick plexiglass tank measuring 0.61 m long, 0.61 m wide and 0.92 m high, with an extension out on one side with dimensions 0.30m long, 0.127 m wide and 0.76 m high. A schematic of the tank and extension is shown in Figs. 3.1a and 3.1b. The experiments were carried out in this extension for the ease of the photography, with the large part of the tank being required to maintain the bulk fluid temperature. This extension was fitted with various plexiglass 'spacers' and a copper plate assembly to vary the experimental set-up.

An angle iron frame was built to support the tank and extension, and it was fitted with a special support for the camera for the close-up photographs. The tank was fitted with a plywood lid on which the various measuring instruments and probes could be placed for easy access.

The large part of the tank was insulated with 0.0127 m (1/2 in.) thick styrofoam sheets, held in place by a

1 COPPER PLATE ASSEMBLY
2 PLEXIGLASS SUPPORT
3 CONSTANT TEMPERATURE BATH FOR BULK FLUID TEMPERATURE
4 CONSTANT TEMPERATURE BATH FOR THE COPPER PLATE

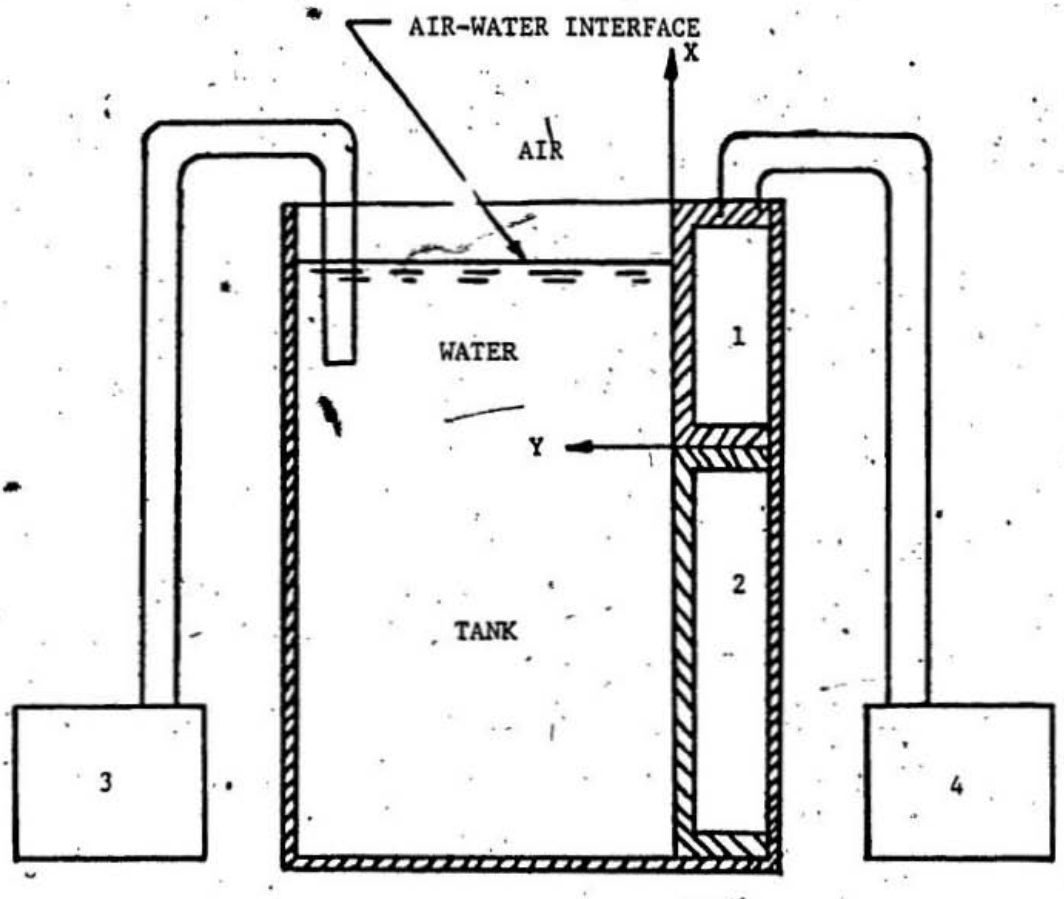

Fig. 3.1 a The Schematic of the Experimental Set-Up (Side View)

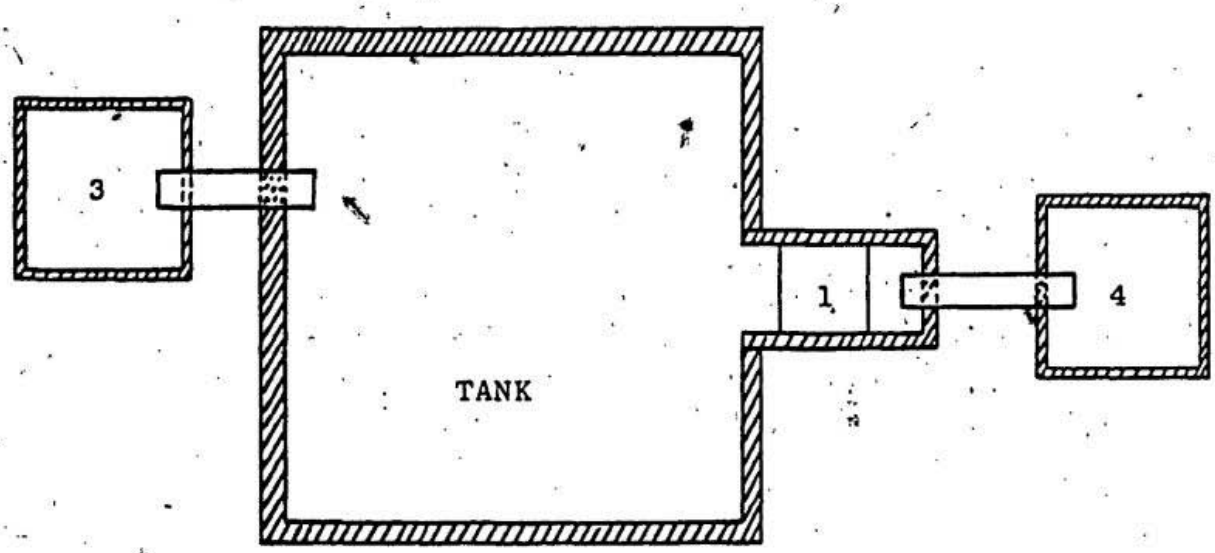

1 COPPER PLATE ASSEMBLY

3 CONSTANT TEMPERATURE BATH FOR BULK FLUID TEMPERATURE

4 CONSTANT TEMPERATURE BATH FOR THE COPPER PLATE

Fig. 3.1 b The Schematic of the Experimental Set-Up (Top View)

0.0127 m (1/2 in) plywood frame.

A coil of 0.0127 m (1/2 in.) copper tubing was placed in the tank and connected via clear tubing to a constant temperature bath for control of the water temperature. A circulating pump was also connected to the tank by 0.0508 m (2 in.) PVC pipe. This was used for mixing up the water in the tank. Figure 3.2 shows the actual equipmental set-up.

3.3.2 The Copper Plate Assembly

To eliminate the problem of forming uniform ice sheets for each experiment, it was decided to use a copper plate assembly instead of an actual ice surface. This assembly consisted of a 0.0254 m (1 in.) thick plexiglass frame (0.10 m wide x 0.127 m on top and 0.254 m long) with a channel cut along its front, top and bottom. The copper plate was screwed to the plexiglass frame, with a gasket for sealing, to cover this channel. This channel allows for circulation of the constant temperature fluid (anti-freeze) from a constant temperature bath (Lauda Kryomat) via appropriate fittings and clear tubing (refer to Fig. 3.3).

To go along with the copper plate assembly there were two plexiglass spacers, 0.127 m deep. The spacers and copper plate assembly had notches cut in both sides of the

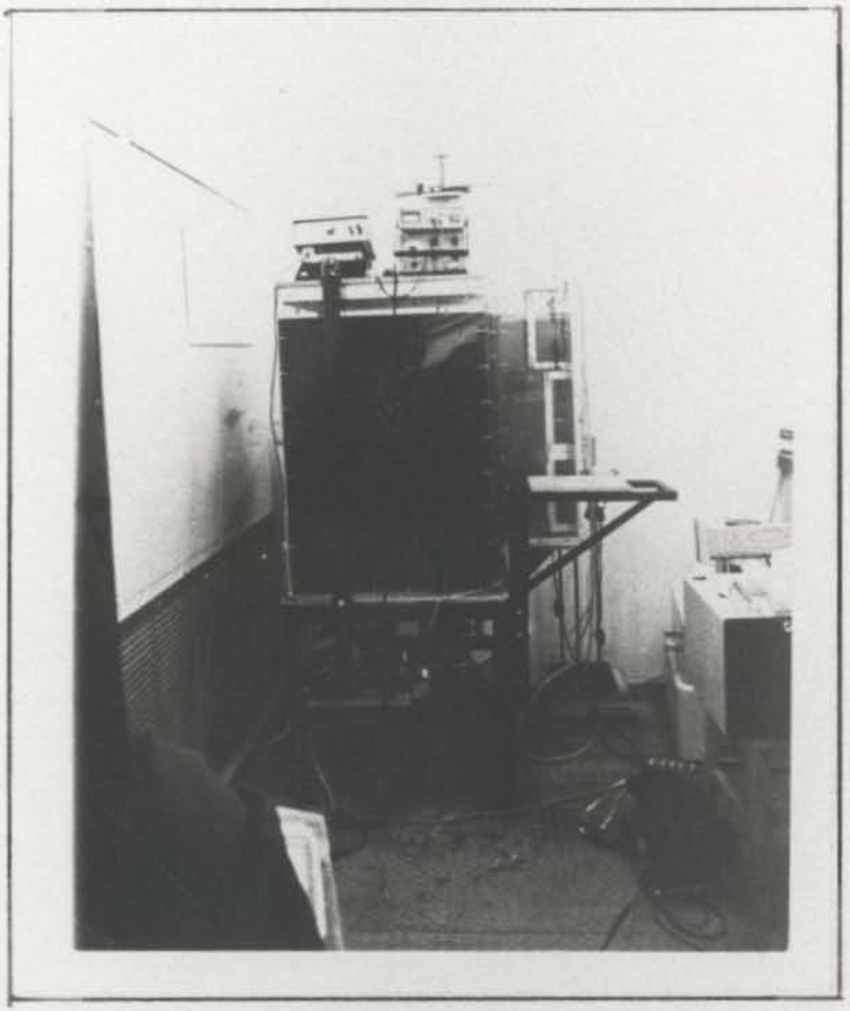

Fig. 3.2 A Pictorial View of the Experimental Set-Up

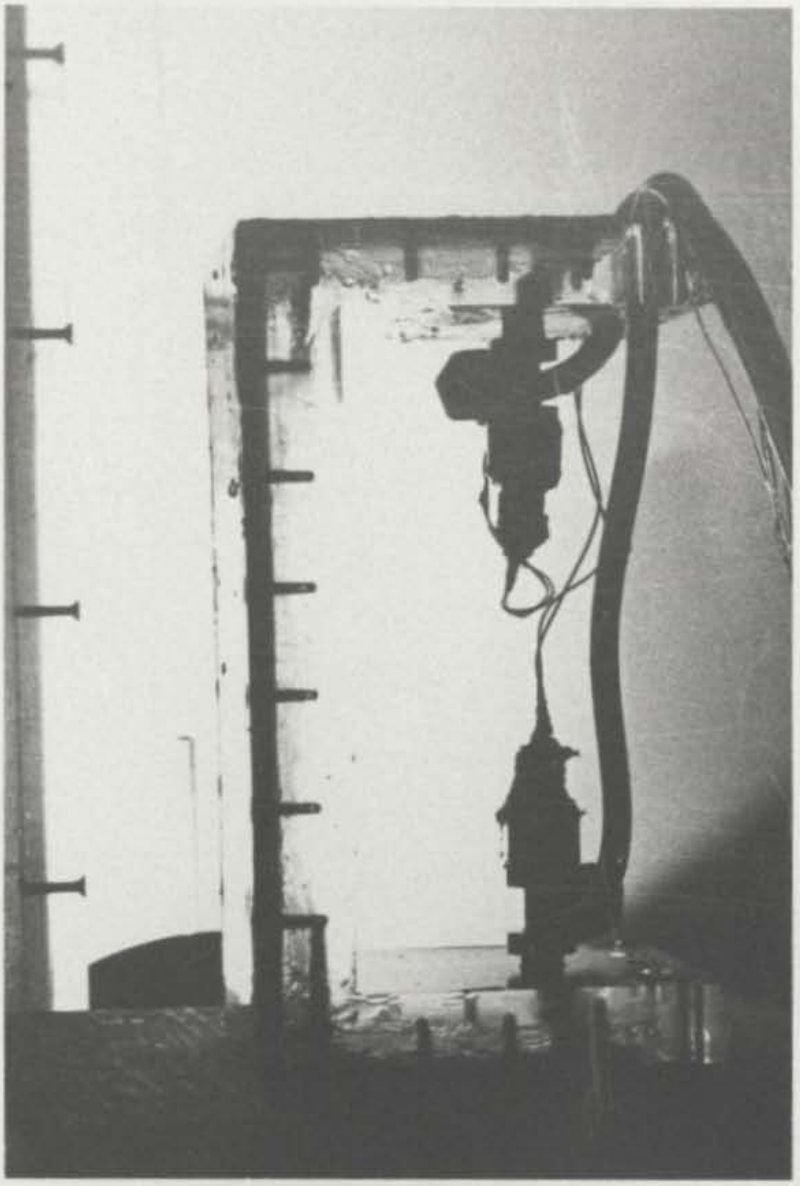

Fig. 3.3 The Copper Plate Assembly

back of their frames which fit over guides in the tank extension. This secured their position during the experiments.

3.3.3 The Temperature Probe

For the temperature measurements several options were examined such as thermocouples, thermistors, RTD's, etc. Of the choices available, it was decided to go with the thermistor for the following reasons:

1. It has a linear temperature-voltage characteristics over the temperature range of interest.
2. It is available in very small sizes 1.27×10^{-4} m (0.005 in.).
3. It is easily calibrated - no ice bath required.
4. It has a stable output.
5. It has been used in similar applications with success.

The thermistor selected was a Thermometrics Model BR14PA103N-L, bead diameter 3.6×10^{-4} m (0.014 in.) with platinum alloy leads 2.54×10^{-5} m (0.001 in.) in diameter. It was necessary to make an appropriate probe to hold this thermistor. This consisted of a 0.0127 m (1/2 in.) stainless steel tube, 0.610 m long, set into a two-piece plexiglass block for adjustment of the probe. Two 22-gauge hypodermic needles were mounted in the end of this block. The thermistor was mounted across the tips of these needles, by

soldering. Copper wire leads were connected to the back of the needles and carried up through the stainless steel tube to the measuring instruments. An adjustment screw on the plexiglass block assured tightness of the thermistor across the needles. The needles being 0.0381 m (1-1/2 in.) long allowed the bulk of the probe to be outside the boundary layer and therefore not affect the flow.

The thermistor was calibrated using a calibrated thermometer. The calibration curve is shown in Fig. 3.4.

3.3.4 The Velocity Probe

For the velocity measurements there were two possibilities examined: (1) a hot-wire anemometer probe, or (2) the thymol blue indicator solution with a platinum wire probe. The hot-wire anemometer was considered because it had previously been used successfully for low velocity measurements and some of the equipment was already available at the university. After some experimentation with the equipment on hand, it was decided to go with the other method due to the costs involved in purchasing other necessary pieces of equipment.

The technique for the use of the thymol blue indicator solution with platinum wire probe, has been developed by Baker [23] and had been used in a similiar

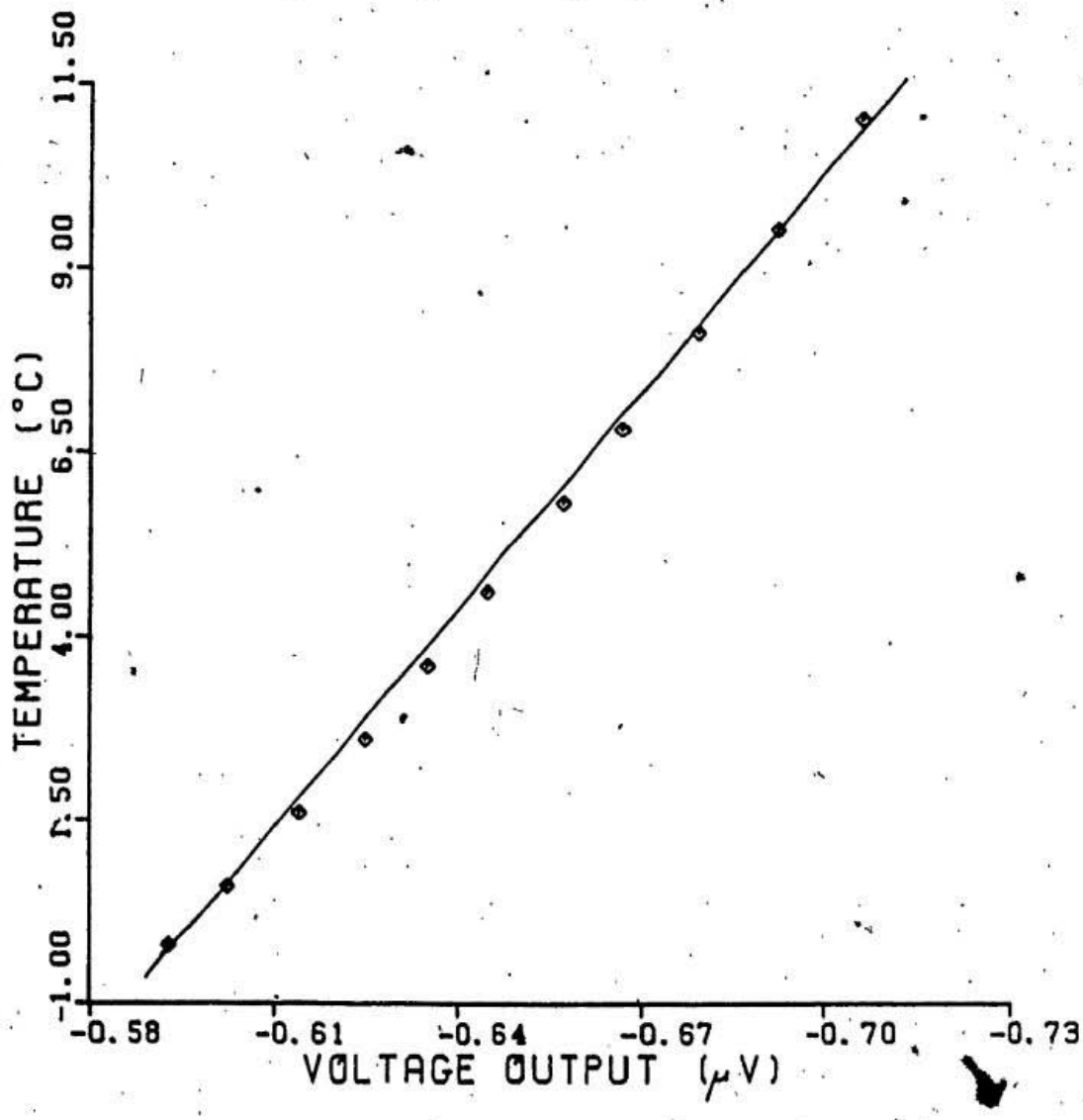

Fig. 3.4 The Thermistor Calibration Curve

application by Wilson & Vyas [22].

The thymol blue solution is 0.01% by weight of thymol blue powder to distilled water. Approximately 30 grams of powder were used for the volume of water in the tank. The solution was prepared as follows: the thymol blue powder was added to the water turning it a deep red; it was then titrated to its endpoint (pH 8) by adding 1N-NaOH* until it turns the solution deep blue; it was then brought past its end point by adding 1N-HCl*, turning the solution orange. The circulating pump on the tank was used to mix the solution. The solution in the tank was now ready such that the pulsing of a voltage across the platinum probe would turn the solution blue at the probe due to a proton transfer near the wire.

The platinum probe itself was made at the glass-shop at the university and consisted of a 0.008 m diameter glass tube 0.610 m long with a 0.076 m end piece bent at right angle to the main tube. The 1.2×10^{-4}m (.005 in.) diameter platinum wire was soldered to a length of

---

* 1N Solution = $\frac{\text{No. of GEW solute}}{\text{No. of litres of solution}}$

1GEW (Gram Equivalent Weight) HCl = 36.5g HCl

1GEW NaOH = 40g NaOH

copper wire and run through the glass tube. Approximately 0.050 m of the platinum wire was left extending out the end of the short piece of tube and this end was heat-sealed closed to securely hold the wire. The top of the glass tube was left open and the copper wire extended out of it to be connected to a voltage source.

3.3.5 The Positioning Device

To position the probes for an experiment a specially designed positioner was assembled. For the vertical movement an assembly from the Unislide company, model A4015-K2M with a travel of 0.276 m, was used with one end modified so as to be fitted with three levelling legs for positioning in brass holes in the tank lid. The travelling part of the positioner was also modified to hold the actual probe by means of a plate at right angle to the slide. Horizontal movement of the probe was provided by a Delron-Precision Slide (500 series) spring loaded x-y positioner, that the company itself modified to hold the micrometer. The micrometer used was a Mitutoya micrometer head - Model 297.101, with a travel of 0.05 m in graduations of 5×10^{-6} m. It is also equipped with a zeroing scale that allows readings to 1×10^{-5} m with a digital read-out. The actual clamp for the probes was attached to one end of the

x-y positioner with the micrometer head being its means of travel.

When assembled this device allowed for accurate positioning of the probe along the length of the ice surface. After the probe was positioned at the ice surface, it could be moved horizontally out through the boundary layer for temperature measurement purposes. Fig. 3.5 shows the positioning device used.

3.3.6 The Measuring Instruments

3.3.6.1 Temperature Measurement

As temperature measurements were taken using from the thermistor probe and thermocouples (bulk fluid temperature), it was necessary to have a measuring device to handle both. The electronics shop in Technical Services at Memorial University built a Wheatstone Bridge amplifier (to amplify the micro-volt output of the probes) that could be connected to a digital voltmeter (DVM). Fig. 3.6 shows the wiring diagrams. The DVM used was a Fluke model 8610A Digital Multimeter set in a range of 0-2V. The amplifier device allowed for reading of up to 8 thermocouples (Probe-Amp switch in the AMP position and the 2-9V batteries on) or the thermistor probe (Probe-Amp switch in PROBE position and the 1.5 V battery on). All wire connections

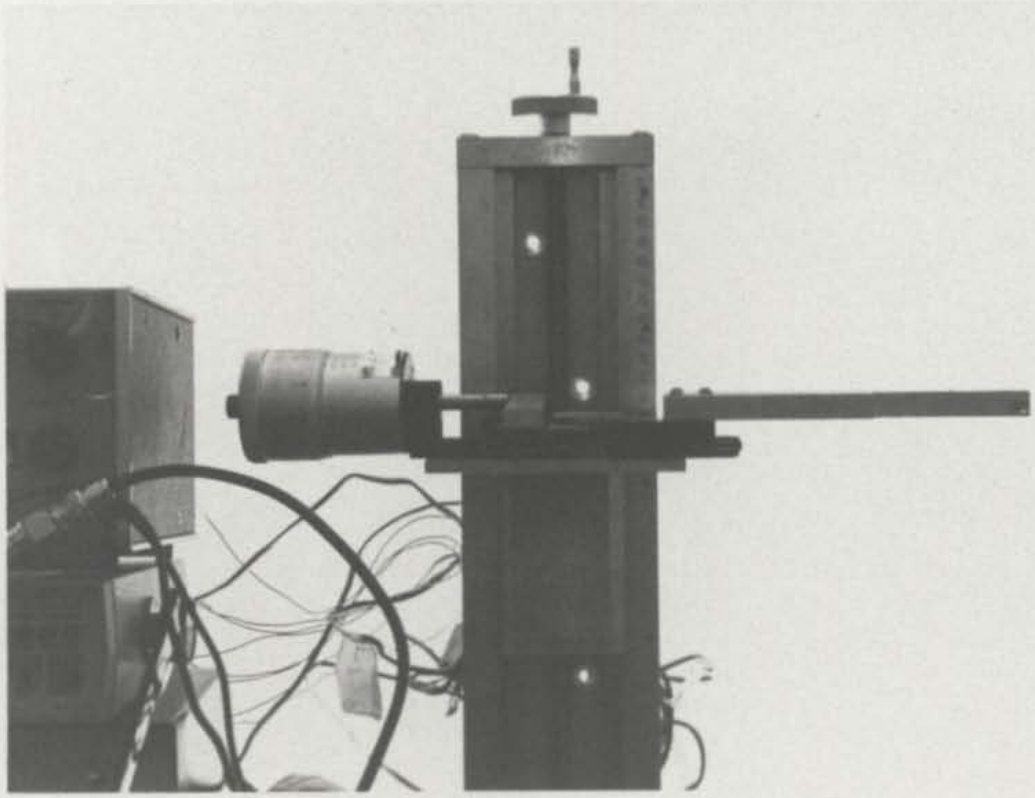

Fig. 3.5 A Pictorial View of the Positioning Device

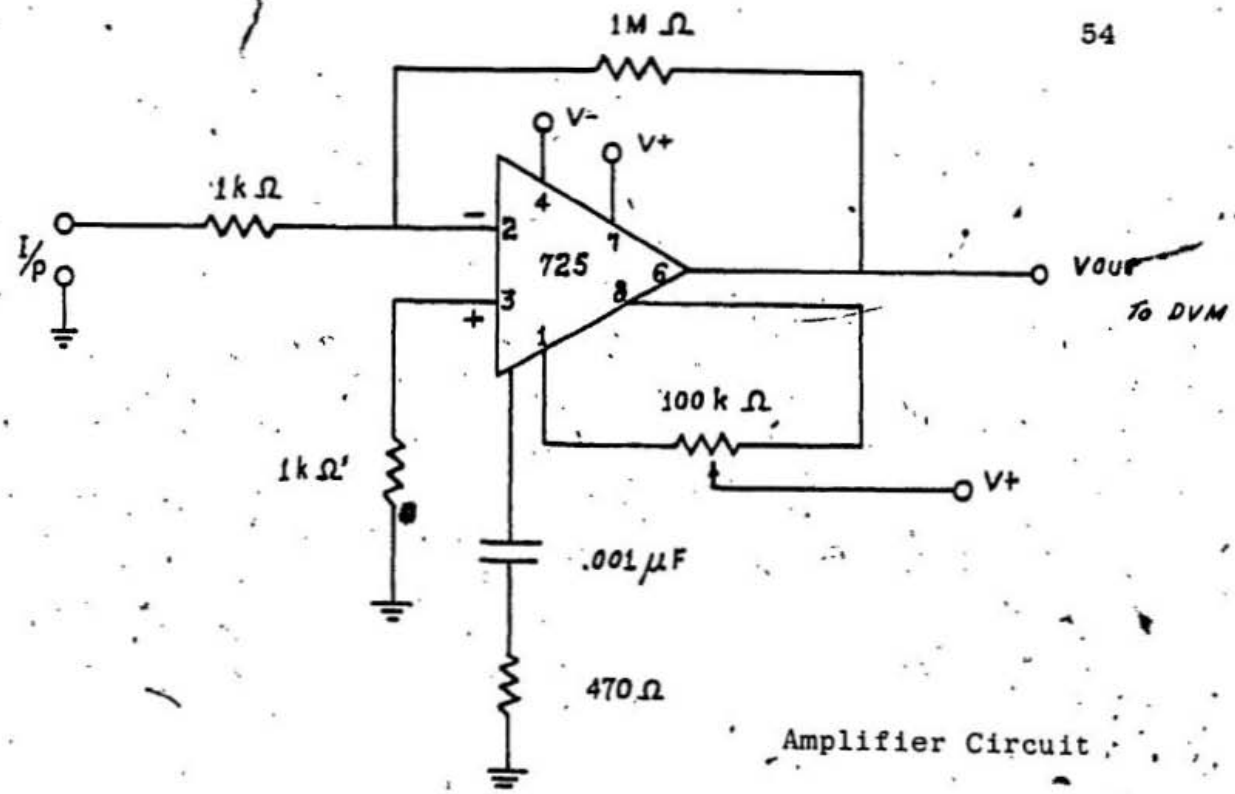

Amplifier Circuit

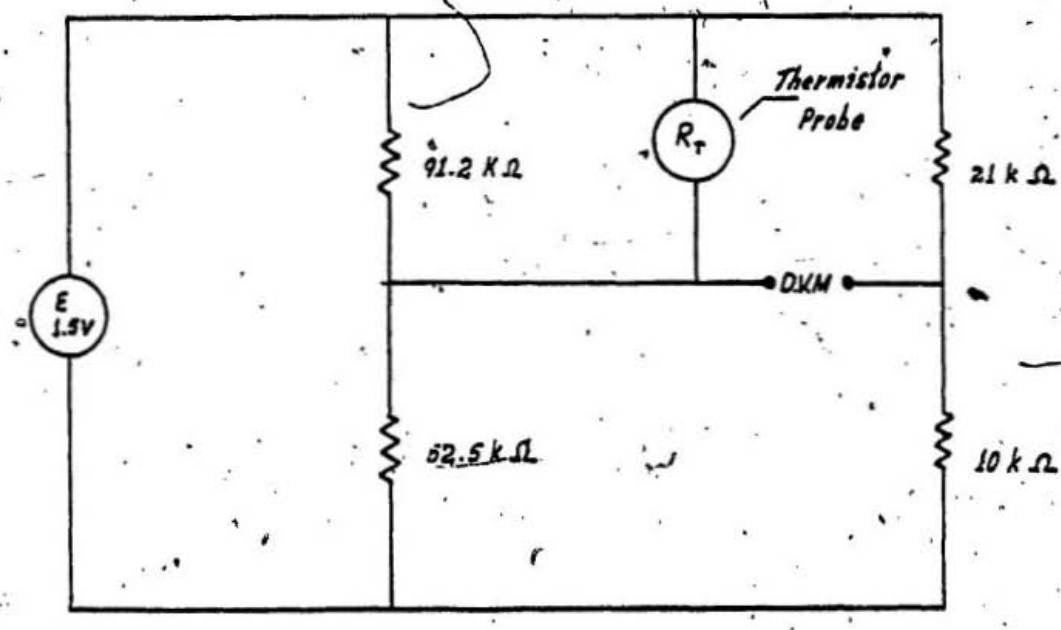

Wheatstone-Bridge Circuit

Fig. 3.6 Probe-Amp Wiring Diagrams

were made through the back of the device to minimize the tangle on the tank lid where the equipment was situated (refer to Figs. 3.7a and 3.7b).

3.3.6.2 Velocity Measurement

A HP 3310A Function Generator was used in conjunction with the platinum wireprobe. This particular instrument gave the appropriate pulses (square waves) when set to 0.01 Hz. The voltage could also be varied (usually to a maximum of 5V so as not to produce too many hydrogen bubbles at the probe itself which would affect the flow). The voltage variation increases the intensity of the blue dye produced. Actual settings of the function generator were determined by observation, depending on the type of flow.

Connections from the generator to the probe were as follows: one side from a BNC to two alligator clips to be connected; one to the copper wire at the probe and the other one in the water to complete the circuit. The other side of the BNC went to a digital multicounter (Fluke Model 1900A). This device was used to determine the exact frequencies and period of the pulses generated. Fig. 3.7a shows the connections between the various devices and Fig. 3.7b shows the measurement devices.

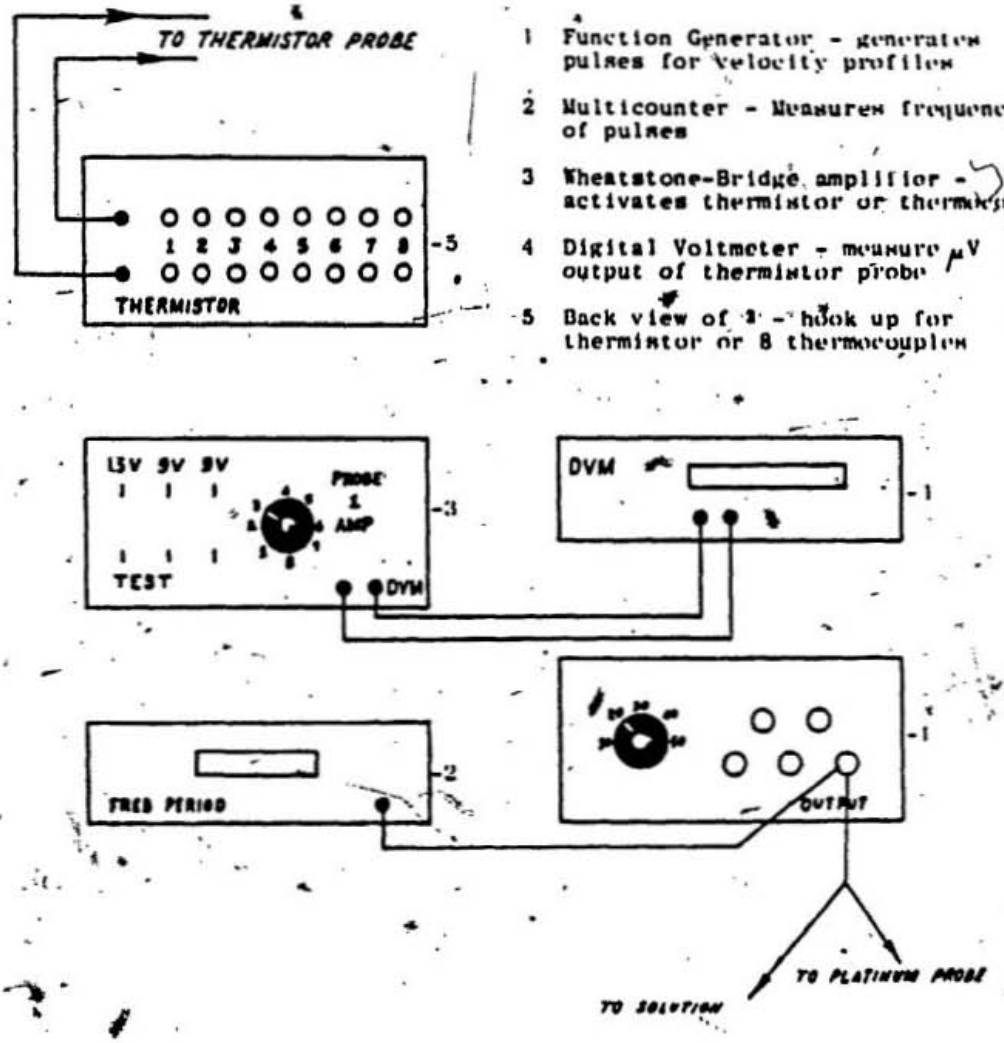

Fig. 3.7 a The Schematic of the Measurement Devices

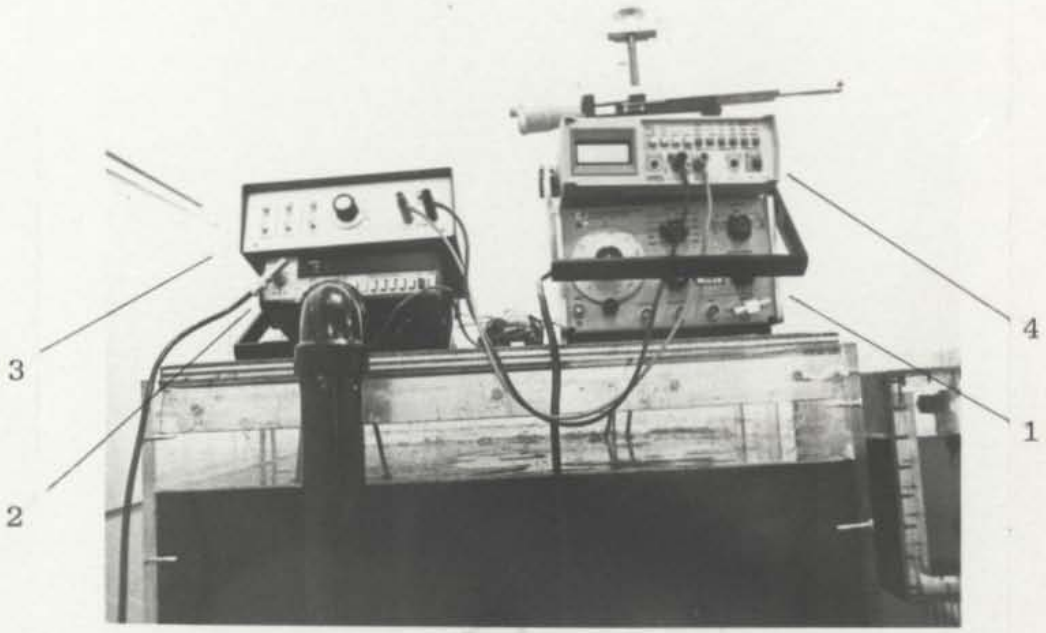

1 FUNCTION GENERATOR

2 MULTICOUNTER

3 WHEATSTONE-BRIDGE AMPLIFIER

4 DIGITAL VOLTMETER

Fig. 3.7 b A Pictorial View of the Measurement Devices

3.3.6.3 The Photographic Equipment

The camera equipment used to record the velocity profiles consisted of the following items:

1. The Hasselblad camera (Model 500C) with 12 exposure back.
2. The 80 mm-lens.
3. The extension tube.
4. The 0.5 mm-proxar lens.
5. The cable release.
6. The two quartz lamps for illumination (positioned behind the tank extension).

The camera was fitted onto a special stand which allowed movement in three directions (support frame of a NIKON Autocollimator Model 6D) which was supported on a part of the tank frame.

The camera setting was f 2.8 for 1/60 second using TRI-X 120 black and white film. The film was developed in the usual method except that HC-110 (dilution B) high contrast developer was used. Color slides using a 35 mm NIKOMAT camera were also taken for presentation purposes.

3.4 The Experimental Procedure

All these experiments were carried out in Cold Room #1 at Memorial University of Newfoundland (S. J. Carew

Building). The room controls and two constant temperature baths were used to adjust and maintain the bulk temperature of the water and the copper plate temperature. The circulating pump on the tank also aided in adjusting the water temperature from one experiment to the next, by mixing up the water.

At least 12 to 14 hours prior to starting an experiment, it was necessary to set the room temperature and connect the larger (Lauda Kryomat TK-30D) constant temperature bath to the copper coil in the tank, set to the same temperature as the room. On the morning of any given experiment, the circulating pump was turned on briefly (at least two hours before starting) to ensure even mixing of the water in the tank. The temperature measurements were taken at various positions in the tank, to check the uniformity, and the bulk fluid temperature was recorded. The Kryomat was then connected to the copper plate assembly, and the Lauda Model BE, RC-3, constant temperature bath, was connected to the copper coil in the tank. This was done because of the greater circulating capacity of the Kryomat making it more useful in setting the temperature of the copper plate assembly. This was carried out at least an hour prior to the experiment. The copper plate assembly and appropriate plexiglass spacers were positioned on the guides in the tank

and everything was left for about 1 hour to allow the water to settle.

Once the water temperature and ice surface were in equilibrium then an experiment could start. The thermistor probe was positioned in the tank at the ice surface. Its vertical position was recorded and the micrometer reading was zeroed. The probe was then moved out from the ice surface in increments of 0.1×10^{-3} m and the corresponding voltages were recorded. Readings were taken out to a distance of 2.0×10^{-2} m from the ice surface. This was repeated at two other recorded vertical positions along the ice surface. When all temperature readings were taken, the platinum wire probe was moved into position. The voltage output frequency was adjusted until a well defined pulse was formed. Photographs were taken with a scaled object in each and the frequency and period of the pulse were recorded. Photographs were taken midway along the ice surface.

Any time a probe was positioned in or out of the boundary layer, the water was allowed to settle before recording any measurements so that the flow would be undisturbed.

Experiments were carried out at various temperatures in the range of 0.95°C to 8.4°C.

3.5 Conclusions

In this chapter, the details of the experimental set-up and the procedures were discussed. In these discussions, the sensitivity, the linearity and the size, which are the selection criteria for the measurement devices, were taken into account.

CHAPTER 4

THE EXPERIMENTAL AND THEORETICAL RESULTS

4.1 Introduction

The problem of heat transfer around a vertical ice wall in fresh water was defined in the first chapter. Previous work in this area, both theoretical and experimental was discussed in some detail in this chapter so that it was clear that there was a need for further work on this topic. In Chapter 2, it was discussed that the modelling of the physical problem could be approached by using a finite-difference technique. In this chapter the mathematical transformation of the governing partial differential equations to a general finite-difference form was also discussed. The experimental technique and the various pieces of equipment used for the temperature and velocity profiles were described in Chapter 3.

In this chapter, the theoretical and experimental results will be presented and discussed. The verification of the theoretical model will be done by comparing these with the experimental results. These theoretical or experimental results include the temperature and the velocity profile, the local as well as the average heat transfer coefficients and the Nusselt number.

4.2 The Verification of the Theoretical Model

In Chapter 2, the continuity equation, the Navier-Stokes equation for two-dimensions and the energy balance equation defining the physical problem were represented by Eqns. (2.1) to (2.4). These equations were then transformed using the finite-difference technique to a general form represneted by Eqn. (2.30). This equation requires the use of the Table 2.1.

The programme developed for the solution of the equation was called CU.FOR and is included in the Appendix A. The grid spacing in the field of interest is shown in the Fig. 2.3 and Tables 2.2a and 2.2b.

4.2.1 The Temperature Profiles

Figs. 4.1 to 4.3 show the variation of the temperature in the zone of interest at bulk fluid temperatures of 0,95°C, 5.6°C and 7.7°C respectively.

Referring to Fig. 2.1 and Figs. 4.1 - 4.3 it can be seen that there is a good agreement between the experimental and theoretical values. The major discrepancy arises at 5.6°C which is mainly due to the nature of the flow at this temperature, i.e. a bi-directional flow was observed. From both the experimental and theoretical results, the local heat transfer coefficients (h_x), were calculated using [29]:

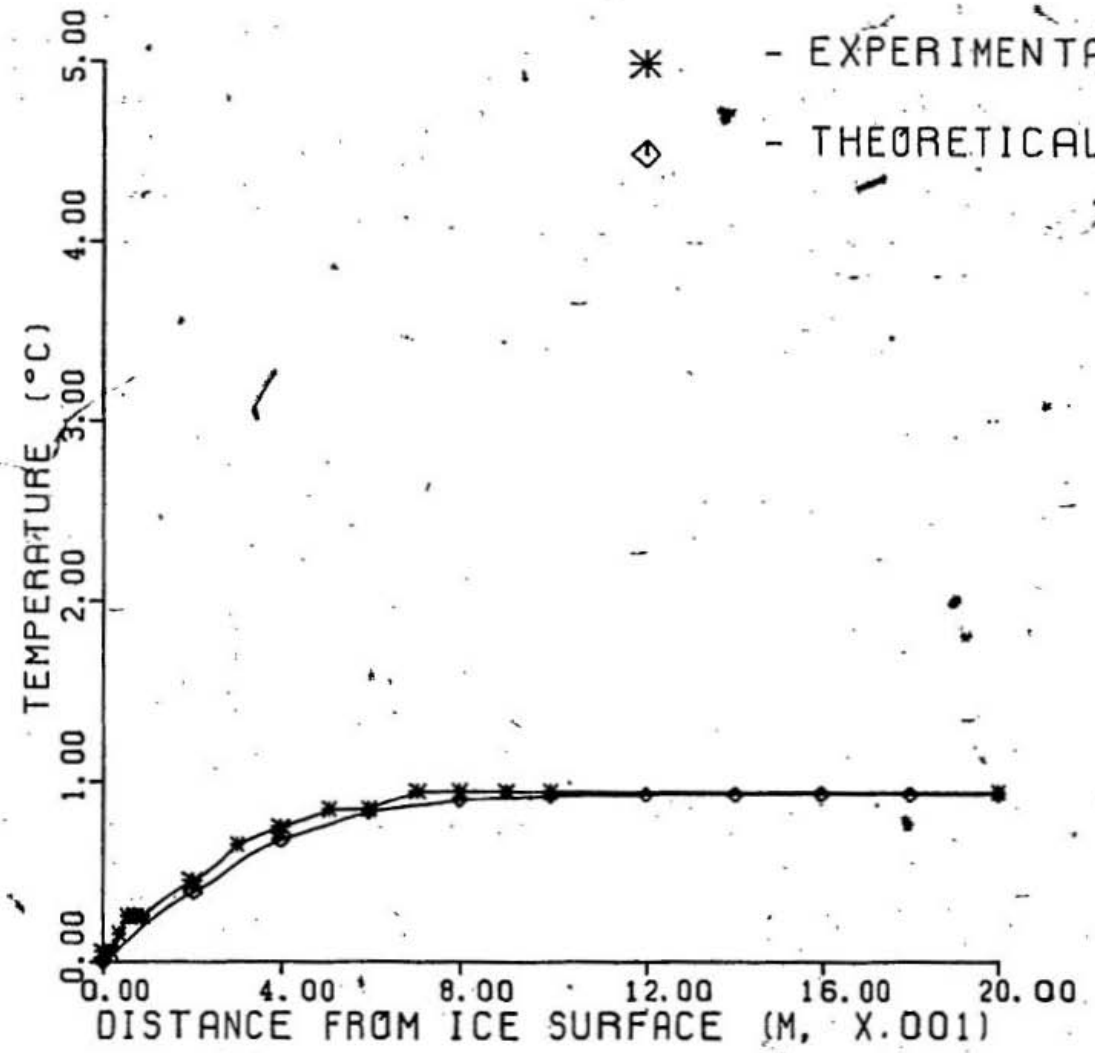

Fig. 4.1 The Temperature Profiles at 0.95°C (X=0.067Om)

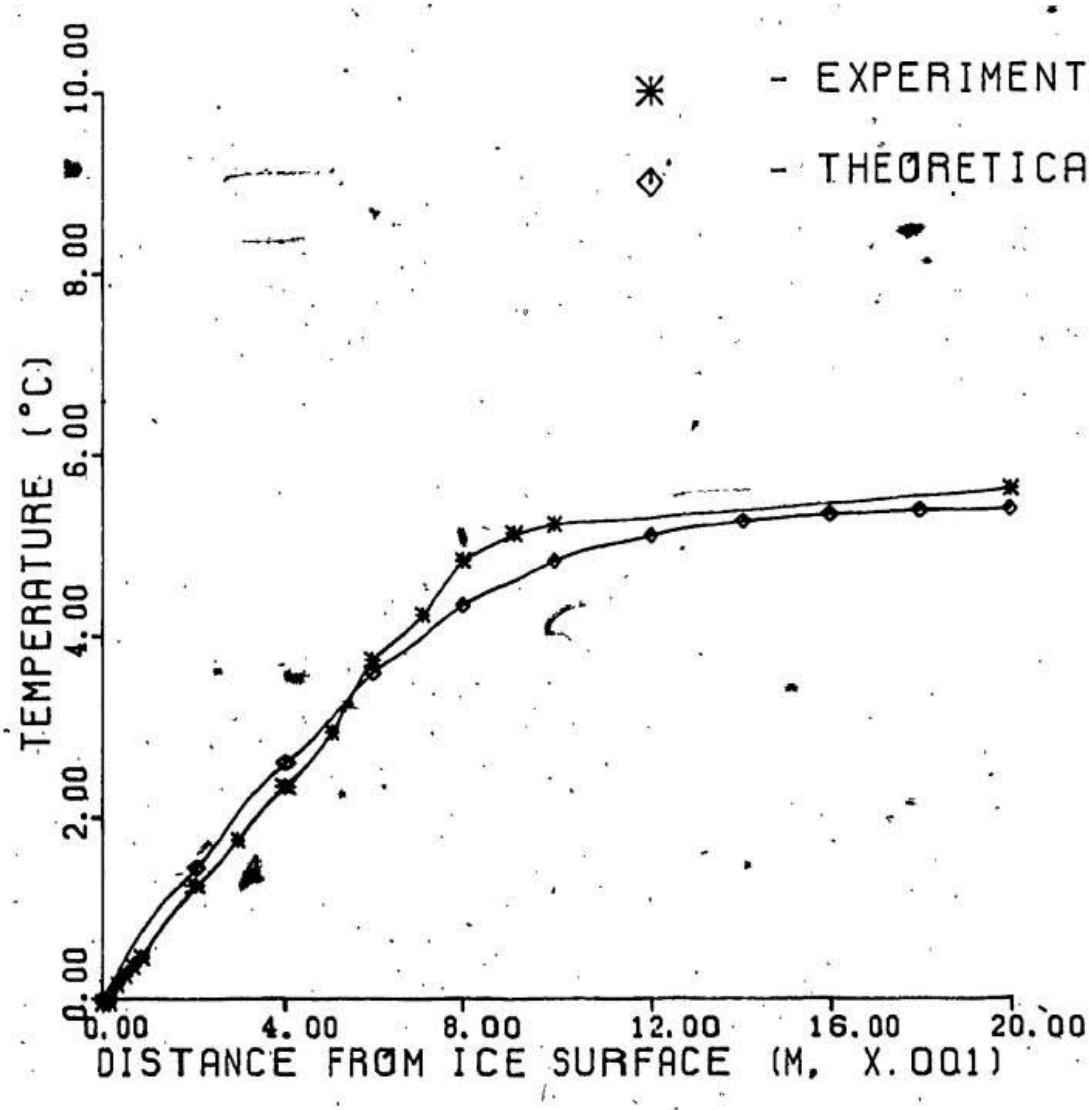

Fig. 4.2 The Temperature Profiles at 5.6°C (X=0.0670m)

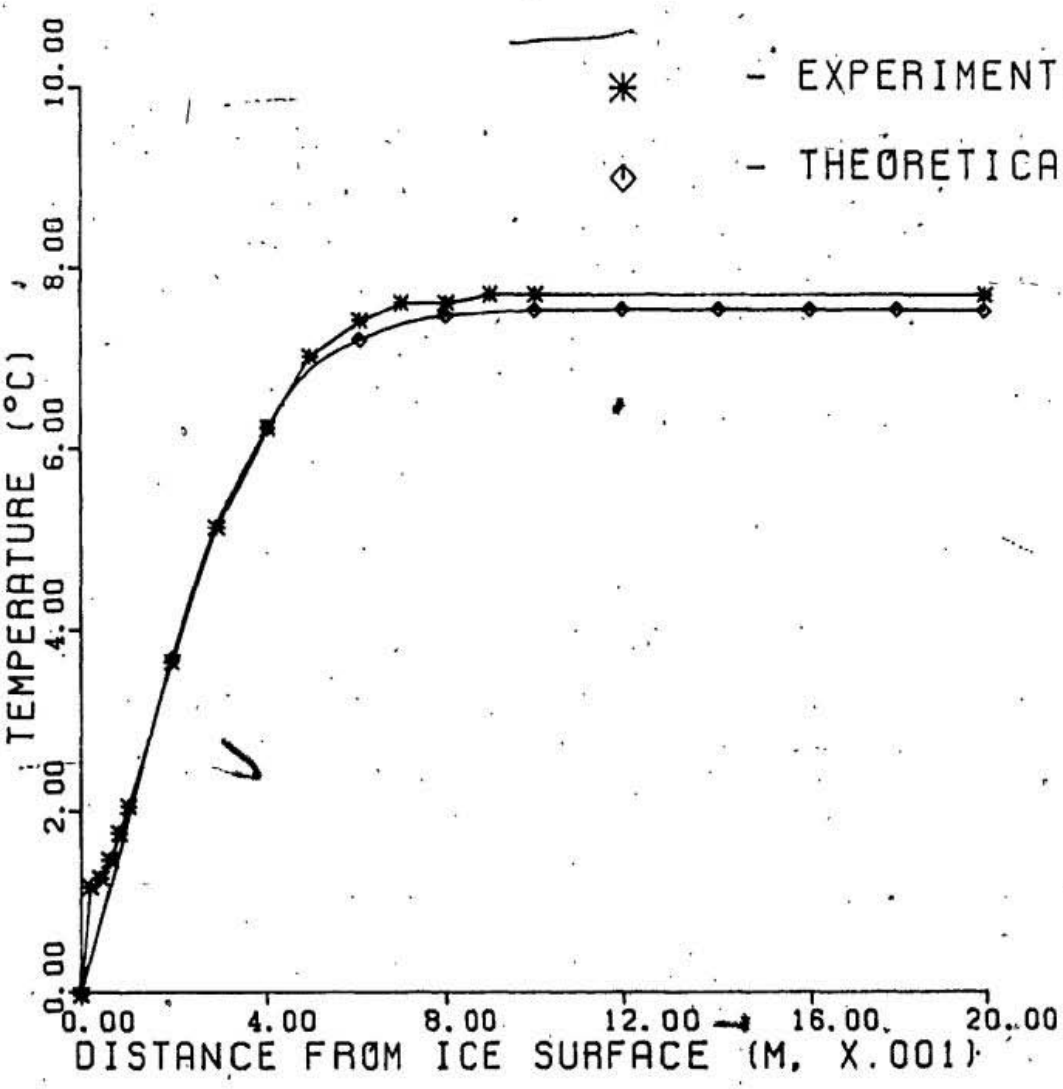

Fig. 4.3 The Temperature Profiles at 7.7°C (X=0.0670m)

$$h_x = \frac{-k}{T_w - T_B} \left(\frac{\partial T}{\partial y}\right)_w \qquad (4.1)$$

where

T_w = temperature at the wall (0.0°C)

T_B = bulk fluid temperature

k = thermal conductivity

$\left(\frac{\partial T}{\partial y}\right)_w$ = slope of the curve at the wall

The h_x values for various temperatures are shown in Table 4.1.

From these values of h_x, the corresponding Nusselt numbers were calculated using:

$$Nu_x = \frac{h_x X}{k} \qquad (4.2)$$

where

X(m) = the vertical position along the ice surface.

These results are also shown in Table 4.1. These results indicate a minimum Nusselt number around 5.6°C which is consistent with findings of other researchers [1].

4.2.2 The Velocity Profiles[30]

The theoretical and the experimental velocity results are shown in the Fig. 4.4. In this figure the

Table 4.1: Experimental and Theoretical Local Heat Transfer Coefficients and Nusselt Number

Temperature °C	h_x, $(\frac{\text{watts}}{m^2 °C})$		Nu_x	
	Exp.	Theo.	Exp.	Theo.
0.95	140.8	122.6	16.5	13.2
5.6	64.6	74.3	7.5	8.6
7.7	137.6	145.7	15.8	16.7

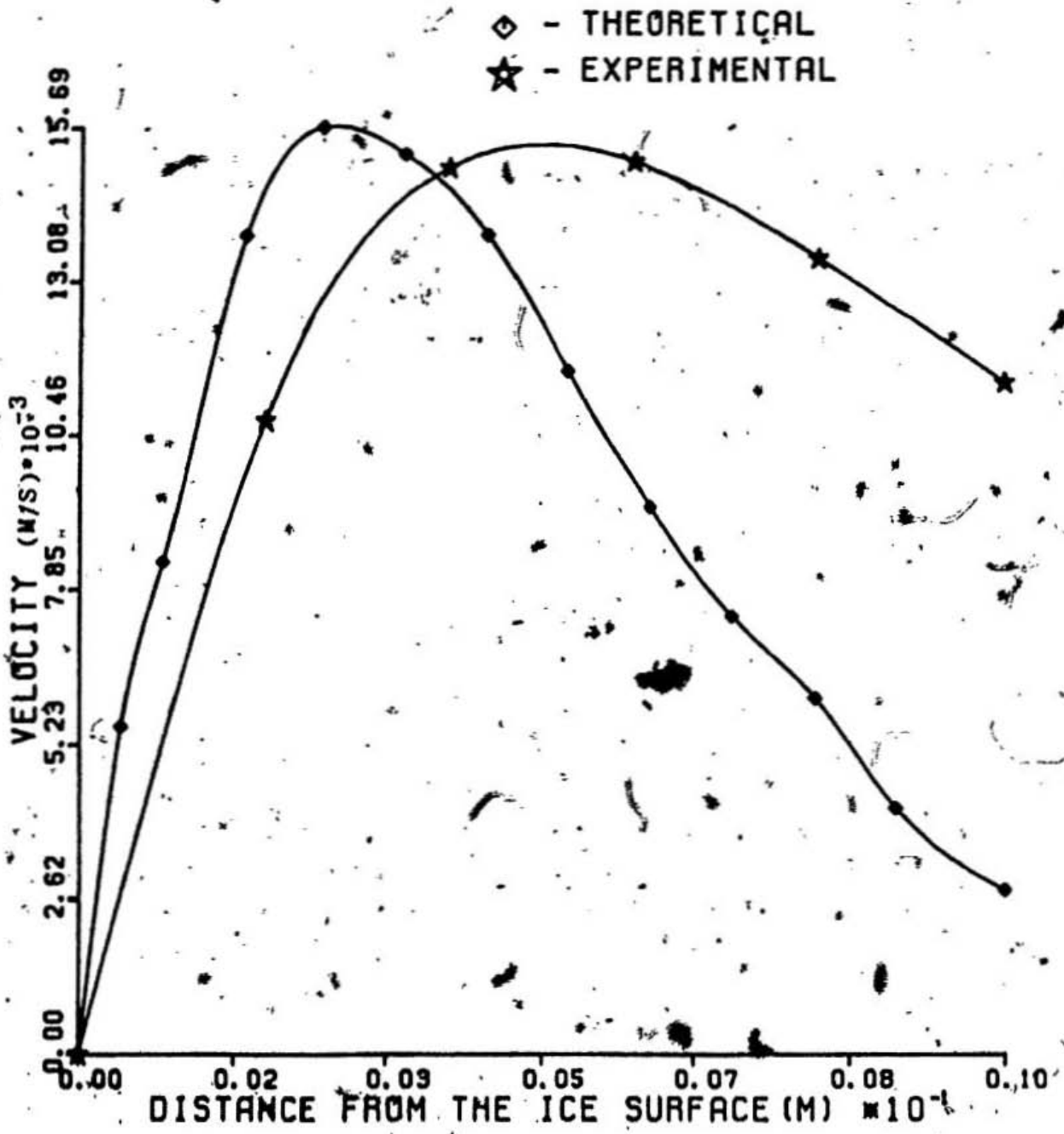

Fig. 4.4 The Velocity Profiles at 1.1°C (X=0.0803m)

velocity profiles look similar, there is a shift in the peaks but the magnitudes of the peaks are close. Fig. 4.5 shows the experimental velocity profile at 4.7°C where one can very clearly see the dual nature of the flow. There is an upward velocity near the wall and downward velocity away from the wall. The velocity is zero at the wall as well as at a distance far away from the wall where the natural convection effects are not present, i.e. the bulk conditions prevail. It should be mentioned here that this figure does not show any theoretical results because the solutions did not converge in this dual flow temperature range. Lee [1] in his thesis has also reported nonconvergence of the solution in the dual flow temperature range.

Fig. 4.6 is a schematic of the observed velocity profiles in the dual flow range. For a bulk fluid temperature of 1.1°C there is a full upward velocity profile which goes to zero at some distance from the ice surface. As the bulk temperature increases to 4.0°C the peak of the velocity profile has decreased and there is the start of a small downflow out from the ice surface. With another increase in temperature to 4.7°C the upward velocity profile has again decreased and the downward profile has increased. The point where the velocity goes to zero between the upward flow and the downward flow has shifted to the left, closer to the ice surface. As the water temperature is again increased

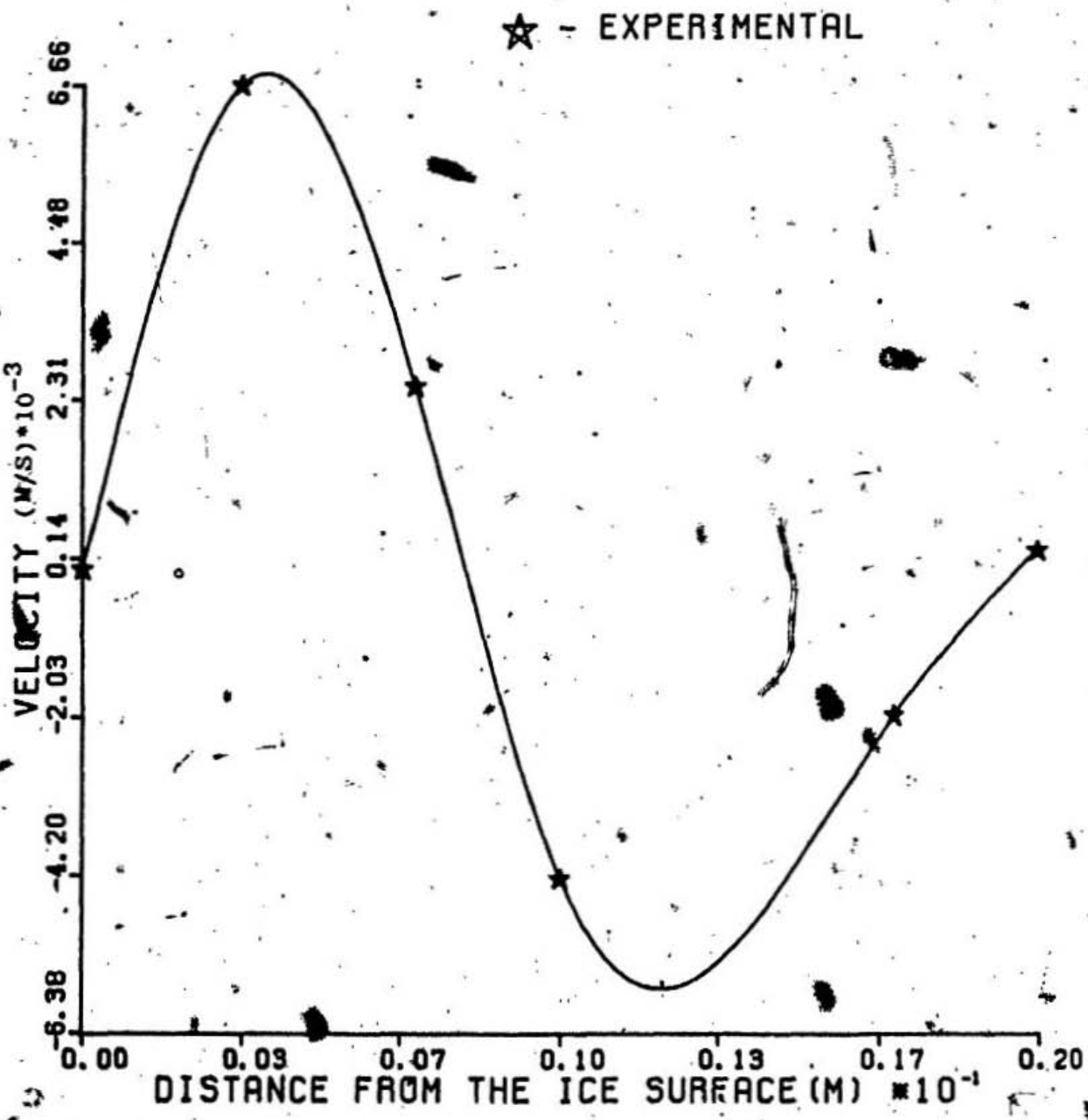

Fig. 4.5 The Velocity Profile at 4.7°C (X=0.0803m)

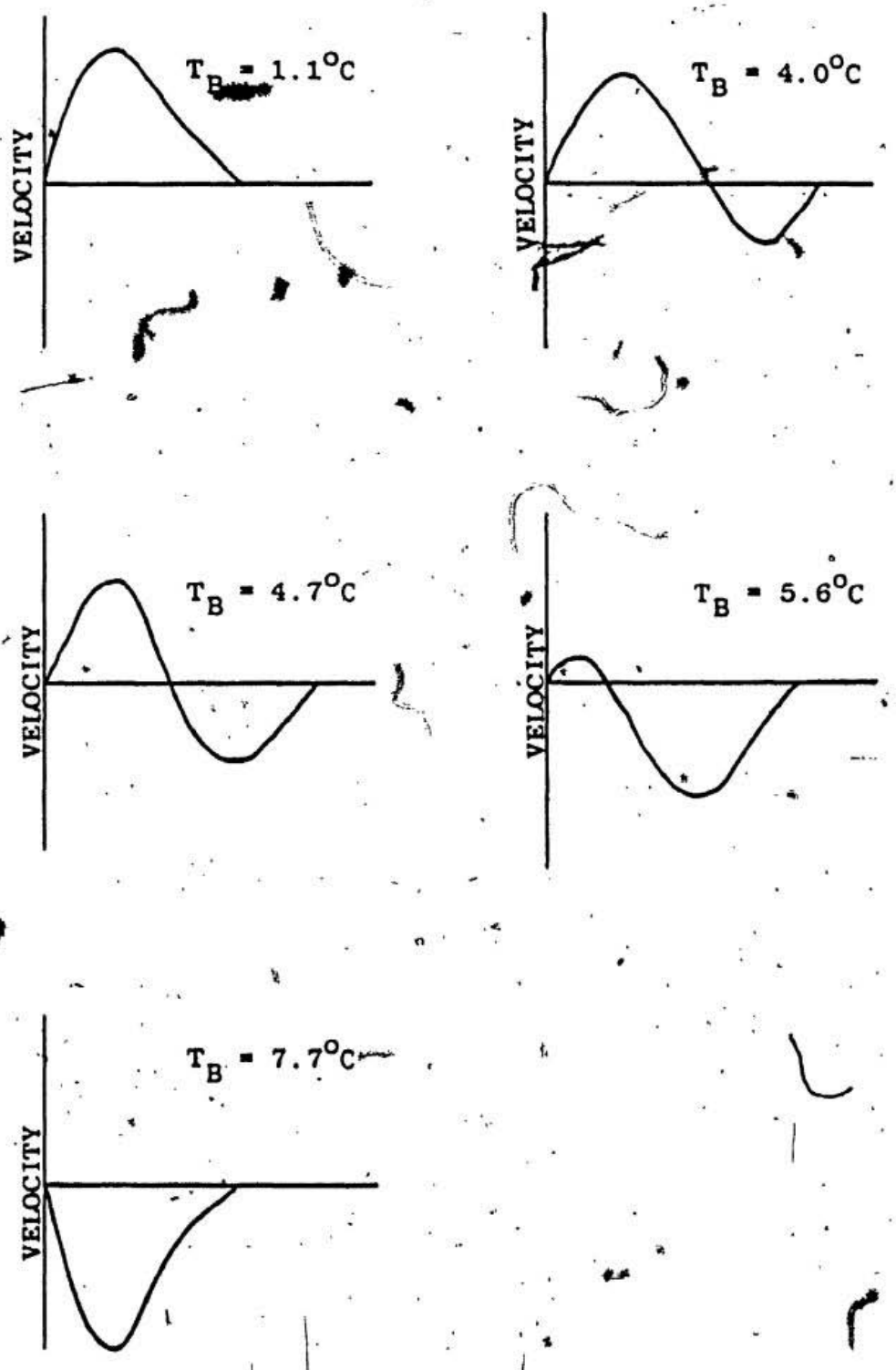

Fig. 4.6 The Observed Velocity Profiles in the Dual Flow Range

to 5.6°C the peak of the upward velocity profile has decreased almost to zero, and the downward profile has again increased. The point of zero velocity has again shifted closer to the ice surface. At a bulk fluid temperature of 7.7°C there is a full downward velocity profile with a peak value greater than that observed at the lower temperatures. There is actually a bulk fluid temperature at which there would be an area of zero velocity near the ice surface before the downward velocity profile. This would correspond to the temperature at which there is a minimum Nusselt number.

4.3 The Extension of the Theoretical Model

4.3.1 The Temperature Field

Fig. 4.7 shows the temperature profile at various values at 1.0°C. It can be clearly seen in this figure that as X increases the slope of the temperature profile at the wall decreases. This implies that the h_x, the local heat transfer coefficient, decreases as X increases. This is because in Eqn. (4.1), h_x is directly proportional to the slope. Similar results can be seen in Fig. 4.8 which is at temperature 3.0°C. Fig. 4.9 shows the temperature profiles at 5.0°C which is in the dual flow range. Table 4.2 shows the variation of h_x as a function of X at 5.0°C. From this figure and the table one can clearly see that h_x at first

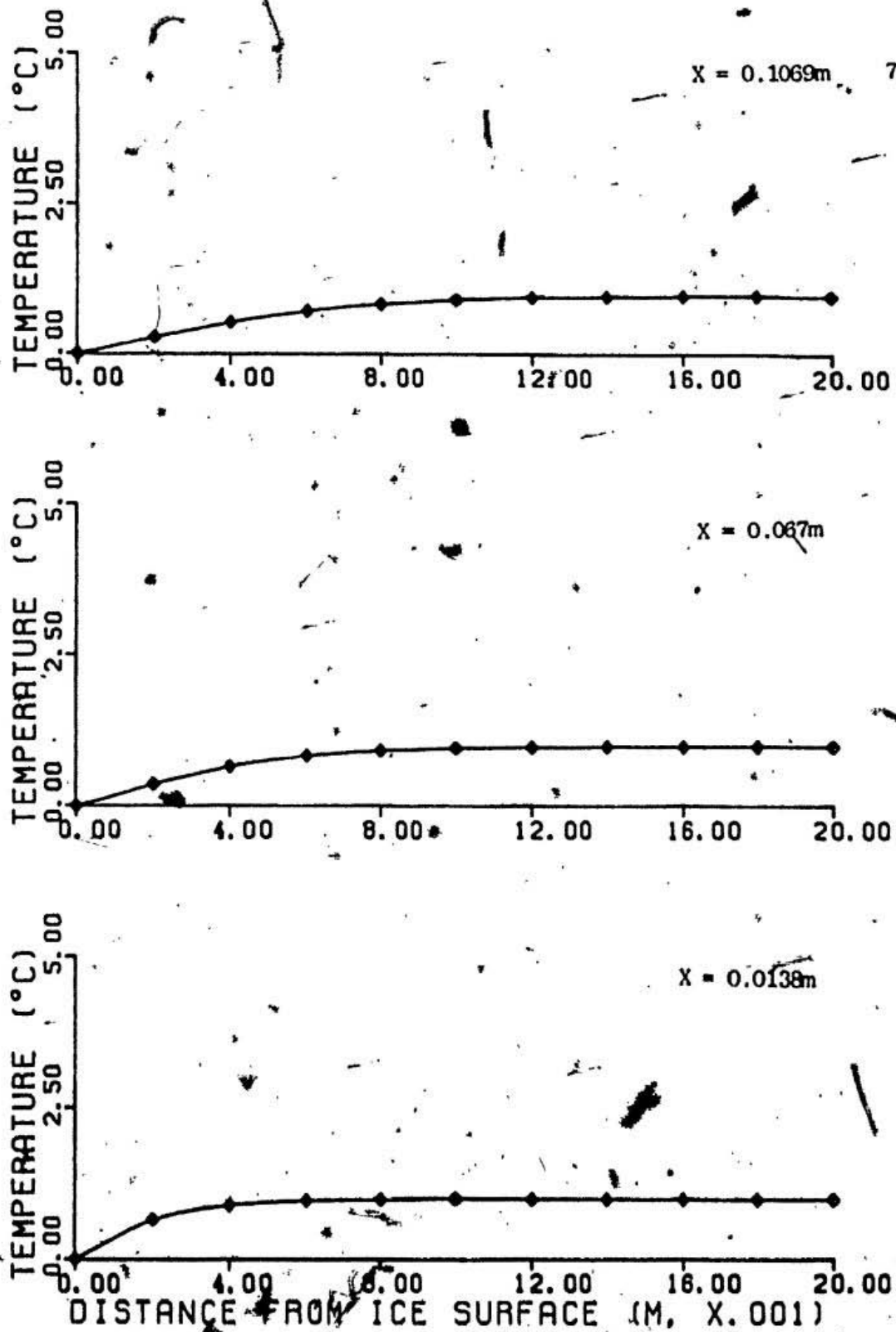

Fig. 4.7 The Temperature Profiles at 1.0°C

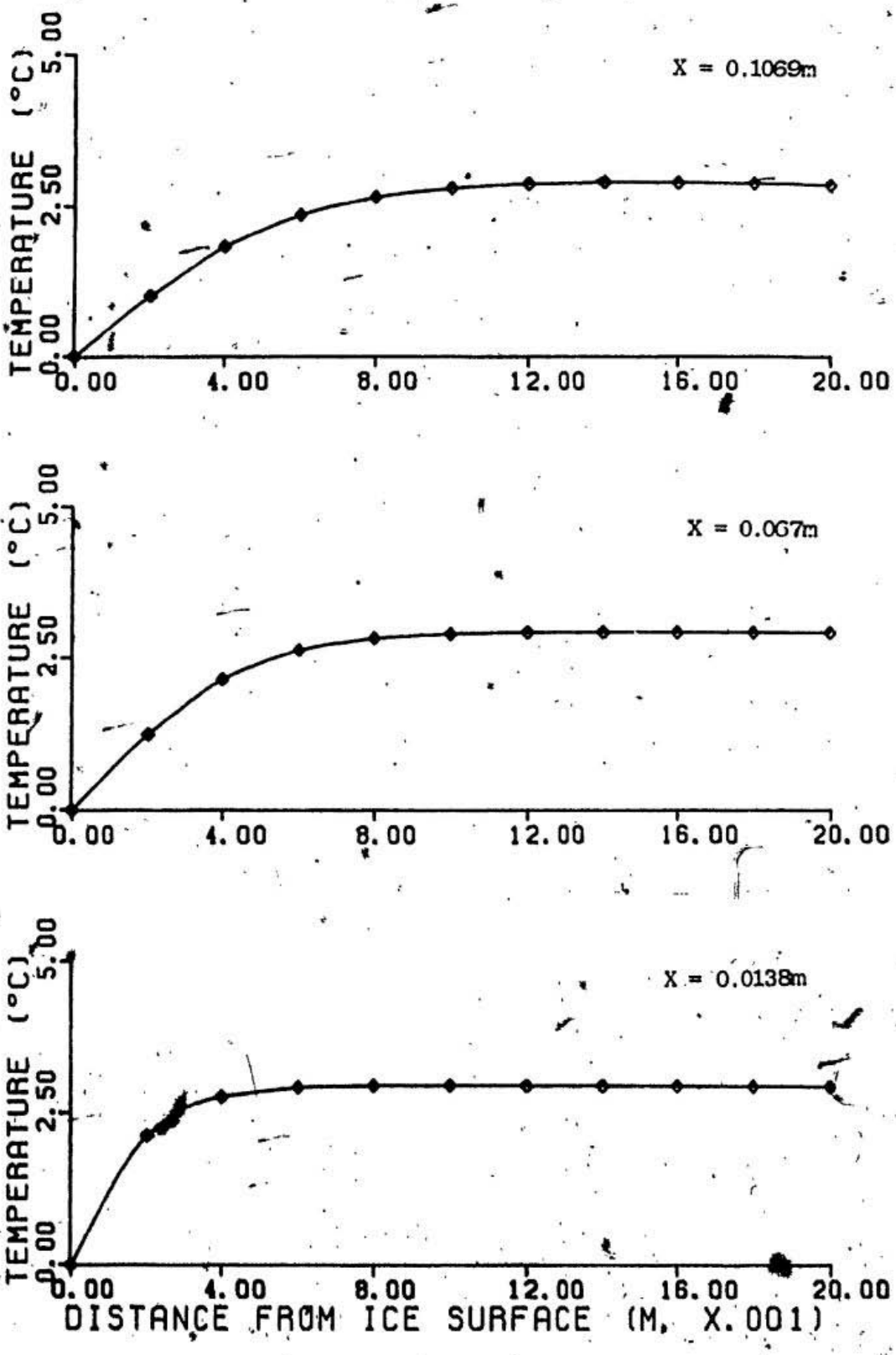

Fig. 4.8 The Temperature Profiles at 3.0°C

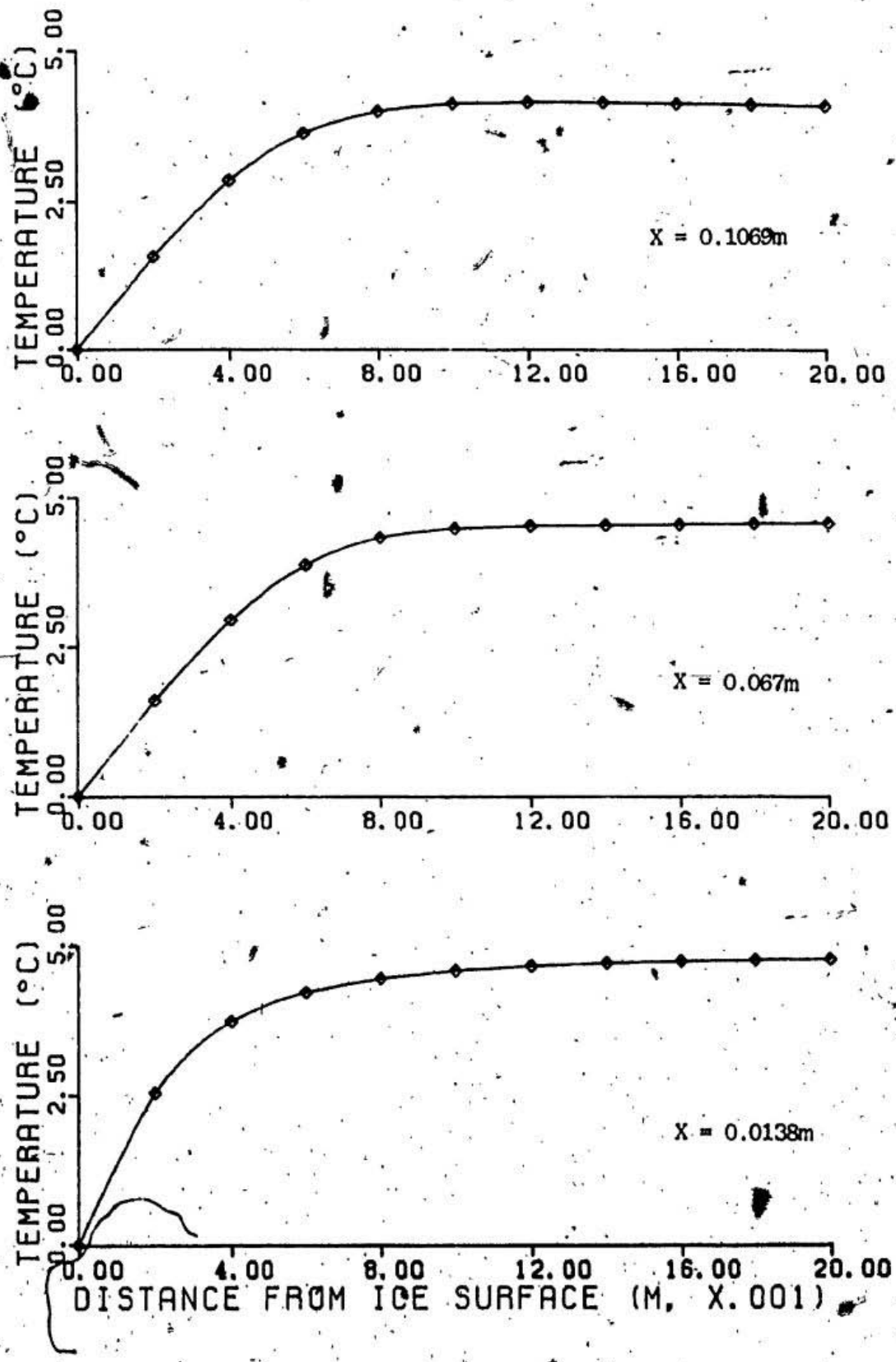

Fig. 4.9 The Temperature Profiles at 5.0°C

Table 4.2: Local Heat Transfer Coefficients at 5.0°C

X(m)	h_x, $(\frac{\text{watts}}{m^2 °C})$
0.0000	147.5
0.0137	123.5
0.0271	110.8
0.0404	102.5
0.0537	96.4
0.0670	92.2
0.0803	90.4
0.0936	93.1
0.1069	97.6
0.1202	100.1
0.1467	100.1
0.1601	98.2
0.1734	91.3
0.1867	71.8
0.2000	71.8

decreases with X and then increases and again it decreases. Since, as reported earlier, the velocity values did not converge in this temperature range, this may not be the actual variations of h_x with X.

The temperature profiles at 7.0°C and 9.0°C are shown in Figs. 4.10 and 4.11 respectively. Both the temperatures are above the dual flow region. In both these figures the slope at the wall increases with the increase of X. This behaviour is opposite to what was observed at temperatures below the dual flow region. This behavior can be explained by the fact that the flow is downwards now at 7.0°C and 9.0°c.

4.3.2 The Velocity Field

The velocity profiles at different locations at 1.0°C and 3.0°C are shown in Figs. 4.12 and 4.13. In Fig. 4.12 the peak velocities increase with an increase of X. All the velocities shown are upward throughout the field of interest. The velocity profile at the lower edge of the plate is flatter as compared to the profiles where X has higher values. This is because the natural convection forces increase with the increase in X. This also explains the increase in the peak values. In addition, in Fig. 4.13, the velocities approach zero far away from the vertical wall. Comparing Figs. 4.12 and 4.13 one can see that the boundary

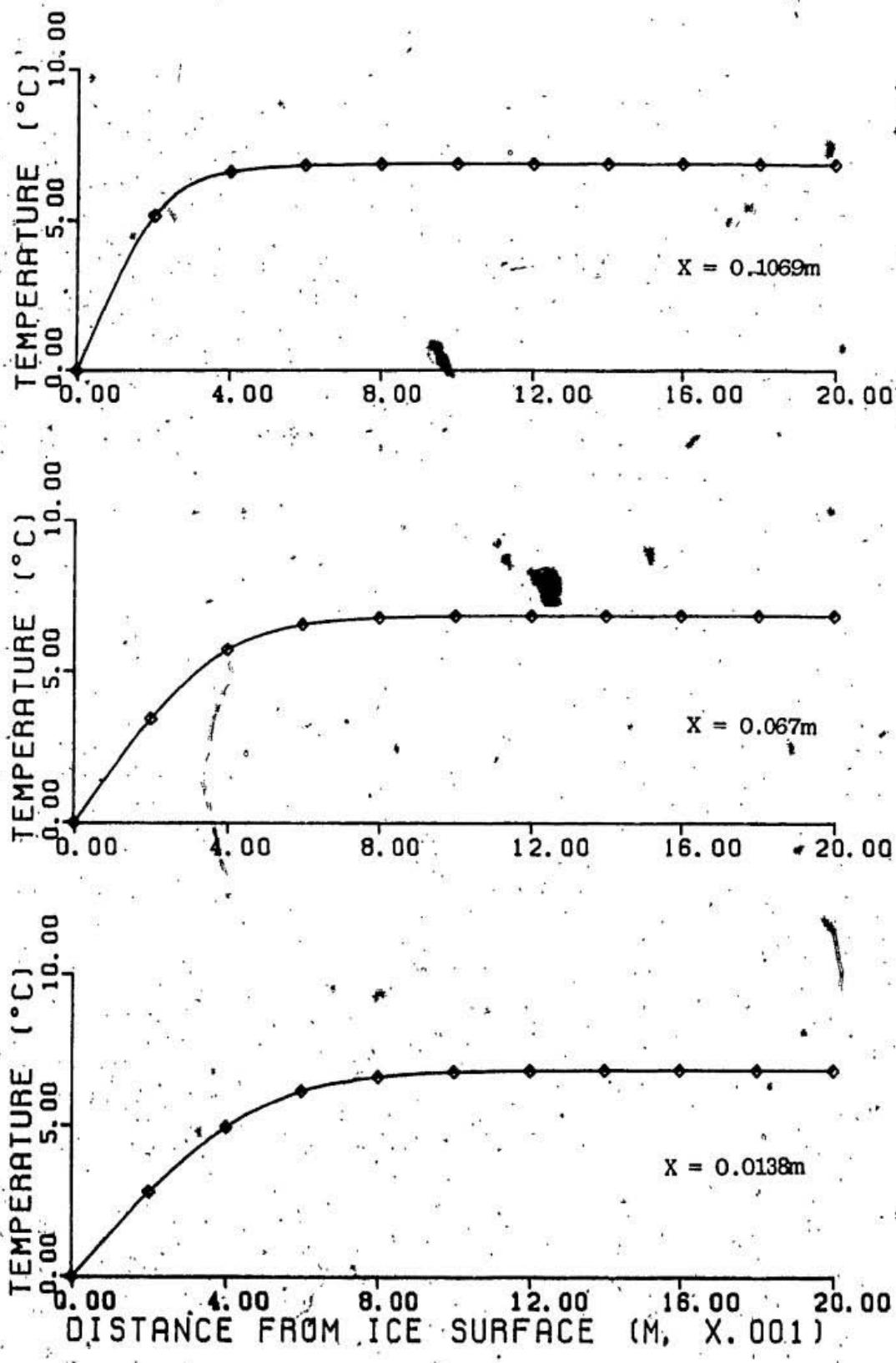

Fig. 4.10 The Temperature Profiles at 7.0°C

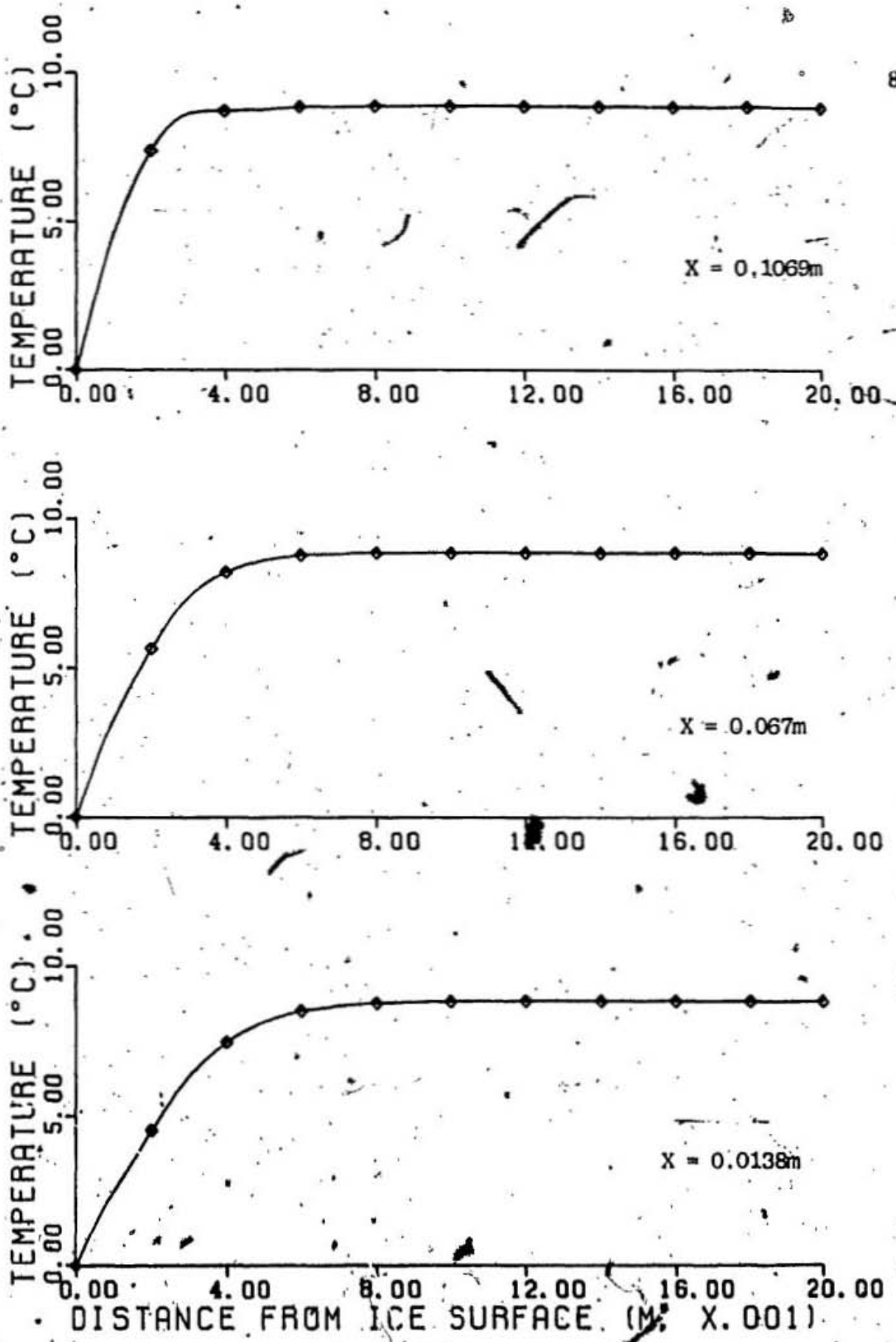

Fig. 4.11 . The Temperature Profiles at 9.0°C

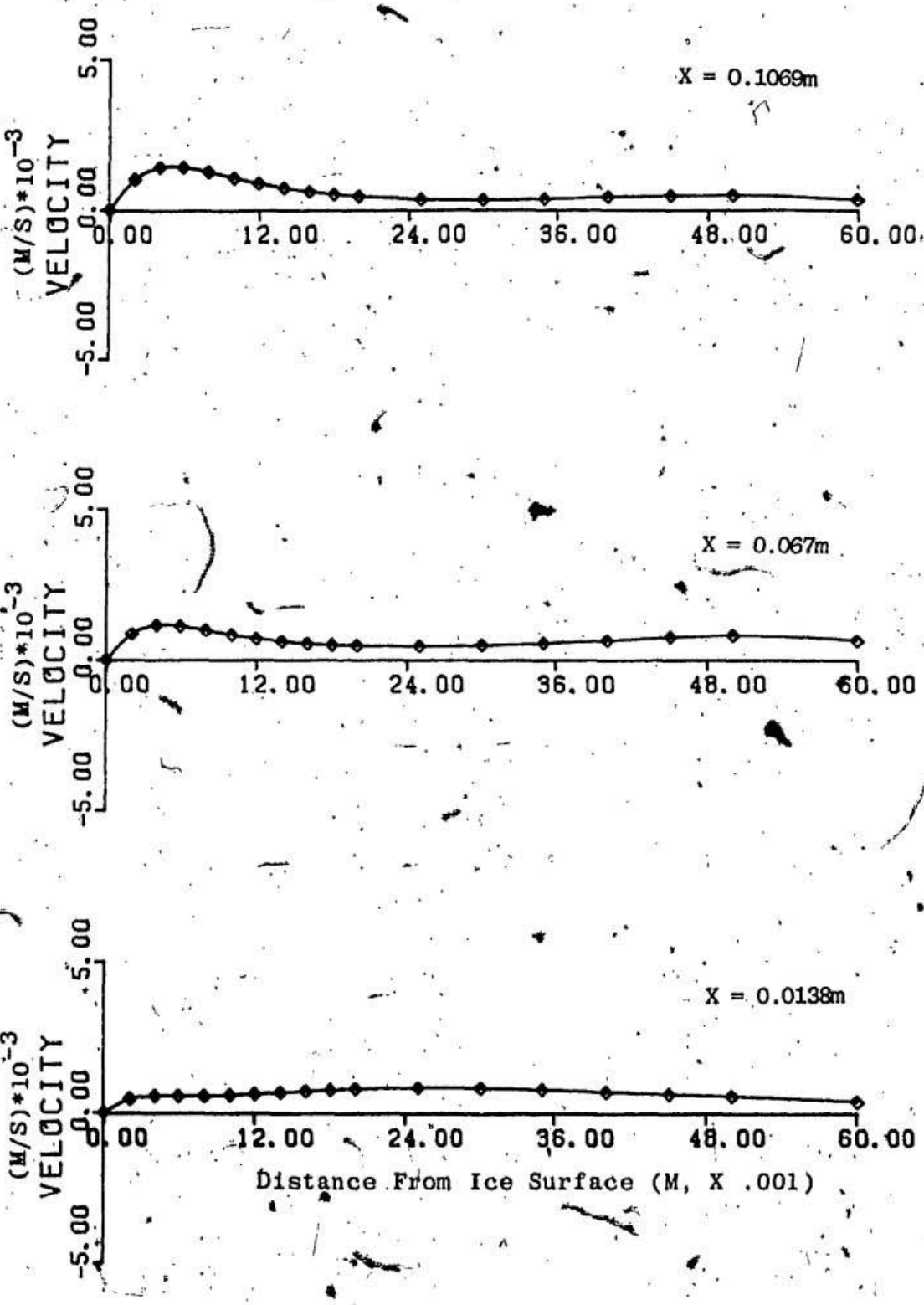

Fig. 4.12 The Velocity Profiles at 1.0°C

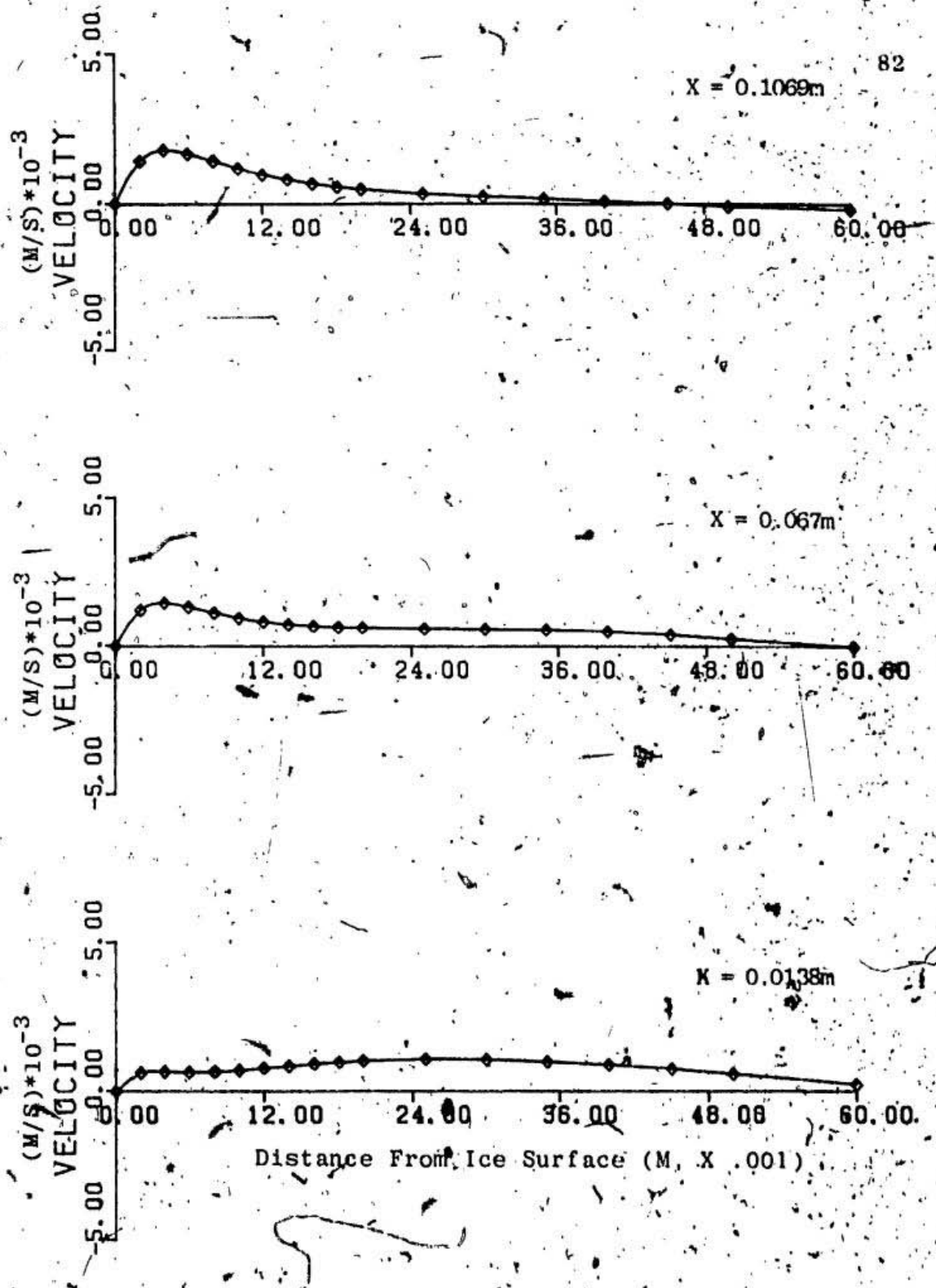

Fig. 4.13 The Velocity Profiles at 3.0°C

layer effects due to the natural convection increase as the temperature increases, i.e. the velocity profiles become sharper.

The velocity profile in the dual flow temperature range, i.e. between 4.0 °C, and 6.0 °C are not reported here because the solutions did not converge in this temperature range. The velocity profiles at 7.0 °C and 9.0 °C are shown in Figs. 4.14 and 4.15.. In both of these figrues, the velocity values are negative because of the downward flow. Since the temperatures for these figures are higher than those in Figs. 4.12 and 4.13 the magnitude of the peaks are much higher and profiles are much sharper. One can also see in these figures that there is a reversed flow far away from the vertical ice surface.

4.4 The Heat Transfer Coefficients and the Nusselt Numbers

The local values of the heat transfer coefficient, h_x, were calculated by using the slopes of the temperature profile at the wall as given in Eqn. (4.1). Then the average value of h_x was calculated using the equation [29]

$$\bar{h} = \frac{\int_0^L h_x \, dx}{L} \qquad (4.3)$$

where L is the length of the vertical ice surface. The local value of the Nusselt number was obtained using Eqn. (4.2).

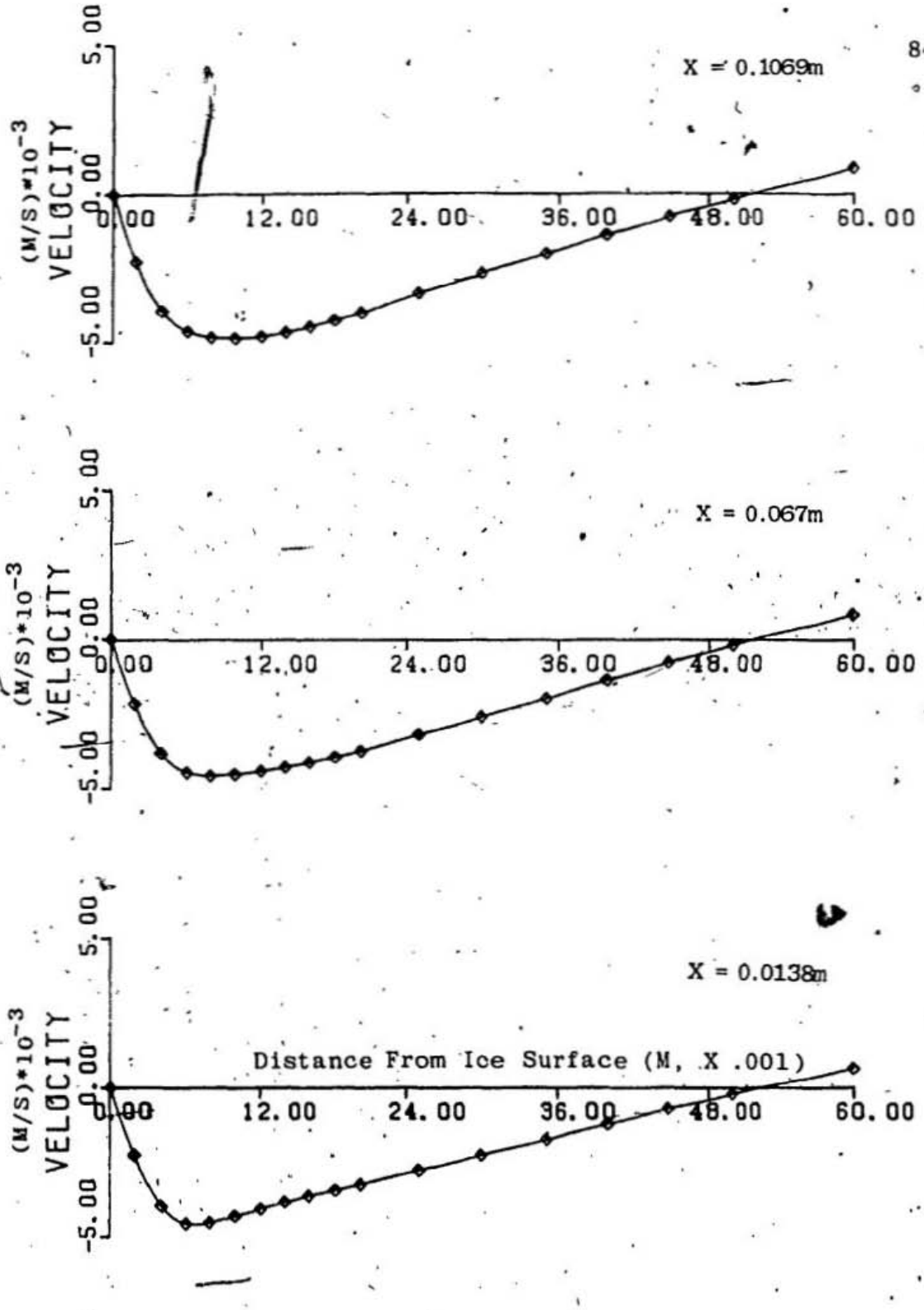

Fig. 4.14 The Velocity Profiles at 7.0°C

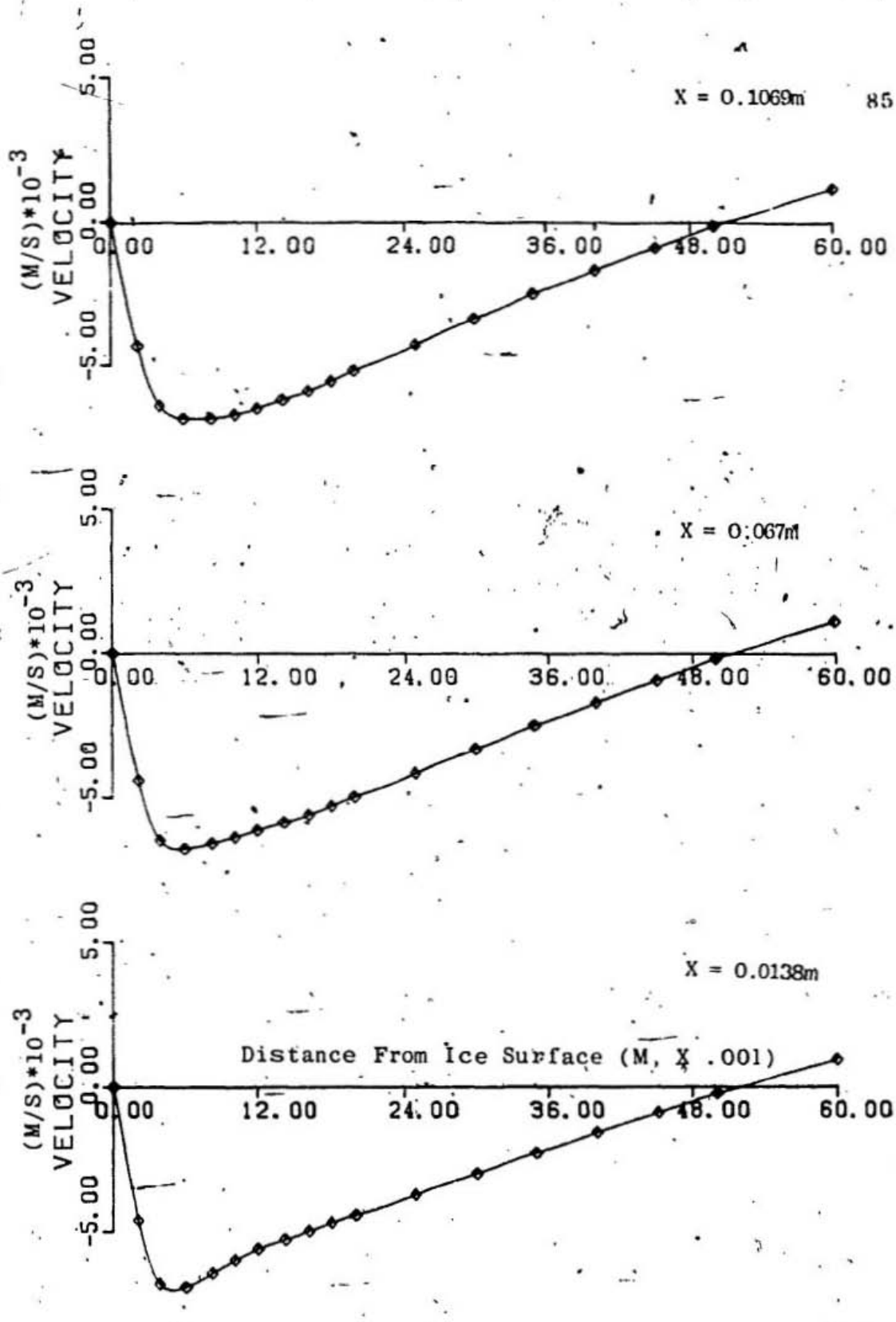

Fig. 4.15 The Velocity Profiles at 9.0°C

The average value of the Nusselt number was calculated using this equation

$$\bar{Nu} = \frac{\bar{h}\, L}{k} \qquad (4.4)$$

Tables 4.3 to 4.6 shows the variation of h_x with X at various temperatures. In Tables 4.3 and 4.4 which are at 1.0°C and 3.0°C the h_x decreases with increase in X whereas at higher temperatures, i.e. at 7.0°C and 9.0°C, (Tables 4.5 and 4.6) h_x increases with an increase in X. This is because the temperature profile slope (refer to Figs. 4.7 and 4.8) decreases with increases in X and since from Eqn. (4.1), h_x is directly proportional to the slope, h_x must also decrease with an increase in X. In the case of h_x variation with X at higher temperatures (refer to Figs. 4.9 and 4.10), the slopes increase with increase in X and therefore, h_x also increases with the increase in X.

Figs. 4.16 and 4.17 show the variations of $\bar{h}$ and $\bar{Nu}$ with temperature respectively. Both of these figures are similar. The results obtained by other researchers is shown in Fig. 1.1 which is also similar. All these figures show that $\bar{Nu}$ or $\bar{h}$ at first increases with the increase in the temperature; then decreases to a minimum value in the dual flow temperature range and then increases again with the temperature. The decrease of $\bar{h}$ or $\bar{Nu}$ can be understood by

Table 4.3: Local Heat Transfer Coefficients at 1.0°C

X(m)	h_x, $(\frac{watts}{m^2 °C})$
0.0000	186.3
0.0137	153.9
0.0271	136.9
0.0404	126.1
0.0537	118.3
0.0670	112.3
0.0803	107.3
0.0936	103.0
0.1069	98.9
0.1202	95.3
0.1467	92.1
0.1601	88.3
0.1734	80.7
0.1867	64.6
0.2000	64.6

Table 4.4: Local Heat Transfer Coefficients at 3.0°C

X(m)	h_x, $(\frac{watts}{m^2 °C})$
0.0000	205.4
0.0137	174.2
0.0271	156.5
0.0404	144.9
0.0537	136.4
0.0670	129.8
0.0803	124.3
0.0936	120.4
0.1069	115.6
0.1202	111.8
0.1467	108.6
0.1601	105.4
0.1734	97.2
0.1867	77.6
0.2000	77.6

Table 4.5: Local Heat Transfer Coefficients at 7.0°C

X(m)	h_x, $(\frac{watts}{m^2 °C})$
0.0000	117.0
0.0137	113.9
0.0271	115.5
0.0404	118.6
0.0537	123.1
0.0670	128.6
0.0803	135.2
0.0936	143.3
0.1069	153.2
0.1202	165.4
0.1467	180.2
0.1601	197.7
0.1734	214.9
0.1867	229.4
0.2000	229.4

Table 4.6: Local Heat Transfer Coefficients at 9.0°C

X (m)	h_x, $(\frac{watts}{m^2 °C})$
0.0000	147.1
0.0137	152.1
0.0271	155.6
0.0404	159.4
0.0537	163.9
0.0670	169.1
0.0803	175.4
0.0936	182.9
0.1069	191.9
0.1202	202.7
0.1467	215.2
0.1601	228.0
0.1734	240.4
0.1867	287.9
0.2000	287.9

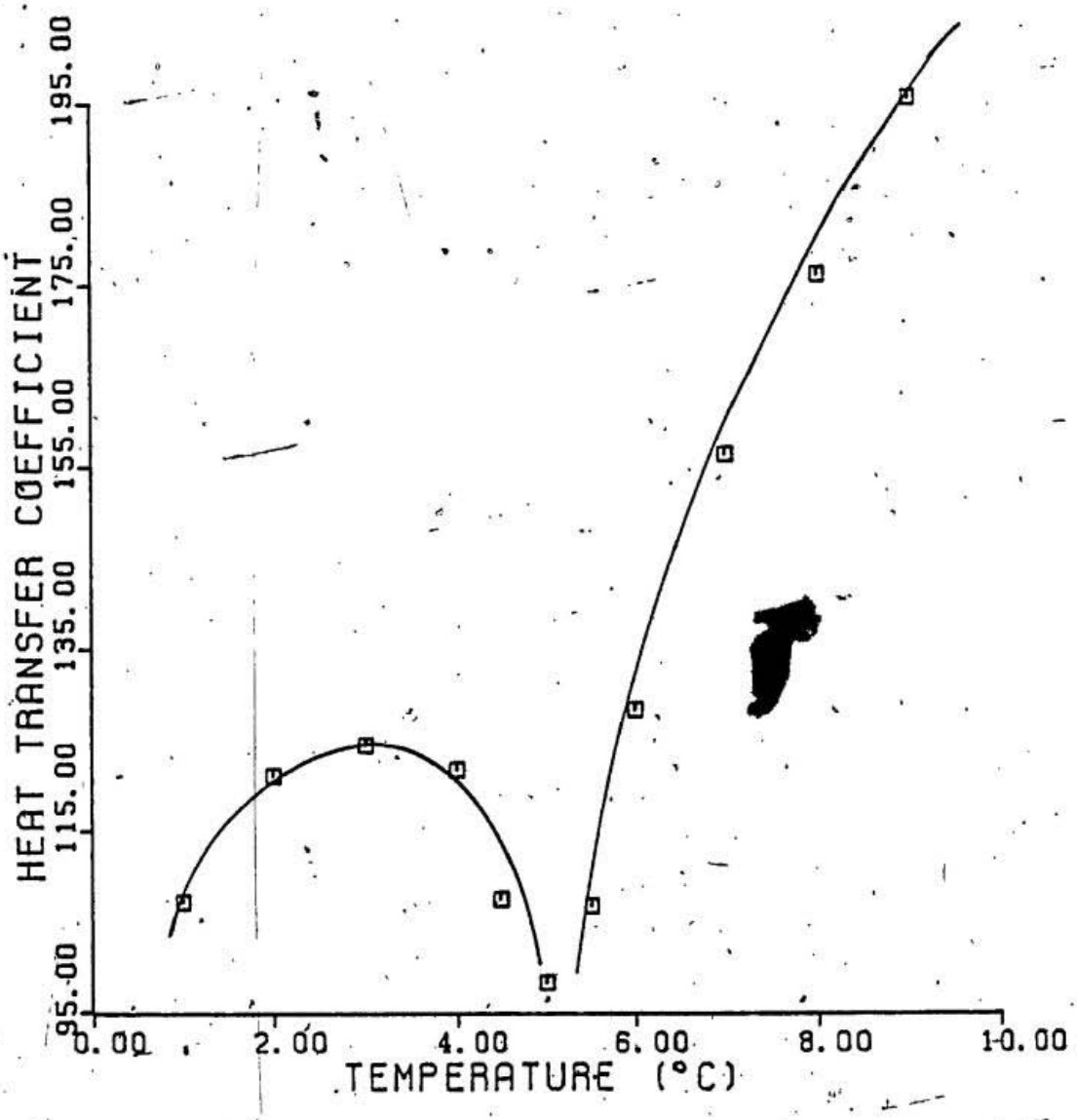

Fig. 4.16 The Average Heat Transfer Coefficient as a Function of Temperature

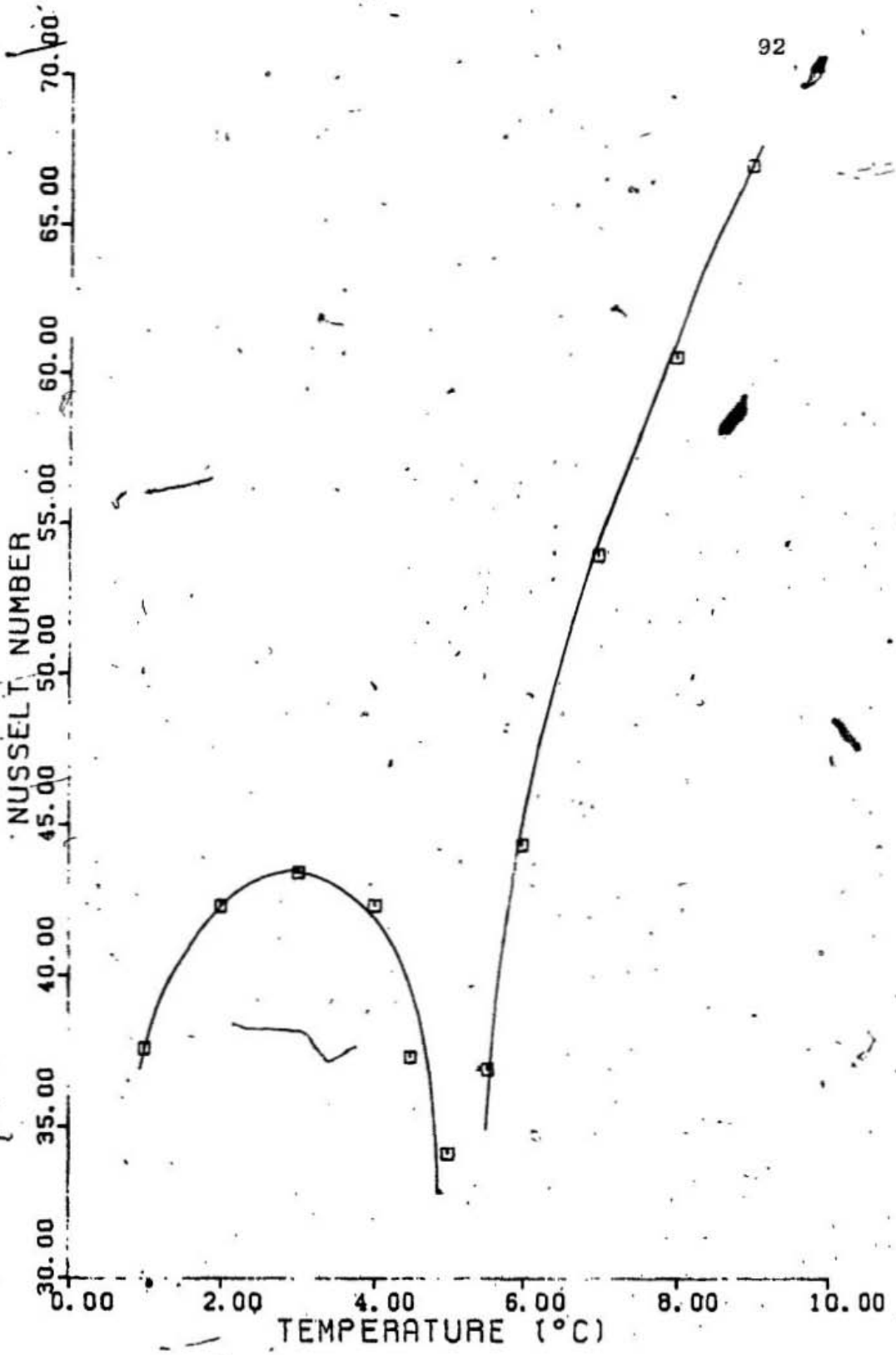

Fig. 4.17 The Average Nusselt Number as a Function of Temperature, L = 0.2 m

referring to Fig. 4.6. In this figure the peak upward velocity decreases with the increase in the temperature. The slope of the velocity curve at the wall is also decreased. Therefore, the convective heat transfer process which depends upon the variations of u with y, also decreases. This leads to the decrease in the slope of the temperature profile, and thus the heat transfer coefficient. This trend continues with the increase in the temperature until the peak upward velocity decreases to zero as given in the Fig. 4.6. When the temperature is increased further, the flow at the wall reverses and the absolute value of the slope of the velocity profile starts increasing. It should be pointed out here that when the slope of the velocity profile is zero, the heat transfer can be only due to the conduction process; there would be no convective process at this temperature. As the temperature increases above the reverse flow temperature at the wall, the slope of the velocity profile increases, thus the slope of the temperature profile also increases. Thus, the minimum value of $\bar{h}$ or $\bar{Nu}$ can be understood in terms of the variation of the absolute value of the slope of the velocity profile.

Table 4.7 shows the variation of h_x and Nu_x, at $X = 0.067m$ with increase in the temperature. One can clearly see that the behaviour of h_x in this case is similar to $\bar{h}$ or $\bar{Nu}$.

Table 4.7: Local Heat Transfer Coefficients and Nusselt Number (X_x = 0.0067 m)

Temperature °C	h_x, $\left(\frac{\text{watts}}{m^2\,°C}\right)$	Nu_x
1.0	103.1	12.1
2.0	116.4	13.6
3.0	119.7	13.9
4.0	116.0	13.5
4.5	111.3	12.98
5.0	93.1	10.78
5.5	58.2	06.74
6.0	108.8	12.57
7.0	143.3	16.51
8.0	165.5	19.01
9.0	182.9	20.90

It is worth mentioning here that at very low bulk temperatures such as around 1 °C, the melting rate of ice will be very small. Therefore, the values computed for h_x, $\bar{h}$ and $\bar{Nu}$ will be very close to the values obtained if the melting of the ice is also included which would involve inclusion of an additional term in the energy equation.

The results shown in Fig. 4.17 compare favourably with those obtained by Bendall and Gebhart [10] and Gebhart and Mollendorf [11]. In these two references, the results are tabulated for a plate length of 0.303 m. For other plate lengths one should use the equation [10].

$$(\overline{Nu})_c = \overline{Nu}\left(\frac{L}{0.303}\right)^{3/4} \qquad (4.5)$$

where $(\overline{Nu})_c$ is the corrected Nusselt number. It is worth mentioning here that the results shown in Fig. 1.1 are for $L = 0.7632$ m.

The average heat transfer coefficient values are quite useful in studying the overall heat transfer process around the vertical ice wall. The principles used in this investigation can be easily extended to the study of the heat transfer process in lakes, rivers and around icebergs where the liquid temperatures are close to the freezing point of water.

4.5 The Conclusions

In this chapter, the temperature and velocity profiles were calculated using the analytical model and the validity of this model was established using the experimental results. Then this model was used to predict these profiles at various locations along the vertical ice wall and at various temperatures. The heat transfer coefficients, h_x and $\bar{h}$ and the corresponding Nusselt numbers were calculated using the slopes of the temperature profile. Based on these studies, the following conclusions can be drawn:

1. The analytical model developed in Chapter 2 predicts the temperature and velocity profiles reasonably well in the lower as well as the higher temperature ranges.
2. In the lower temperature range h_x decreases with the increase in X.
3. In the higher temperature range h_x increases with the increase in X.
4. In the lower temperature range there is an upward fluid flow near the ice wall.
5. In the higher temperature range there is a downward fluid flow near the ice wall.
6. There is a dual flow between 4.0°C to 6.0°C. Around 4.0°C, the flow is upwards near the wall and downwards away from the wall. These directions reverse around 5.0°C. The dual flow disappears above 6.0°C.
7. The average values of $\bar{N}u$ and $\bar{h}$ at first increase with the temperature, then decrease to a minimum value in the dual flow range and then increase again with the increase in the temperature.
8. The increase or decrease in the values of $\bar{h}$, $\bar{N}u$ or h_x is directly related to the absolute value of the slope of the velocity profile.

CHAPTER 5

CONCLUSIONS AND RECOMMENDATIONS

5.1 A Brief Discussion of This Investigation

The main objective of this investigation has been to develope a theoretical model of the heat transfer process along a vertical ice wall in fresh water at various temperatures.

A finite difference technique was used to transform the governing steady-state equations to a form suitable for programming on the digital computer. The theoretically obtained results for the temperature and velocity profiles along the ice surface were compared to the experimental values. The local and average heat transfer coefficients and Nusselt numbers were also calculated from the extended model.

5.2 Conclusions

Based on this investigation the following conclusions can be drawn:

1. The theoretical model developed in Chapter 2 predicts the temperature profiles with reasonable accuracy in both the lower and upper temperature ranges.

2. The model also predicts the velocity profiles reasonably well. In both the lower (<4.0°C) and upper (>6.0°C) temperature ranges the directions of flow are correctly predicted, i.e. an upflow for T_B<4.0°C and a downflow for T_B >6.0°C. The results did not converge in the dual flow range.
3. There is a dual flow between 4.0°C and 6.0°C. Around 4.0°C there is an predominant upflow near the ice surface and a small downflow away from the ice surface. This gradually developes as the temperature increases to a full dual flow which then reverses to a small upflow near the ice surface and a predominant downflow farther out, at around 6.0°C. From there a full downflow developes as the temperature is increased.
4. At temperatures below 4.0°C, h_x decreases with an increase in X.
5. At temperatures above 6.0°C h_x increases with an increase in X.
6. The average heat transfer coefficients and corresponding Nusselt numbers at first increase as a function of temperature; then decrease to a minimum in the dual flow range; and then increase again with temperature.

7. This behaviour of $\bar{h}$, $\bar{Nu}$ and h_x as a function of temperature is directly related to the absolute value of the slope of the velocity profile.

5.3 Limitations of the Present Work

The experimental and theoretical work has the following limitations:

1. The velocity measurement technique, although useful in recording the type and direction of the flow is not very accurate in measuring instantaneous velocities.
2. The theoretical and experimental work was carried out for the steady-state condition of ice in fresh water at various bulk temperatures. They do not cover the case of ice melting i.e., the model does not include the phase changes.
3. The length of ice used was relatively small compared to the possible thickness of ice sheets in lakes or rivers in nature.

5.4 Recommendations for Future Work

The model used has been verified with a certain degree of accuracy for the domain of interest selected. It should now be possible to extend this model in the following ways:

1. Introduce an additional term to the energy equation so that the actual melting rate of the ice can be determined.
2. Introduce salinity as one of the governing equations so that the problem of iceberg melting can be examined.
3. Experiment with lasers to develope a better photographic technique for the velocity measurements, so that an instantaneous velocity at various points along the ice surface can be measured for comparison with the theoretical findings.
4. Vary the experimental set-up such that the geometry of the problem changes to include a lower ice surface, so that edge effects and melting from the bottom, can be taken into account.

REFERENCES

1. Lee, J. J., "Melting of a Vertical Ice Wall by Natural Convection into Pure or Saline Water", M. Eng. Thesis, Memorial University, Nfld., 1979.

2. Dumoré, J. M., Merk, H. J. and Prins, T. A., "Heat Transfer from Water to Ice by Thermal Convection", Nature, London, Vol. 172, 1953, pp. 460-461.

3. Merk, H. J., "The Influence of Melting and Anomalous Expansion on the Thermal Convection in Laminar Boundary Layers", Applied Scientific Research, Section A, Vol. 4, 1954, pp. 435-452.

4. Ede, A. J., "The Influence of Anomalous Expansion on Natural Convection in Water", Applied Scientific Research, Vol. 5, 1955, pp. 458.

5. Schenk, J. and Schenkels, F. A. M., "Thermal Free Convection from an Ice Sphere in Water", Applied Scientific Research, Vol. 19, 1968, pp. 465.

6. Vanier, C. R. and Tien, Chi, "Free Convection Melting of Ice Spheres", AICHE Journal, Vol. 16, 1970, pp. 76-82.

7. Saitoh, T., "Natural Convection Heat Transfer from a Horizontal Ice Cylinder", Applied Scientific Research, Vol. 32, 1976, pp. 429-451.

8. Oborin, L. A., "Special Features of Free Convection in Water at Temperatures Below 277°K", Journal of Engineering Physics, Vol. 13, 1967, pp. 429.

9. Schechter, R. S. and Isbin, H. S., "Natural-Convection Heat Transfer in Regions of Maximum Fluid Density", A.I.Ch.E. Journal, Vol. 4, 1958, pp. 81-89.

10. Bendell, M. S., and Gebhart, B., "Heat Transfer and Ice-Melting in Ambient Water Near its Density Extremun", International Journal of Heat and Mass Transfer, Vol. 19, 1976, pp. 1081-1087.

11. Gebhart, B. and Mollendorf, J. C., "Buoyancy-Induced Flows in Water under Conditions in which Density Extremun May Arise", Journal of Fluid Mechanics, Vol. 87, 1978, pp. 673-708.

12. Queresh, F. Z., and Gebhart, B., "Vertical Natural Convection with a Uniform Flux Condition in Pure and Saline Water at the Density Extremun", Sixth International Heat Transfer Conference, Toronto, Canada, Vol. 2, 1978.

13. Sesonske, Alexander, "Velocity and Temperrature Distributons About a Horizontal Cylinder in Free Convection Heat Transfer", A.I.Ch.E Journal, Vol. 7, 1961, pp. 352-353.

14. Josberger, E. G., "Laminar and Turbulent Boundary Layers Adjacent to Melting Vertical Ice Walls in Salt Water", Ph.D Thesis, University of Washington, Seattle, 1979.

15. Josberger, E. G. and Martin, S., "A Laboratory and Theoretical Study of the Boundary Layer Adjacent to a Vertical Melting Ice Wall in Salt Water", Journal of Fluid Mechanics, Vol. 11, 1981, pp. 439-473.

16. Carey, V. P. and Gebhart, B., "Visualization of the Flow Adjacent to a Vertical Ice Surface Melting in Cold Pure Water", Journal of Fluid Mechanics, Vol. 107, 1981, pp. 37-55.

17. Yen, Yin-Chao, "Onset of Convection in a Layer of Water Formed by Melting Ice from Below", The Physics of Fluids, Vol. 11, 1968, pp. 1263-1270.

18. Yen, Yin-Chao and Galea, F., "Onset of Convection in a Wath Layer Formed Continuously by Melting Ice", The Physics of Fluids, Vol. 12, 1969, pp. 509-516.

19. Huppert, H. E. and Turner, J. S., "On Melting Icebergs", Nature, Vol. 271, 1978, pp. 46-48.

20. Huppert, H. E. and Josberger, E. G., "The Melting of Ice in Cold Stratified Water", J. Physical Oceanography, Vol. 10, 1980, pp. 953.

21. Wilson, N. W. and Lee, J. J., "Melting of a Vertical Ice Wall by the Free Convection in Fresh Water", Journal of Heat Transfer, Vol. 103, 1981, pp. 13-16.

22. Wilson, N. W. and Vyas, B. D., "Velocity Profiles near a Vertical Ice Surface Melting into Fresh Water", Journal of Heat Transfer, Vol. 101, 1979, pp. 313-317.

23. Baker, D. J., "A Technique for the Precise Measurement of Small Fluid Velocities", Journal of Fluid Mechanics, Vol. 26, 1966, pp. 573-575.

24. Jaluria, Y. and Gebhart, B., "On Transition Mechanisms in Vertical Natural Convection Flow", Journal of Fluid Mechanics, Vol. 66, 1974, pp. 309-337.

25. Warner, C. Y., "Turbulent Natural Convection in Air Along a Vertical Flat Plate", Ph.D. Thesis, University of Michigan, 1966.

26. Hishida, M. and Nagano, Y., "Simultaneous Measurements of Velocity and Temperature in Nonisothermal Flows", Journal of Heat Transfer, Vol. 100, 1978, pp. 340-345.

27. Vliet, G. E. and Liu, C. K., "An Experimental Study of Turbulent Natural Convection Boundary Layers", Journal of Heat Transfer, 1969, pp. 517-531.

28. Gosman, A. D., Pun, W. M., Runchal, A. K, et al., "Heat and Mass Transfer in Recirculating Flows", Academic Press, London and New York, 1969.

29. Holman, J. P., "Heat Transfer", McGraw-Hill, Inc. New York, 1976.

30. Dutton, C. R. and Sharan, A. M. "Analytical and Experimental Studies of the Heat Transfer Around a Vertical Ice Wall in Fresh Water at Various Temperatures", Offshore Mechanics and Arctic Engineering Conference, Dallas, TX, 1985.

APPENDIX A

DESCRIPTION AND LISTING OF THE COMPUTER PROGRAMME

The programme used for the solution of the finite-difference form of the governing equations is CU.FOR. The programme is written in the Fortran language and was run on the DEC VAX 11/785 computer at Memorial University.

Figs. 2.4a and 2.4b show the flow diagrams for this programme. This programme consists of several subroutines, the main one being EQN which carries out up to 1500 iterations each for the solution of the vorticity, stream function and temperature equations.

All the properties, except density, are constant for any bulk fluid temperature and are evaluated at

$$\frac{T_B - T_{ice}}{2}$$

The density relationship used is

DENS = 1000. + AO + T * (A1 + T * (A2 + T * (A3 + T * A4)))

where

$T = T_B - 4.0$

A_0 = .65263594E-5

A_1 = -.19559673E-3

A_2 = -.79633407E-4

A_3 = .78565026E-4

A_4 = -.7027333OE-6

with similar expressions for the other properties. The density value was updated for each new temperature value.

The convergence criteria used was 0.001. The residual was calculated as

$$RS = 1. - \frac{\text{OLD Value}}{\text{NEW value}}$$

for each node and the maximum value was saved to determine convergence. Convergence was obtained with as low at 700 to 800 itertions at the higher temperatures.

This programme can be easily modified to include additional terms such as salinity, as it is written in a general form.

```
      DIMENSION A(21,21,8),BE(21),BW(21),BN(21)
     1  ,BS(21),GETW(12),GETF(12),GETT(12)
      BYTE FILNAM(80)
      COMMON/CNUMBR/NW,NF,NT,NRO,NMU,NV1,NV2,NVSQ,IE,IV
     1  /CGEO/IN,INM,JN,JNM,IMIN(21),IMAX(21),X1(21),X2(21),R(21),NCORD
     1  /CGEN/ROREF,ZMUREF,NMAX,NPRINT,IP,CC,PR(9),RP(9),RSDU(9)
      READ(5,4) FILNAM
4     FORMAT(80A1)
      FILNAM(80)=0
      READ(5,6) TB
6     FORMAT(F5.2)
C
      OPEN(UNIT=7,NAME=FILNAM,DISPOSE='SAVE',ACCESS='SEQUENTIAL',
     1  TYPE='NEW')
C     INPUT DATA
C
      DATA RP/9*1.0/
      DATA NMAX,NPRINT,IP,CC/1500,50,2,.001/
      DATA ROREF,NCORD,IN,JN/1000.,1,21,21/
      DATA IMIN,IMAX/21*2,21*20/
      DATA NW,NF,NT,NRO,NMU,NV1,NV2,NVSQ,IE,IV/1,2,3,4,5,6,7,8,4,2/
      DATA X1/0.0,1.5,3.0,4.0,5.0,5.5,6.0,6.5,7.0,7.5,8.0,8.2,8.4,8.6,
     1  8.8,9.0,9.2,9.4,9.6,9.8,10.0/
      DATA X2/0.0,2.0,4.0,6.0,8.0,10.0,11.38,12.71,14.04,15.37,16.70,
     1  18.03,19.36,20.69,22.02,23.36,24.68,26.01,27.34,28.67,30.0/
      FACTOR=.01
      DO 333 I=1,21
      X1(I)=X1(I)*FACTOR
      X2(I)=X2(I)*FACTOR
333   CONTINUE
C
C     STARTING PROGRAM
C
      DATA N1,N2,N3/21,21,8/
      INM=IN-1
      JNM=JN-1
C
2     CONTINUE
C
      CALL GRID(N1,N2,N3,BE,BW,BN,BS)
      CALL INIT(N1,N2,N3,A,TB)
      NITER=0
1     CONTINUE
      CALL DENSIT(N1,N2,N3,A,I,J,NRO)
      NITER=NITER+1
      CALL EQN(N1,N2,N3,A,BE,BW,BN,BS)
      IF((NITER+NPRINT-IP)/NPRINT.NE.NITER/NPRINT) GO TO 10
10    CONTINUE
      IF (NITER.EQ.NMAX) GO TO 8
      RES=0.
      DO 7 K=1,IE
      IF(ABS(RES).LT.ABS(RSDU(K))) RES=RSDU(K)
7     RSDU(K)=0.0
      IF(ABS(RES).GT.CC.OR.NITER.LE.5) GO TO 1
      GO TO 9
8     WRITE(7,600)NITER
9     CONTINUE
      CALL VELDIS(N1,N2,N3,A)
      CALL RANGE(A,N1,N2,N3,GETW,GETF,GETT)
750   FORMAT(1X,12F5.2/1X,12F5.2/1X,12F5.2)
500   FORMAT(I5,3F10.5)
600   FORMAT(I5)
      DO 22 J=1,JN
22    WRITE(7,550)  (A(I,J,3),I=1,IN)
```

```
      DO 33 K=6,7
      DO 44 J=1,JN
44    WRITE(7,550) (A(I,J,K),I=1,IN)
33    CONTINUE
      CLOSE(UNIT=7)
550   FORMAT(1X,7F14.6/1X,7F14.6/1X,7F14.6)
      STOP
      END
C
C     END OF OPERATING PROGRAM. START OF BLOCK DATA
C
C
C     END OF BLOCK DATA. START OF INITIALIZING SUBROUTINE
C
      SUBROUTINE INIT(N1,N2,N3,A,TB)
      DIMENSION A(N1,N2,N3)
      COMMON /CNUMBR/NW,NE,NT,NRO,NMU,NV1,NV2,NVSQ,IE,IV
     1 /CGEO/IN,INM,JN,JNM,IMIN(21),IMAX(21),X1(21),X2(21),R(21),NCORD
     1 /CGEN/ROREF,ZMUREF,NMAX,NPRINT,IP,CC,PR(9),RP(9),RSDU(9)
C
C     SET VALUES IN STORE TO ZERO
C
      DO 30 J=1,JN
      DO 30 I=1,IN
      IF(TB.LE.5.0) GO TO 34
      A(I,J,NW)=-0.10
      A(I,J,NE)=-0.10
      GO TO 35
34    A(I,J,NW)=0.10
      A(I,J,NE)=0.10
35    A(I,J,NV1)=0.
      A(I,J,NV2)=0.
30    A(I,J,NT)=TB
      DO 32 J=7,21
      A(IN,J,NT)=0.0
32    CONTINUE
      T=(A(1,JN,NT)-A(IN,JN,NT))/2.
      DO 33 I=1,IN
      DO 33 J=1,JN
33    A(I,J,NMU)=VISC(T)
C
C
      RETURN
      END
C
C     END OF INITIALIZING SUBROUTINE. START OF ITERATION SUBROUTINE
C
      SUBROUTINE EQN (N1,N2,N3,A,BE,BW,BN,BS)
      DIMENSION A(N1,N2,N3),BE(N1),BW(N1),BN(N2),BS(N2)
      COMMON/CNUMBR/NW,NE,NT,NRO,NMU,NV1,NV2,NVSQ,IE,IV
     1 /CGEO/IN,INM,JN,JNM,IMIN(21),IMAX(21),X1(21),X2(21),R(21),NCORD
     1 /CGEN/ROREF,ZMUREF,NMAX,NPRINT,IP,CC,PR(9),RP(9),RSDU(9)
      DXISQ=(X1(IN)-X1(INM))**2
      DO 11 J=2,JNM
      IL=IMIN(J)
      IH=IMAX(J)
      DO 11 I=IL,IH
1     CONTINUE
      CALL SORCE(N1,N2,N3,A,SOURCE,I,J,NW)
      CALL CONVEC(N1,N2,N3,A,AE,AW,AN,AS,I,J,NW)
      RSQ=R(J)*R(J)
      BBE=2.*RSQ*BE(I)
      BBW=2.*RSQ*BW(I)
      BBN=(R(J+1)*R(J+1)+RSQ)*BN(J)
```

```
      BBS=(R(J-1)*R(J-1)+RSQ)*BS(J)
      IF(I.EQ.INM.AND.J.LE.JNM) GO TO 12
16    TERM2=0.0
      GO TO 13
12    TERM1=-3.*(A(INM,J,NF)-A(IN,J,NF))/RSQ/DX1SQ/(A(I,J,NRO))
      TERM2=.5*(AE+A(I+1,J,NMU)*BBE)
      A(I+1,J,NW)=TERM1
13    CONTINUE
C
      ANUM=(AE+A(I+1,J,NMU)*BBE)*A(I+1,J,NW)
     1 +(AW+A(I-1,J,NMU)*BBW)*A(I-1,J,NW)
     2 +(AS+A(I,J-1,NMU)*BBS)*A(I,J-1,NW)
     3 +(AN+A(I,J+1,NMU)*BBN)*A(I,J+1,NW)+SOURCE
      ADNM=AE+AW+AN+AS+A(I,J,NMU)*(BBE+BBW+BBN+BBS)+TERM2
      IF (ADNM.EQ.0.0) GO TO 11
      Z=A(I,J,NW)
      A(I,J,NW)=ANUM/ADNM
      RS=1.-Z/A(I,J,NW)
      A(I,J,NW)=Z+RP(NW)*(A(I,J,NW)-Z)
      IF(ABS(RS).GT.ABS(RSDU(NW))) RSDU(NW) =RS
11    CONTINUE
C
C     SECTION FOR STREAM FUNCTION
C
      DO 21 J=2,JNM
      IL=IMIN(J)
      IH=IMAX(J)
      DO 21 I=IL,IH
      CALL SORCE(N1,N2,N3,A,SOURCE,I,J,NF)
      RISQ=1./R(J)/R(J)
      ROP=A(I,J,NRO)
      BBE=4./(A(I+1,J,NRO)+ROP)*RISQ*BE(I)
      BBW=4./(A(I-1,J,NRO)+ROP)*RISQ*BW(I)
      BBN=16./(A(I,J+1,NRO)+ROP)/((R(J+1)+R(J))**2)*BN(J)
      BBS=16./(A(I,J-1,NRO)+ROP)/((R(J-1)+R(J))**2)*BS(J)
      ANUM=BBE*A(I+1,J,NF)+BBW*A(I-1,J,NF)+BBN*A(I,J+1,NF)
     1 +BBS*A(I,J-1,NF)+SOURCE
      ADNM=BBE+BBW+BBN+BBS
      IF(ADNM.EQ.0.0) GO TO 21
      Z=A(I,J,NF)
      A(I,J,NF)=ANUM/ADNM
      RS=1.-Z/A(I,J,NF)
      A(I,J,NF)=Z+RP(NF)*(A(I,J,NF)-Z)
      IF(ABS(RS).GT.ABS(RSDU(NF))) RSDU(NF)=RS
21    CONTINUE
C
C
      K=3
      T=(A(IN,1,NT)-A(1,1,NT))/2.
      PR(3)=(CP(T)*VISC(T))/COND(T)
      DO 31 J=2,JNM
      IL=IMIN(J)
      IH=IMAX(J)
      DO 31 I=IL,IH
C
C
      CALL CONVEC(N1,N2,N3,A,AE,AW,AN,AS,I,J,K)
C
      BPP=A(I,J,NMU)
      BBE=(A(I+1,J,NMU)+BPP)/PR(K)*BE(I)
      BBW=(A(I-1,J,NMU)+BPP)/PR(K)*BW(I)
      BBN=(A(I,J+1,NMU)+BPP)/PR(K)*BN(J)
      BBS=(A(I,J-1,NMU)+BPP)/PR(K)*BS(J)
C
```

```
C
60      ANUM=(AE+BBE)*A(I+1,J,K)+(AW+BBW)*A(I-1,J,K)+(AN+BBN)*A(I,J+1,K)
     1  +(AS+BBS)*A(I,J-1,K)
C
        ADNM=AE+AW+AN+AS+BBE+BBW+BBN+BBS
        IF (ADNM.EQ.0.) GO TO 31
        Z=A(I,J,K)
        A(I,J,K)=ANUM/ADNM
C
        RS=1.-Z/A(I,J,NT)
        A(I,J,K)=Z+RP(K)*(A(I,J,K)-Z)
C
        IF(ABS(RS).GT.ABS(RSDU(NT))) RSDU(NT)=RS
31      CONTINUE
41      CONTINUE
        CALL BOUND(N1,N2,N3,A)
        RETURN
        END
C
C
C
        SUBROUTINE CONVEC(N1,N2,N3,A,AE,AW,AN,AS,I,J,K)
        COMMON/CNUMBR/NW,NF,NT,NRO,NMU,NV1,NV2,NVSQ,IE,IV
     1  /CGEO/IN,INM,JN,JNM,IMIN(21),IMAX(21),X1(21),X2(21),R(21),NCORD
     1  /CGEN/ROREF,ZMUREF,NMAX,NPRINT,IP,CC,PR(9),RP(9),RSDU(9)
        DIMENSION A(N1,N2,N3)
C       CALCULATION OF CONVECTION TERMS
C
        DV=R(J)*(X1(I+1)-X1(I-1))*(X2(J+1)-X2(J-1))
        G1PW=(A(I,J+1,NF)-A(I,J-1,NF)+A(I-1,J+1,NF)-A(I-1,J-1,NF))/DV
        G1PE=(A(I,J+1,NF)-A(I,J-1,NF)+A(I+1,J+1,NF)-A(I+1,J-1,NF))/DV
        G2PS=(A(I-1,J,NF)-A(I+1,J,NF)+A(I-1,J-1,NF)-A(I+1,J-1,NF))/DV
        G2PN=(A(I-1,J,NF)-A(I+1,J,NF)+A(I-1,J+1,NF)-A(I+1,J+1,NF))/DV
        APP=1.
C
        AE=0.5*APP*(ABS(G1PE)-G1PE)
        AW=0.5*APP*(ABS(G1PW)+G1PW)
        AN=0.5*APP*(ABS(G2PN)-G2PN)
        AS=0.5*APP*(ABS(G2PS)+G2PS)
C
        RETURN
        END
C
C       SUBROUTINE FOR CALCULATION OF BE,BW,BN,BS
C
        SUBROUTINE GRID (N1,N2,N3,BE,BW,BN,BS)
        DIMENSION BE(N1),BW(N1),BN(N2),BS(N2)
        COMMON/CNUMBR/NW,NF,NT,NRO,NMU,NV1,NV2,NVSQ,IE,IV
     1  /CGEO/IN,INM,JN,JNM,IMIN(21),IMAX(21),X1(21),X2(21),R(21),NCORD
     1  /CGEN/ROREF,ZMUREF,NMAX,NPRINT,IP,CC,PR(9),RP(9),RSDU(9)
C
C
C
        DO 11 J=1,JN
11      R(J)=1.0
C
        DO 21 I=2,INM
        DX1=1./(X1(I+1)-X1(I-1))
        BW(I)=DX1/(X1(I)-X1(I-1))
21      BE(I)=DX1/(X1(I+1)-X1(I))
C
        DO 22 J=2,JNM
        DX2=0.5/(X2(J+1)-X2(J-1))
        BS(J)=(1.+R(J-1)/R(J))/(X2(J)-X2(J-1))*DX2
```

```
22      BN(J)=(1.+R(J+1)/R(J))/(X2(J+1)-X2(J))*DX2
C       WRITE(5,101)  (X1(I),I=1,IN)
C       WRITE(5,102)  (X2(I),I=1,IN)
101     FORMAT(1X,25HDISTANCES IN DIRECTION-1/1X,7F10.5)
102     FORMAT(1X,25HDISTANCES IN DIRECTION-2/1X,7F10.5)
        RETURN
        END
C
CC
CC
C
CC      SUBROUTINE TO DETERMINE VALUES AT BOUNDARIES
C
        SUBROUTINE BOUND(N1,N2,N3,A)
        DIMENSION A(N1,N2,N3)
        DIMENSION DX1(21),DX2(6)
        COMMON/CNUMBR/NW,NF,NT,NRO,NMU,NV1,NV2,NVSQ,IE,IV
      1 /CGEO/IN,INM,JN,JNM,IMIN(21),IMAX(21),X1(21),X2(21),R(21),NCORD
      1 /CGEN/ROREF,ZMUREF,NMAX,NPRINT,IP,CC,PR(9),RP(9),RSDU(9)
C
        YY(YN,YP)=1./1.-(YP/YN)**2
        XX(XN,XP)=1./1.-(XP/XN)**2
        DO 10 I=2,INM
        DX1(I)=1./(X1(I+1)-X1(I-1))
10      CONTINUE
        DX1(1)=1./(X1(2)-X1(1))
        DO 21 I=1,INM
        BB=YY(2.*DX1(I),X1(IN)-X1(IN-1))
        A(I,JN,NT)=BB*A(I,JN-1,NT)-(BB-1.)*A(I,JN-2,NT)
21      CONTINUE
        DO 20 J=2,5
        DX2(J)=1./(X2(J+1)-X2(J-1))
20      CONTINUE
        DX2(1)=1./(X2(2)-X2(1))
        DO 22 J=1,5
        BB=XX(2.*DX2(J),X2(6)-X2(5))
        A(IN,J,NT)=BB*A(IN-1,J,NT)-(BB-1.)*A(IN-2,J,NT)
22      CONTINUE
        RETURN
        END
C
CC
C
        SUBROUTINE DENSIT(N1,N2,N3,A,I,J,K)
        DIMENSION A(N1,N2,N3)
        COMMON/CNUMBR/NW,NF,NT,NRO,NMU,NV1,NV2,NVSQ,IE,IV
      1 /CGEO/IN,INM,JN,JNM,IMIN(21),IMAX(21),X1(21),X2(21),R(21),NCORD
      1 /CGEN/ROREF,ZMUREF,NMAX,NPRINT,IP,CC,PR(9),RP(9),RSDU(9)
C
        DO 20 I=1,IN
        DO 20 J=1,JN
        T=A(I,J,NT)
        A(I,J,NRO)=DENS(T)
20      CONTINUE
        RETURN
        END
C
CC
CC      OUTPUT SUBROUTINE
C
        SUBROUTINE PRINT(N1,N2,N3,A,IN,JN,NBEGIN,NTOTAL)
        DIMENSION A(N1,N2,N3)
        JX=JN/10
        IF(JX.LT.1)  JX=1
```

```
      IX=IN/10
      IF(IX.LT.1)  IX=1
      K=NBEGIN
      DO 10 M=1,NTOTAL
      IF(M.EQ.1)  WRITE(5,50)
      IF  (M.EQ.2)  WRITE(5,60)
      IF(M.EQ.3)  WRITE(5,70)
      DO 2 L=1,JN,JX
      J=JN+1-L
2     WRITE(5,30)  (A(I,J,K),I=1,IN),J
      K=K+1
10    WRITE(5,40)  (I,I=1,IN)
40    FORMAT(1X,11I2/1X,10I2)
50    FORMAT(1X,'VORTICITY DISTRIBUTION')
60    FORMAT(1X,'STREAM FUNCTION')
70    FORMAT(1X,'TEMPERATURE DISTRIBUTION')
30    FORMAT(1X,11F10.5/1X,10F10.5,5X,I2)
      RETURN
      END
C
C
C
C
      SUBROUTINE VELDIS(N1,N2,N3,A)
      DIMENSION A(N1,N2,N3)
      COMMON/CNUMBR/NW,NF,NT,NRO,NMU,NV1,NV2,NVSQ,IE,IV
     1 /CGEO/IN,INM,JN,JNM,IMIN(21),IMAX(21),X1(21),X2(21),R(21),NCORD
     1 /CGEN/ROREF,ZMUREF,NMAX,NPRINT,IP,CC,PR(9),RP(9),RSDU(9)
C
      DO 50 J=2,JNM
      H2=(X2(J)-X2(J-1))/(X2(J+1)-X2(J))
      RX2=R(J)*(X2(J+1)-X2(J-1))
      IL=IMIN(J)
      IH=IMAX(J)
      DO 50 I=IL,IH
      H1=(X1(I-1)-X1(I))/(X1(I+1)-X1(I))
      RX1=R(J)*(X1(I+1)-X1(I-1))
      A(I,J,NV1)=(A(I,J+1,NF)-A(I,J,NF))*H2+(A(I,J,NF)-A(I,J-1,NF))/H2
      A(I,J,NV1)=A(I,J,NV1)/RX2/A(I,J,NRO)
      A(I,J,NV2)=(A(I+1,J,NF)-A(I,J,NF))*H1+(A(I,J,NF)-A(I-1,J,NF))/H1
      A(I,J,NV2)=A(I,J,NV2)/RX1/A(I,J,NRO)
      A(I,J,NVSQ)=((A(I,J,NV1)**2+(A(I,J,NV2))**2))/2.
50    CONTINUE
      RETURN
      END
C
C
C
C
C
      SUBROUTINE SORCE(N1,N2,N3,A,SOURCE,I,J,K)
      DIMENSION A(N1,N2,N3)
      COMMON/CNUMBR/NW,NF,NT,NRO,NMU,NV1,NV2,NVSQ,IE,IV
     1 /CGEO/IN,INM,JN,JNM,IMIN(21),IMAX(21),X1(21),X2(21),R(21),NCORD
     1 /CGEN/ROREF,ZMUREF,NMAX,NPRINT,IP,CC,PR(9),RP(9),RSDU(9)
C
      DATA G/9.81/
      DIF1(PE,PP,PW,X1E,X1P,X1W)=((PE-PP)*(X1P-X1W)/(X1E-X1P)+
     1 (PP-PW)*(X1E-X1P)/(X1P-X1W))/(X1E-X1W)
      DIF2(PN,PP,PS,X2N,X2P,X2S)=((PN-PP)*(X2P-X2S)/(X2N-X2P)+
     1 (PP-PS)*(X2N-X2P)/(X2P-X2S))/(X2N-X2S)
C
      GO TO (1,2,3,3,3,3,3,3)K
C
```

```
C       VORTICITY
C
1       S1=DIF1(A(I+1,J,NVSQ),A(I,J,NVSQ),A(I-1,J,NVSQ),X1(I+1),X1(I),
     1  X1(I-1))*DIF2(A(I,J+1,NRO),A(I,J,NRO),A(I,J-1,NRO),X2(J+1),
     1  X2(J),X2(J-1))
C
        S2=DIF2(A(I,J+1,NVSQ),A(I,J,NVSQ),A(I,J-1,NVSQ),X2(J+1),X2(J),
     1  X2(J-1))*DIF1(A(I+1,J,NRO),A(I,J,NRO),A(I-1,J,NRO),X1(I+1),
     1  X1(I),X1(I-1))
C
        SOURCE=(S1-S2)-G*DIF1(A(I+1,J,NRO),A(I,J,NRO),A(I-1,J,NRO),
     1  X1(I+1),X1(I),X1(I-1))
        RETURN
C
C       STREAM FUNCTION
C
2       SOURCE=A(I,J,NW)
        RETURN
3       SOURCE=0.0
        RETURN
        END
C
        FUNCTION CP(X)
        DATA A0,A1,A2,A3/8.95866E3,-4.05340E1,1.12431E-1,-1.01379E-4/
        T=X+273.15
        CP=A0+T*(A1+T*(A2+T*A3))
        RETURN
        END
C
        FUNCTION COND(X)
        DATA A0,A1,A2,A3,A4/-0.92247,2.8395,-1.8007,0.52577,-0.07344/
        T=(X+273.15)/273.15
        COND=A0+T*(A1+T*(A2+T*(A3+T*A4)))
        RETURN
        END
C
        FUNCTION VISC(X)
        DATA A0,A1/2.414E-5,247.8/
        T=X+133.5
        VISC=A0*10.**(A1/T)
        RETURN
        END
        FUNCTION DENS(X)
        DATA A0,A1,A2,A3,A4/.65263594E-5,-.19559673E-3,-.79633407E-2,
     1  .78565026E-4,-.70273330E-6/
        T=X-4.
        DENS=1000.+A0+T*(A1+T*(A2+T*(A3+T*A4)))
        RETURN
        END
```